Cortical network dynamics during visually-guided motor behavior: Setup development and Preliminary analyses

Von der Fakultät für Mathematik, Informatik und Naturwissenschaften der RWTH Aachen University zur Erlangung des akademischen Grades eine Doktor der Naturwissenschaften genehmigte Dissertation

vorgelegt von

Marcel Jan de Haan,
M.Sc. in Neurosciences,

aus

Den Helder, Niederlande

Berichter: Prof. Dr. Sonja Grün
Prof. Dr. Björn Kampa
Dr. Alexa Riehle

Tag der mündlichen Prüfung: 19-01-2018

PUBLICATION

The following publication forms the content of chapter 2 and was submitted to Journal of Neurophysiology. It is under revision at the time of writing this thesis:

Real-time visuomotor behavior and electrophysiology recording setup for use with humans and monkeys

Marcel J. de Haan, Thomas Brochier, Sonja Grün, Alexa Riehle, Frédéric V. Barthélemy

Abstract: We aimed at exploring large-scale network dynamics in multiple visuomotor areas related to eye-hand behavior under normal or perturbed conditions, both in monkeys and humans. We therefore integrated non-invasive commercially available solutions for eye tracking (EyeLink) and hand kinematics/perturbation (KINARM) into a single experimental setup, with on-line control and synchronous recording of eye and hand positions during interactive hand movement tasks. In order to relate the eye movements to the hand movements, both needed to be optimally represented in a common coordinate system. Our setup controls the two modalities in real-time, and simultaneously outputs behavioral data to an external data acquisition system, with high spatial and temporal precision. We developed an eye calibration method that allows us to track gaze positions relative to visual stimuli presented in the horizontal plane where the hand moves. This calibration method compensates for non-linearities caused by the system's geometry, and transforms eye kinematics into the same coordinate system as hand and targets. Additionally, in monkeys, head-fixation was achieved by a non-invasive mask to improve animal welfare. At the time of submission, there was no contemporary solution meeting all of our experimental requirements in human and monkey participants. Our setup design is the first to allow synchronous, highly precise tracking of eye and hand in a single reference frame, under normal or perturbed conditions. It is applicable to both human and monkey and is designed to record multimodal behavior and cortical network dynamics using a common data format. Finally, our adaptive eye calibration method is compatible with different eye-trackers.

SUMMARY

In natural conditions, primates possess a remarkable coordination of body movements in response to highly complex sensory information from the external world. The properties of our own body and those of the objects we interact with vary over time, yet continuous online adjustments allow for movements to be combined into a smooth and efficient goal-directed behavior. A key contribution to this behavior comes from eye-hand coordination. Studying the neural underpinnings of such coordinated behaviors involves attention, visual processing, visuomotor integration, motor planning and motor control in multiple areas across the brain. This distribution has led to specialized fields in neuroscience that aim to elucidate the contribution of each respective field to visually-guided motor behavior in isolation. However, studying individual systems without taking into account their synergistic relationships diminishes our insight, as isolated behaviors in arguably independent regions of the brain are limited. The main goal of this thesis is to elucidate multi-area coordination during goal-directed behavior and provide new insights into the dynamic processes of continuous predictions and transformations from sensory to motor areas (and back). The questions on how the visual input areas and motor output areas coordinate require an experimental setup with extensive behavioral control, recording capacity of multiple effectors, and dense electrophysiological recordings in multiple relevant brain structures. In my thesis I begin by outlining aspects of visually-guided motor behavior and present classic and current ideas on how the visual input on the retina travels in parallel through a multitude of brain areas, experiencing several stages of reference frame transformation, in order to control motor output of the hand. I subsequently detail the development and testing parameters of the *Real-time Integrated Visuomotor behavior & Electrophysiology Recording* (RIVER) setup. This setup had to fulfill the following requirements: 1) both eye and hand positions must be expressed in the same coordinate space; 2) the setup must have real-time control over eye and hand movements within the task environment, 3) movements must be continuously tracked and recorded under any experimental condition, 4) the setup must be optimized to allow for electrophysiological recordings in human/monkey participants, and 5) the setup must have the ability to output synchronized data of behavioral and experimental events with all electrophysiological recordings. I present preliminary behavioral data from a monkey trained to perform a sequential point task in the RIVER setup, and briefly discuss the surgical procedures and outcome of multi-electrode array (MEA) implantation. Finally, I present our findings from noise correlation analysis on massively parallel electrophysiology data from a parallel reach-to-grasp project.

ZUSAMMENFASSUNG

Primaten besitzen unter natürlichen Bedingungen eine bemerkenswerte Koordination von Körperbewegungen als Reaktion auf hoch komplexe sensorische Informationen aus der externen Umgebung. Der Zustand unseres eigenen Körpers und der der Objekte mit denen wir interagieren variiert mit der Zeit, jedoch erlaubt uns eine gleichzeitige Anpassung unserer Bewegungen ein gleichmäßiges, effizientes und Ziel-gerichtetes Verhalten. Eine Schlüsselkomponente dieses Verhaltens ist die Auge-Hand-Koordination. Die Erforschung der neuronalen Grundlagen und Prinzipien eines solchen Koordinationsverhalten involviert die Untersuchung von multiplen Arealen des Gehirns zuständig für Aufmerksamkeit, visuelle Verarbeitung, visuomotor Integration, Bewegungsplanung und -kontrolle. Diese Notwendigkeit führte zur Entstehung eines speziellen neurowissenschaftlichen Bereichs, welcher sich zur Aufgabe gesetzt hat in Isolation die Anteile jedes respektiven Areals zu visuell-kontrollierten Bewegungsabläufen zu untersuchen. Allerdings reduziert diese Vorgehensweise, die die individuellen Systeme ohne deren synergetischen Zusammenhang betrachtet, unseren Einblick, weil isoliertes Verhalten von „unabhängigen“ Gehirnregionen eher selten ist. Das Hauptziel dieser Doktorarbeit ist multi-areale Koordination durch Ziel gerichtetes Verhalten aufzuklären und neue Einblicke in die dynamischen Prozesse von kontinuierlichen Vorhersagen und Transformationen zwischen sensorischen und motorischen Arealen zu schaffen. Die Frage wie sich visuelle und motorische Areale miteinander koordinieren, benötigt einen experimentellen Aufbau mit einer aufwendigen Verhaltenskontrolle, Aufnahmekapazitäten mit multiplen Effektoren, und dichten elektrophysiologischen Aufnahmen in verschiedenen relevanten Gehirnstrukturen. In meiner Arbeit beginne ich zunächst damit die Aspekte von viuell-gesteuertem Motorverhalten darzustellen und klassische und moderne Ideen zu präsentieren, die erklären wie visuelle Stimuli von der Retina parallel über eine Vielfalt von Gehirnarealen geleitet werden und dabei mehrere Bezugsrahmen durchwandern um später die Motorik der Handbewegung zu kontrollieren. Ich führe nacheinander im Detail auf wie man einen Echtzeit integrierten visuomotorischen Verhaltens und elektrophysiologischen Aufnahmeaufbau (Real-time Integrated Visuomotor behavior & Electrophysiology Recording; RIVER) entwickelt und dessen Einstellungen testet. Dieser Aufbau musste dabei die folgenden Bedingungen erfüllen: 1) Beide Augen und Hand Positionen musste im gleichen Koordinatensystem darzustellen sein; 2) Der Aufbau musste innerhalb der Aufgabenumgebung in Echtzeit Kontrolle über Augen und Handbewegungen behalten; 3) Bewegungen müssen unter jeglichen experimentellen Bedingung kontinuierlich verfolgt und aufgezeichnet werden können; 4) der Aufbau muss so optimiert sein, dass elektorphysiologische Aufzeichnungen bei menschlichen Teilnehmern und Affen möglich sind; und 5) der Aufbau muss die Möglichkeit besitzen

Daten des Verhaltens und allen experimentellen Events mit allen elektrophysiologischen Signalen synchron aufzuzeichnen. Ich präsentiere zudem vorläufige Verhaltensdaten eines Affen, der in einer sequenziellen Zeige Aufgabe im RIVER Aufbau trainiert wurde, und diskutiere kurz die chirurgischen Prozeduren und das Resultat der Implantation des Multi-Elektroden-Arrays (MEA). Zum Schluss präsentiere ich die Ergebnisse der Noise-Korrelationsanalyse der massiv-parallelen elektrophysiologischen Daten eines parallel durchgeführten Greif-Experiments (reach-to-grasp project).

TABLE OF CONTENTS

LIST OF FIGURES

LIST OF TABLES

1 INTRODUCTION

The notions of vision and visual perception are often confounded, which is also the case for other sensory modalities such as hearing, touch, and taste. In the early days of behavioral experimentation, vision was regarded as the key to the mind; a gateway to understanding how the subjective experiences of the external world was formed by a physical stimulus. This gave rise to the field of psychophysics, which focuses on the relationship between the characteristics of a stimulus and the sensory experience, and fields of neuroscience dedicated to study the neural bases of various sensory systems (Kandel et al. 2000). The discovery of the phenomenon of blindsight in 1963 by Weiskrantz and Cowey initiated a shift in neuroscientific vision research by proposing different distinct types of visual processing in the brain. A person with blindsight has a lesion in the primary visual cortex, yet retains the ability to detect and respond to visual stimuli presented in their visual field, despite being unaware of these stimuli. This dissociation between phenomenal experience of stimuli and the ability to access information conveyed by those stimuli showed that behavior does not need to be guided by conscious perception of sensory information. Though the discovery has since met with criticism (Overgaard 2012), it did spark the exploration of parallel visual pathways, leading to the proposition of two independent visual systems (Trevarthen et al. 1968; Schneider et al. 1969; Ingle et al. 1973) and the further distinction by Ungerleider & Mishkin (1982) of a dorsal stream ("where" pathway) and a ventral stream ("what" pathway), to process spatial and object features, respectively. Goodale and Milner reinterpreted and characterized features of these streams based on a large body of anatomical and electrophysiological work, leading to the most popular interpretation of these separate visual pathways to date, separating the visual control of actions from the conscious perception of the world, or vision-for-action and vision-for-perception, respectively (Goodale & Milner 1992, Milner & Goodale (2006) Revision from 1995). In the 25 years since then, a sharp separation between vision-for-action and vision-for-perception has largely been replaced by a recognition that both streams interact considerably, and are likely functionally integrated. Nevertheless, the distinction has expanded the prevailing interpretation of vision as a system for perceiving the world to include vision as a system for movement control. Indeed, when we consider the most primitive forms of vision, the function seems to be entirely devoted to adjusting movements as a response to changes in light. The construction of the most basic eye in certain protozoa consists of just two cells: a photoreceptor that detects light and a pigment

cell that provides shading (Lenci et al. 2001). The photoreceptor is directly connected to ciliated cells, which engage the animal to move when lighting conditions change. Increasing the number of photoreceptors and the complexity of motion through muscle tissue we get a more varied behavior from a multi-cellular organism, such as the zebrafish, in which different sets of retinal ganglion cells project onto distinct areas of the brain to activate appropriate motor behaviors (Gebhardt et al. 2013). In higher organisms, such as humans and monkeys, the parallel demands of increased cognitive understanding of our surrounding through perception, and motor responsiveness to objects within our surrounding through action, have shaped the organization of the visual pathways in the brain. It turns out that visual areas involved with recognizing a steering wheel (vision-for-perception) are broadly distinct from those areas that program and control hand movements in order to use a steering wheel (vision-for-action; Goodale 2011). A crucial contribution to such goal-directed behavior is the control of the coordination between binocular eye movements and reach-to-grasp arm/hand movements, known as eye-hand coordination. This gives us the ability to perform different types of visually-guided reaches in a variety of conditions, with a fast eye movement (saccade) to an object preceding, followed by guiding the hand towards this object. These are common abilities that allow us to interact with objects in the external world, yet are complex with regard to the underlying neural mechanisms (Crawford et al. 2003). Various cortical and subcortical structures are distinctly modulated by behavioral features, such as eye positions/movements (Anderson et al. 1990; Galletti et al. 1995; Tolias et al. 2001; Ito et al. 2011) or hand positions (Thura et al. 2008). This may be even further complicated when the visual stimulus guiding the movement is different from the actual object, such as a computer mouse activating a cursor on a computer screen (Sailer et al. 2005, Sayegh et al. 2013, 2014).

In this thesis we will explore the neural bases of eye-hand coordination within the extended dorsal route, by focusing primarily on the influence and importance of naturalistic eye behavior on hand motor control. Our understanding of goal-directed action has traditionally been derived from behavioral studies, neuroanatomically derived imaging studies (i.e. functional magnetic resonance imaging, fMRI) and large-scale electrophysiology (electro-encephalogram, EEG) studies. In order to record the activity of populations of single neurons on a large scale, the last few decades of technological advances has seen some decidedly clever hybrid solutions, such as the use of electrocorticogram-electrode grids (ECoG; Rubehn et al. 2009, Bastos et al. 2015), optetrodes (Anikeeva et al. 2011), and cannula-electrode devices (Greger et al. 2007). It has also seen a significant expansion of traditional

extracellular recording capacity, covering larger cortical surfaces with greater spatial resolution and sustainable recording quality (Campbell et al. 1991; Nordhausen et al. 1996; Nicolelis et al. 1997; Cheung 2007; Kelly et al. 2007; Crist and Lebedev 2008; Charvet et al. 2010; Chase et al. 2012; Fernández et al. 2014). Now multi-electrode arrays are capable of recording the activity of hundreds of neurons in parallel to explore the behavioral impact on a large amount of neurons, individually or as part of a functional network, for example. However, as far as I know no single study has endeavored doing massively parallel recordings of single-neuron activities from *all* main areas involved in continuous visually-guided motor behavior, i.e., from visual input to motor output. Data from a single subject engaged in a goal-directed behavior with extracellular recordings along this extended vision-for-action path would yield a wealth of scientific knowledge about the cortical mechanisms underlying visuomotor coordination, integration and interaction. Questions concerning information transmission between the visual and motor cortical areas, and back, could be better explored, together with the relationship between eye and hand movements and their neuronal correlates. It will allow us to compare anticipatory activity for stimulus onset prediction and movement preparation between all areas, and show how and where the system corrects the main stream of information when the visual environment or a tracking movement is perturbed. Such an ambitious scientific endeavor must overcome several practical obstacles, however, such as the limitations in electrode technology: how many electrodes can fit on a current generation multielectrode array (MEA), how small can the connector be made to place several of them on a small area, how much data can be processed in parallel and at what temporal resolution. In parallel, strict experimental features need to be established that allow us to record both eye and hand movements, and have the ability to control naturalistic coordinated eye-hand behavior during a variety of tasks. What kind of participants should we engage? Humans possess a great ability to perform visually-guided motor tasks, but are not suited when it comes to recording brain activity, with only non-invasive options available in healthy subjects. The next best candidate would be a monkey with reaching and pointing capabilities akin to humans, as well as the capability to learn and understand complex visually guided motor tasks, and with a large enough cranium surface to house all the electrode connectors. Finally, a conceptual limitation comes from the relatively rigid perspective of research groups specialized in one cortical area at a time. The body of work describing the influence of a single complex behavior, involving a multitude of effectors, on a single area is rich in both the vision and motor neuroscience fields. In contrast, studies on coordination between cortical

areas that are far apart from each other, yet behaviorally connected in relation to goal-directed behavior, have been relatively sparse. In order to answer questions related to vision-for-action that extend beyond the higher visual areas, to structures involved in visuomotor transformation and motor control, it is imperative to first critically evaluate the state-of-the-art in multiple areas (visual, parietal, motor), and establish what is needed to push the scientific and technological frontier into multi-systemic sensorimotor coordination forward.

This chapter aims to familiarize the reader to important aspects of vision-for-action, and outlines the basic functional and structural connectivity between the cortical and subcortical areas involved in visually-guided motor behavior. Within this behavior, the focus will be on coordination of eye and hand movements, with emphasis on how unrestrained eye movements affect hand motor control and cortical modulation in different areas of the brain. Finally, a number of studies aimed at elucidating specific contributions of single and multiple cortical areas to visually-guided behavior are critically evaluated with respect to their content and the experimental methods they employed. This will provide a basic understanding of the current scientific landscape, before presenting the development of the Real-time Integrated Visuomotor behavior & Electrophysiology Recording (RIVER) in Chapter 2.

1.1 Vision-For-Action

The two-streams hypothesis was first suggested in 1982 based on evidence from a number of electrophysiological, anatomical and behavioral studies (Figure 1.1; Ungerleider & Mishkin 1982).

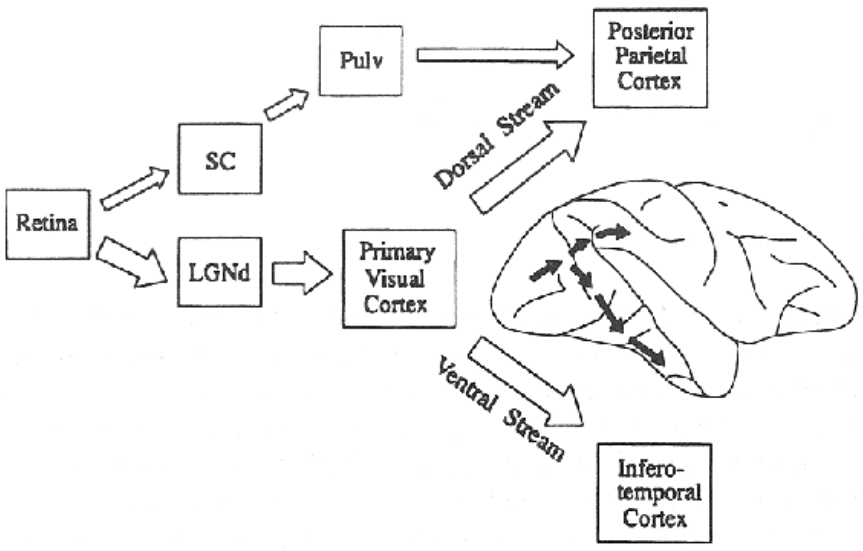

Figure 1.1: Diagram from retinal input to dorsal and ventral streams (Originally from Milner & Goodale 1995, revised in 2006).

It showed that two cortical regions received independent sets of projections from the primary visual cortex (V1): the ventral stream reaching the inferotemporal cortex (IT), and the dorsal stream reaching the posterior parietal cortex (PPC). Their interpretation was largely inferred from behavioral evidence in lesion studies, arguing that the ventral stream is involved in visual object processing and recognition (the "what" pathway), whereas the dorsal stream is involved in processing object location in space relative to the observer (the "where" pathway). Patients suffering from *visual agnosia* after damage of the occipitotemporal region showed difficulty in recognizing and describing object features, even though they were able to interact normally with these objects, and navigate around them (Goodale et al. 1991). Conversely, those suffering from *optic ataxia* after damage of the posterior parietal region were able to recognize objects without difficulty, but misreached in the contralesional visual field and had difficulty in preshaping the hand for grasping (Andersen et al. 2014). In the decade after developing this hypothesis, studies in anatomy and electrophysiology of visual areas led to a deeper knowledge of structural and functional connectivity between the involved regions. An adjustment of the original theory was most famously described in the paper '*Separate visual pathways for perception and action*' (Goodale & Milner 1992) and offered a perspective more focused on the output requirements than on the input distinctions. Their contention was that the perceptual experience of the world may have been a more recently evolved functional module than those controlling actions within it. Object recognition and understanding features of the environment have been shown to develop slower in the infant/childhood stages of a primate's life, than how to navigate within our environment (Dekker et al. 2011). This suggests a strong connection between memory and the ventral stream in order to use past experience to interpret the present, a feature not obviously necessary when walking or responding to a moving visual stimulus. However, the correct handling of an object controlled by the extended dorsal stream, such as using a steering wheel, must access the ventral part in order to cue the appropriate motor behavior (Schenk & McIntosh 2010). In fact, driving is a good example in which the dorsal route uses continuous visual input to adjust handling of the car, and the ventral route is used by the dorsal route to initiate the behavior, while processing cues in the landscape that hold information. An interdependence of highly-salient low-information cues, such as a traffic sign occurrence, and less-salient high-information cues, such as the meaning of the symbols on the traffic signs, underlines the need for the constant interpretation of the external world (ventral) to better help us interact with it (dorsal). If we extend this interplay between visual pathways to include the motor systems, an argument can

be made that the dorsal stream, in a broad sense, is specialized for visuomotor control, rather than spatial vision. This perspective has been largely vindicated over the years, with a vibrant research community dedicated to elucidate the role of vision in motor planning and execution, and vice versa (Sarlegna et al. 2003; Mirabella et al. 2007). This increased insight into the complicated patchwork of higher visual and parietal areas involved in visuomotor integration/transformation took the 'dorsal vs ventral route' hypothesis and refined the functional role of the dorsal route with more recent findings (Jeannerod 1995 (early review); Cohen & Andersen 1998; Rizzolatti & Matelli 2003). They suggested a dorsal-dorsal stream that controls actions on-line and a ventral-dorsal stream that is also responsible for action organization, but also plays a role in space perception and action understanding. This has been broadly shown in studies elucidating the interaction between the dorsal and ventral stream in sensorimotor control of complex object-oriented reaching behaviors, such as skilled grasp (Himmelbach & Karnath 2005; Polanen & Davare 2015). Sensorimotor integration is indeed approached less from a perspective of either a pure sensory field of research or a pure motor field of research, but still retains a general separation, most noticeable in textbooks. In a review by the original author Melvyn Goodale (2011) a comprehensive retrospective of 25 years of research into the visual control of reach-to-grasp movements is given. In hindsight, it formed the conceptual starting point of my project, by emphasizing the contribution and coordination of multiple areas to visually driven action.

1.2 Visually-Guided Motor Behavior

At the turn of the 20th century, tentative principles of bodily motion in response to visual input, or other sensory input (Cattel & Fullerton 1892), were explored with a clear message towards psychological research to include the physchophysics of voluntary movement, and not just work on the relationship between perception and stimulus (Woodworth 1899). Since then, integrated sensorimotor behavior has been studied in a variety of conditions, species and fields. Though these varied contributions are valuable and important, the focus of this thesis is directed at humans and monkeys, specifically macaque, and a common visually-guided motor behavior. For example, when an object appears in the visual field, a cascade of events is induced in the visual pathways and higher areas. Consequently, the head and eyes move to bring the image of this object onto the fovea and the hand moves in to reach it. The entire sequence lasts a fraction of a second, but encompasses numerous cortical (and sub-cortical) areas of the brain. These areas work together in initiating coordinated movements,

necessitating multiple effectors to complete a single goal-directed behavior. To perform this coordinated behavior, it is crucial that the reference systems of both visual input and motor output are linked by using precise transformation rules. This is naturally achieved by a cognitive map, a mental representation that connects the eye and hand positions in space when the movements of the hand involve a direct interaction with the object that is being viewed. Such a direct mapping structure was defined as a *standard mapping* (Wise et al. 1996; Vercher et al. 1994; Battaglia-Mayer et al. 2001; Archambault et al. 2009; Hawkins et al. 2013). However, in some specific conditions, eye and hand movements are dissociated, leading to a *non-standard mapping* (Wise et al. 1996). For example, a mouse cursor on a screen moves in a different plane than the hand movement on the mouse pad. Such a condition does not prevent us from performing an eye-hand coordination task, but it does require additional spatial and cognitive re-mapping processes. When studying eye-hand coordination during such behaviors, it is essential to track the eye and the hand positions continuously and precisely during the entire behavior to get an understanding of their coordination (Vercher et al. 1994; Mooshagian et al. 2014). This is especially important for the understanding of brain activities and interactions between brain areas that enable us to perform such tasks, in particular when trying to disentangle their cumulative and independent influence during the visuomotor neuronal processing (Boussaoud et al. 1998; Cisek et al. 2005; Yttri et al 2013). It has been shown that the same task executed in a standard or a non-standard mapping condition generates different patterns of neuronal activity in different brain regions, and the degree of difference depends on the level of dissociation between visual input and motor output (Connolly et al. 2000; Mascaro et al. 2003; Reina & Schwartz 2003; Gorbet et al. 2004; Gail et al. 2009; Granek et al. 2010; Hawkins et al. 2013; Sayegh et al. 2013,). Therefore, in the framework of this thesis the description of the visually-guided motor behavior is based on any motor behavior that uses visual input to continuously guide and adjust hand movements in the same coordinate space for reaching a sequence of task-related goals in a variety of conditions. This is an important characterization of the behavior to keep in mind, as it dictates the development and requirements of the experimental setups, the choice of the electrophysiological recording sites, and the procedures to be set for training the macaque monkeys.

1.3 Modern & Ancient Pathways of Behavior

The expression of behavior described above emanates, for a large part, from cortical structures that are evolutionary relatively recent in mammals. It would therefore be prudent to first consider how primitive vertebrate organisms achieved analogous motor behavior when they lack any of the brain structures so prominently studied in vision and motor research. Why did we develop such a large cortical surface dedicated to processing, integrating and transforming sensorimotor behavior? How do the phylogenetically older subcortical areas contribute to the structural and functional differentiation we can see in the primate neocortex? Why did our visual system differentiate further into a dorsal and ventral pathway? These questions in themselves merit dedicated graduate work from several evolutionary neurobiologists, but I feel it is useful to briefly touch on how the ancestors of mammals moved and interacted with the world, compared to our modern cognitive capabilities. When we regard vertebrate sensorimotor integration in its developmental infancy, the leap from stationary water organisms that simply grabbed whatever floated by to mobile predators using distance sensors, like smell and sight, to guide their movements was a pivotal point in brain evolution. Early organisms, such as the lamprey, distinguished themselves from the previous evolutionary branch by having a telencephalon, the pre-adaptation of the modern cerebrum and basal ganglia, which received sensory information from vision and olfactory receptors concentrated in their heads via the ventral thalamus. This primitive version of the basal ganglia is important for control of motor behavior and appears to be similarly organized as in mammals. Afferents from the optic nerve and olfactory bulb project to the ventral thalamus and are subject to basal ganglia influence before reaching the brainstem (reticulospinal neurons), which in turn activates spinal cord locomotor networks to elicit goal-directed locomotion (Grillner et al. 2000). A more illustrative example of lamprey sensorimotor behavior is shown in Figure 1.1 from a paper on the transformation of olfactory input into motor output (Derjean et al. 2010). This sensorimotor functioning has allowed lampreys to survive, move through and interact with their environment for over 360 million years (Gess et al. 2006). This is an impressive feat considering they did so without much anatomical change in that time, having specialized early and successfully, and without developing the need for a neocortex. The clear, goal-directed foraging behavior based on central pattern generators (CPGs) and reflexes kept the lampreys unchanged all this time, yet our own evolutionary path has brought forth an explosion of cortical complexity and diversity.

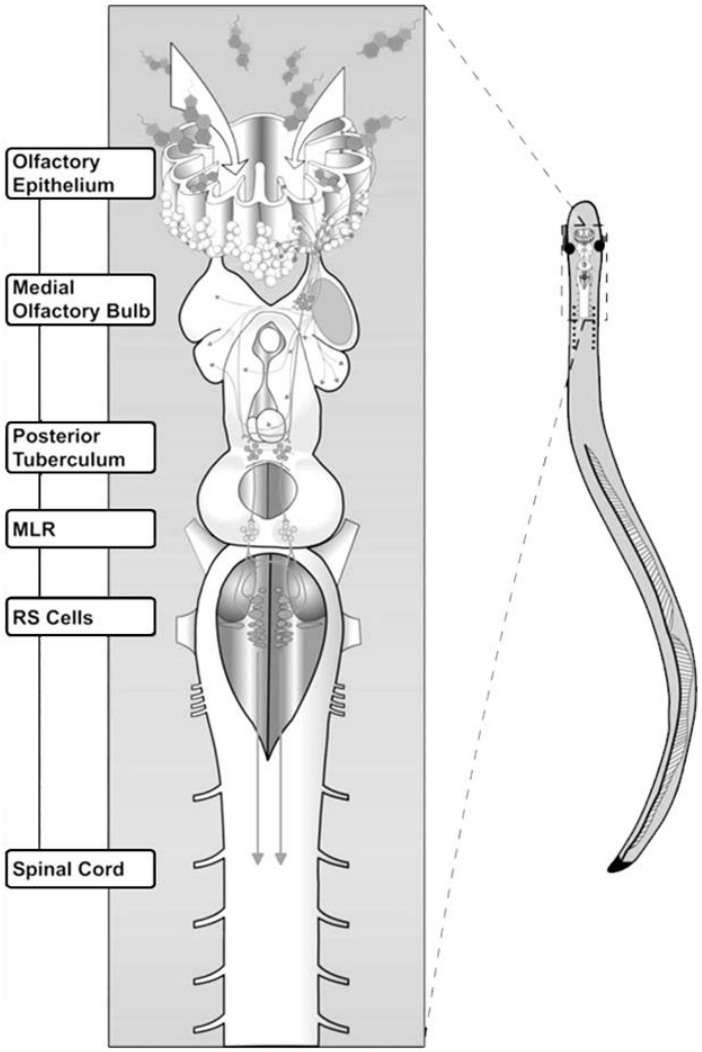

Figure 1.2: Schematic representation of the olfactory-locomotor circuitry in lampreys. Figure 8 from Derjean et al. 2010. Abbreviations: MLR = mesencephalic locomotor region; RS Cells = Reticulospinal cells.

The primate brain builds on the foundation of the lamprey by having the same analogous structures (sensory input, thalamus, basal ganglia, and spinal cord), but developed an additional sensorimotor processing powerhouse in response to the pressures of evolutionary mechanisms: the neocortex. This late addition had to deal with the increased demands of a more diverse external environment. Suddenly the brain needed to control not just the head and body, but also multiple limbs, the skeletomuscular system, the neuroendocrine system. It would have to merge and process additional sensations such as stereo sound, proprioception, the division of olfaction into smell and taste, binocular vision, color vision, object motion in a different medium; it would have to compensate for the greater influence of gravity and use balance organs to maintain posture; it would have to do all this faster and more successful than the competing organism fighting for survival. With several dozen structures in the frontal lobe and parietal areas that contribute to motor control, and several dozen structures in the visual system charged with processing highly complex sensory inputs, it is important to note

that our ancestors got along fine without any of this, and thrived with the most basic features of a sensorimotor system. We primates, however, are dependent on the integration of projections arising from different areas in the neocortex with the descending projections of our vertebrate ancestors to complete our own version of goal-directed behavior (Butler 2000; Shadmer & Wise 2005; Retaux & Kano 2010). Considering the humble list of structures needed to establish the behavior of the lamprey, what are the areas needed in the primate brain to establish our behavior?

1.4 Anatomy of the Visually-Guided Motor Behavior

An intuitive way to describe any behavior is by describing a simple sequence of events in time; monkey sees, monkey does. However, this hierarchy is difficult to maintain when we drop down to the level of cortical network dynamics, and researchers cluster to their own systems of interest in the motor or visual domain, or focus on connecting areas of the parietal cortex or subcortical structures separately. Out of all these systems, vision has always enjoyed an immense interest and captured the imagination of many students, whereas the motor system is generally regarded to have as much appeal as "a 1949 report on farm futures" (Graham 1990). Studying the unified contribution of both systems in a single behavior will hopefully elevate our interest in the motor system and place the visual system in a much more collaborative context. This necessitates the inclusion of secondary/supplementary structures in both systems, as well as areas specifically dedicated to visuomotor integration. To decide which areas are good candidates for electrophysiological recordings during this behavior, we would first have to consider which areas are involved in this behavior from the functional, structural and anatomical literature, and then to consider which areas are accessible with electrode arrays, if this is the recording technology we decided to use. Though several elaborate reviews and connectivity papers did go deep into a single system, and even connected to parts of neighboring systems (locally or functionally), I was unable to find a single complete vision-to-action structural map, speculative or otherwise. I therefore spent several months at the beginning of my PhD project researching and creating my own extended vision-for-action connectivity map. The guiding principle was to map cortical and subcortical areas out by simply regarding information transmission to start at the visual input and end at the motor output. Subsequently, I added the areas that may be required to establish continuous coordination between vision and motor systems as visual information is updated in real-time in order to adjust action. These latter areas would rely on more reciprocal information

transmission between them via subcortical and parietal structures. The questions posed to populate this map were: which areas are certainly involved in this type of behavior, and which areas are in contention but speculated to be involved?

1.4.1 Visual Areas: Retina & Subcortical Structures

The retina is often seen as a passive collection of photodiodes, tasked with counting photons, transforming the result in electrical activity and then sending these impulses on to the brain. However, it houses a variety of internal circuits that already shape incoming visual information before it is transmitted along the optic nerve, and is in fact part of the central nervous system (CNS), with an organization similar to the rest of the neural structures. Before leaving our eye, an image is captured by 125 million receptor cells, which converge on 10 million bipolar cells, which, in turn, converge on 1 million retinal ganglion cells (Dragoi & Tsuchitani 2016). These cells further differentiate into parasol and midget ganglion cells, and carry independent parallel streams of information about stimulus size, color and movement to the parvocellular (P) and magnocellular (M) layers of the lateral geniculate nucleus (LGN) lateralized via the optic chiasma. A third LGN layer, known as the koniocellular (K) layer, consists of a group of heterogeneous cells which introduced complexity to an area which, until recently, has been seen as physiologically clean and simple (Casagrande 1994; Hendry et al. 2000). For example, its direct connection to higher-level visual area MT/V5 is argued to contribute to the blindsight phenomena (Schmid et al. 2010). This opens up the discussion to view the LGN as something more than a simple relay station to V1.

In contrast, the same retinal outputs reach the relatively large Pulvinar nuclei which have reciprocal connections with numerous structures in the cerebral cortex. It is perhaps best regarded as a secondary visual pathway to higher-level visual areas analog to LGN's primary visual pathway to V1, and is considered a key structure for visual salience/attention and oculomotor action (Grieve et al. 2000; Arend et al. 2008), with evidence for subcortical contributions to the dorsal and ventral streams (Kaas & Lyon 2007) and motion processing (Casanova et al. 2001). Both structures are next to each other and belong to an ancient part in the diencephalon known as the thalamus. In parallel, retinal outputs also reach a midbrain structure just below the thalamus, the superior colliculus (SC), a principal component of the subcortical visual system including its important involvement in eye movement generation (Figure 1.3).

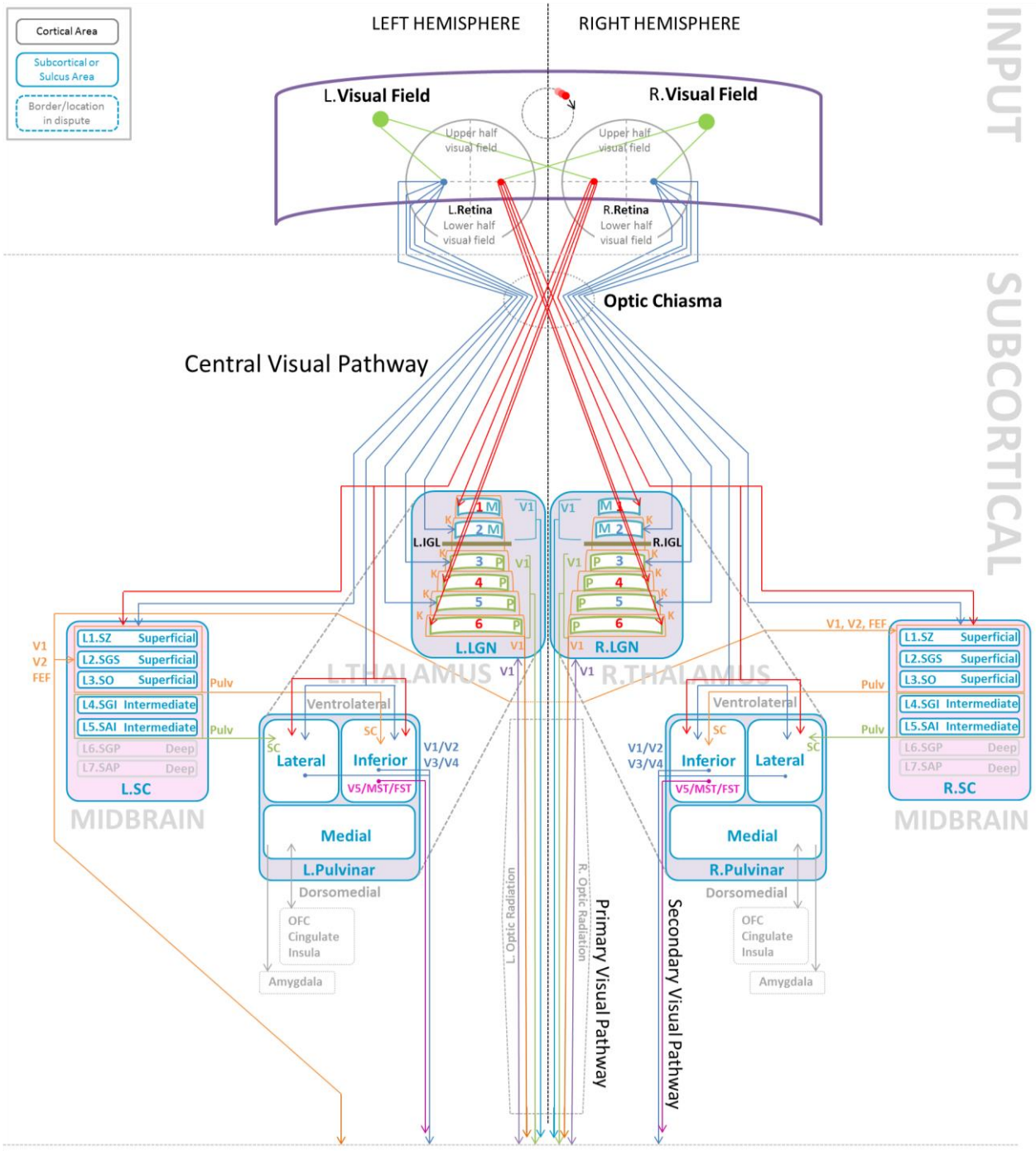

Figure 1.3: Structural connectivity map: *visual input & subcortical areas*. Abbreviations: LGN = Lateral Geniculate Nucleus; IGL = Intrageniculate Leaflet; M-Cells = Magnocellular Cells; P-Cells = Parvocellular Cells; K-Cells = Koniocellular cells; SC = Superior Colliculus (or Tectum); SC L1.SZ = Statum Zonale; SC L2.SGS = Stratum Griseum; SC L3.SO = Stratum Opticum; SC L4.SGI = Stratum Griseum Intermediate; SC L5.SAI = Stratum Album Intermediate; SC L6.SGP = Stratum Griseum Profundum; SC L7.SAP = Stratum Album Profundum; Pulv = Pulvinar; OFC = Orbitofrontal Cortex. The color codes of pathways are arbitrary, but consistent between figures.

It is an area that receives direct inputs from many structures contributing to visually-guided motor behavior: the visual input itself (retina), primary and secondary visual areas (V1, V2),

posterior parietal cortex (PPC) and motor area (FEF; frontal eye field). It is hypothesized that in early human development, a newborn's interaction with the visual world initially draws on innate SC circuits, showing poor acuity and shape perception but good motion perception (Bridge et al. 2016). This underlines the continued contribution of the SC to orienting eyes, head and body towards a stimulus, by employing multisensory integration and sending oculomotor signals to lower structures in the brain stem. The vast reciprocal connections of SC, together with indirect inhibitory influences of the basal ganglia, lead to saccadic eye movements, visual fixation, attention modulation, and oculomotor commands (Kandel et al. 2005). We react to a visual stimulus when it falls into our visual field by unconsciously moving our eyes, head and body towards it. Before the image reaches any cortical structure, it has been compressed and processed for use in fast-acting, reflexive actions leftover from a vertebrate ancestor that needed little more to survive.

1.4.2 Visual Areas: V1 and Higher-Level Visual Systems

The visual input finally reaches our first cortical structure located in the calcarine sulcus of the medial occipital lobe, at the back of the head: the primary visual cortex, or V1 (see Figure 1.4). This specialized structure is perhaps the best-studied cortical structure of the brain and is divided into six anatomically and functionally distinct layers, as it is the case for all cortical areas. Input from the LGN is received by V1 layer 4, which is divided into sublayers corresponding to input from the magnocellular layer and the parvocellular layer of the LGN. This compressed input contains a retinotopic map of the visual field of the two eyes, which is subject to cortical magnification (Daniel & Whitteridge 1961). Simple and complex V1 cells receive and process this input, both responding strongly to oriented edges and gratings (Hubel & Wiesel 1959; Adams & Horton 2003). Besides stimulus position, orientation and spatial frequency (gratings), V1 cells are commonly selective for direction of stimulus motion, color (blobs in layer 3), and stereoscopic integration (Mante & Carandini 2005), later necessary for the perception of depth. The functional architecture is very unique, in that it is highly organized, with neurons of the same orientation preference and eye dominance lining up through the layers following a columnar architecture (Hubel & Wiesel 1968, 1974; Paik & Ringbach 2011). These features vary when observing a neighboring column, with changing response to stimulus orientation (vertical, horizontal, diagonal) and eye inputs (left, right, binocular).

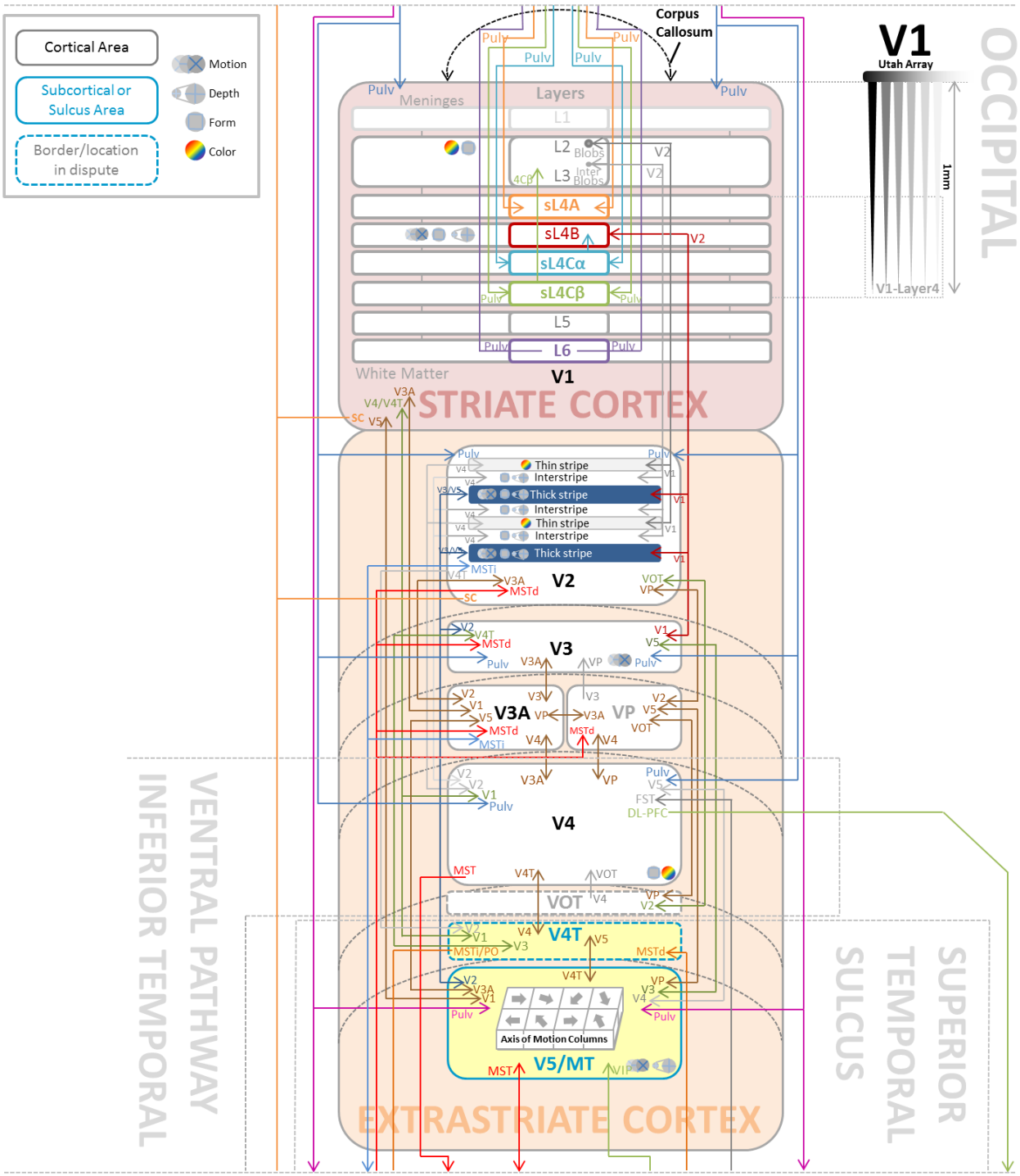

Figure 1.4: **Structural connectivity map: *V1 & higher visual areas*.** Abbreviations: V1 = Primary Visual Cortex (Striate Cortex); V2 = Visual Area 2 (Extrastriate); V3 = Visual Area 3 (Extrastriate); V3A = V3 Accessory Area (Extrastriate); VP = Ventral Porsterior Area (Extrastriate); V4 = Visual Area 4 (Extrastriate); VOT = Ventral Occipato-Temporal Area (Extrastriate); V4T = V4 Transitional Area (Extrastriate); V5/MT = Visual Area 5/Medial Temporal Area (Extrastriate). The color codes of pathways are arbitrary, but consistent between figures.

Columns with neurons that share similar response properties are able to communicate via horizontal connections with each other, creating an intricate pattern of interconnectivity

between orientation-specific columns, known as a hypercolumn (Hubel & Wiesel 1977; Buxhoeveden & Casanova 2002). These hypercolumns receive, transform and predominantly send their outputs via reciprocal connections to the secondary visual cortex, V2, with lesser connections to V3, V4 and V5 as well as feedback connections to the LGN and SC. Taken together, V1 and V2 encompass almost a quarter of the neocortical surface, with most of the corticocortical projections neurons in V2 projecting back to V1 (Anderson 2009). Though area V2 shares similar response properties with V1, most V2 cells are binocularly driven with obvious structural differences between the areas. V2 contains a typical repeating pattern of pale-thin-pale-thick stripes, each receiving different projections from V1 layers originating from the parvocellular and magnocellular layers of the LGN. This segregation remains selectively intact in V2, as a sublayer of V1 layer 4 projects from the extended M pathway to the thick stripes in V2. These stripes connect to higher visual areas that process motion, marking the beginning of the dorsal route. In contrast, blobs in V1 layer 2-3 project from the extended P pathway to the thin stripes and pale stripes in V2, These stripes connect to higher visual areas concerned with color, form and depth, marking the beginning of the ventral route (Roe & Ts'o 1997; Shipp & Zeki 2002; Kandel et al. 2005; Sincich et al. 2010).

Besides V1, area V2 projects to multiple higher visual cortical areas V3 (V3A, VP), V4 (V4T, VOT), and V5/MT (middle temporal area), which all receive direct input from the Pulvinar, including V2 (Felleman & Van Essen 1991; Manitini et al 2012). The region known as V3 (and V3A) is still somewhat controversial as the exact extent is in dispute, yet it has been shown that cells in this area are sensitive to complex motion properties similar to V5/MT, which is an area V3 projects to directly, as well as another motion processing area, the medial superior temporal area (MST; Gegenfurtner et al. 1997; Tootell et al. 1997). Area V4 is traditionally part of the ventral stream and generally regarded as important to object recognition. Yet this area shows strong connections with multiple areas in the intraparietal sulcus generally regarded as being part of the extended dorsal stream, suggesting it plays a role in spatial vision and attention (Ungerleider et al. 2008; Roe et al. 2012). The final visual area in the classical dorsal route is V5, better known as MT (Dubner & Zeki 1971). This area contains a high concentration of neurons selectively tuned to speed and direction of a moving stimulus, and organized according to a columnar architecture (Albright et al. 1984). MT receives direct input from the Pulvinar, LGN, and all the lower visual areas (V1 – V4), and projects to what could be tentatively regarded as visuomotor areas: the ventral intraparietal area (VIP) and MST (Ungerleider & Desimone 1986).

1.4.3 Visuomotor Areas: Structures in the Sulci and Beyond

With visual area MT we are shifting from connectivity between and within subcortical structures and surface cortical structures to cortical structures located within the posterior sulci of the brain. Due to their location, these areas are more difficult to access, but are regarded as key components in visuomotor transformation (see Figure 1.5). The area that has the strongest connections with MT is MST (medial superior temporal area); both located close to each other, yet with different topographical positions in humans and macaque monkeys. Even though human cortical expansion means that MST is located in the inferior temporal sulcus (ITS) in humans and superior temporal sulcus (STS) monkeys, their functional properties are equivalent (Maunsell & Van Essen 1983; Tanaka et al. 1986; Wunderlich et al 2002). I will outline anatomical connectivity based on the topography of the macaque monkey in the interest of clarity, but a review by Grefkes & Fink (2005) explores species differences in the PPC. Functional areas and connectivity seem to follow a parallel logic between human and monkey. The differently sized receptive fields of neurons in MST suggests it is split into an area involved in smooth pursuit movements (MSTl, small receptive fields), and an area important in processing optic flow (MSTd, large receptive fields), but studies have shown evidence that both MST areas contribute to motion perception alongside MT (Ilg 2008). In parallel, MT and MST both have direct projections to the ventral region of the intraparietal sulcus (IPS) known as VIP. The IPS, and indeed the entire PPC, contributes functionally to visuomotor behavior involving eye-hand movements towards targets, object manipulation, and visuospatial attention (Grefkes & Fink 2005), but is also involved in other sensory and cognitive functions, such as multimodal integration, attentional control, and (spatial) working memory (Swisher et al. 2007; Bray et al. 2015). It is important to note here that there are a multitude of parallel processes occurring in most of these visuomotor areas. VIP is distinguished on the basis of its neuronal response properties to speed and direction of a moving visual stimulus and stimuli near the face, with some changes in activity related to smooth pursuit eye movements, but not to saccadic eye movements. This led to the hypothesis that, much like other visual areas in the dorsal stream, VIP may be involved in the processing of visual motion (Colby et al. 1993). Additionally, it is connected directly to the motor cortex, specifically the dorsal premotor cortex (PMd), but also to the parieto-occipital area (PO) and area 7a in the superior parietal lobule (SPL). The lateral, medial, posterior and anterior parts of the IPS (LIP, MIP, PIP, AIP) share this level of connectivity, by extending into the frontal eye fields (FEF), the prefrontal cortex (PFC), and the primary motor cortex (M1; Shadmehr &

Wise 2005). The IPS seems to be a bridge between many cortical structures, yet it is functionally difficult to map extensively due to its inaccessibility and rare occurrence of lesions in this area, which in two patients only led to a spatial-attentional deficit (Gillebert et al. 2011). This somewhat typifies the dichotomy of this region: there is a large distribution of connectivity in the posterior sulci with other areas of the brain, but access to explore its function is very limited, and lesion studies in these areas show milder behavioral deficits than lesions in the primary visual or motor cortices.

Controversies about the topographical distinction following functional studies are part of the scientific landscape, such as the organization of V3 and PO (Gatass et al. 2015), but are inevitable when pushing the frontier forward.

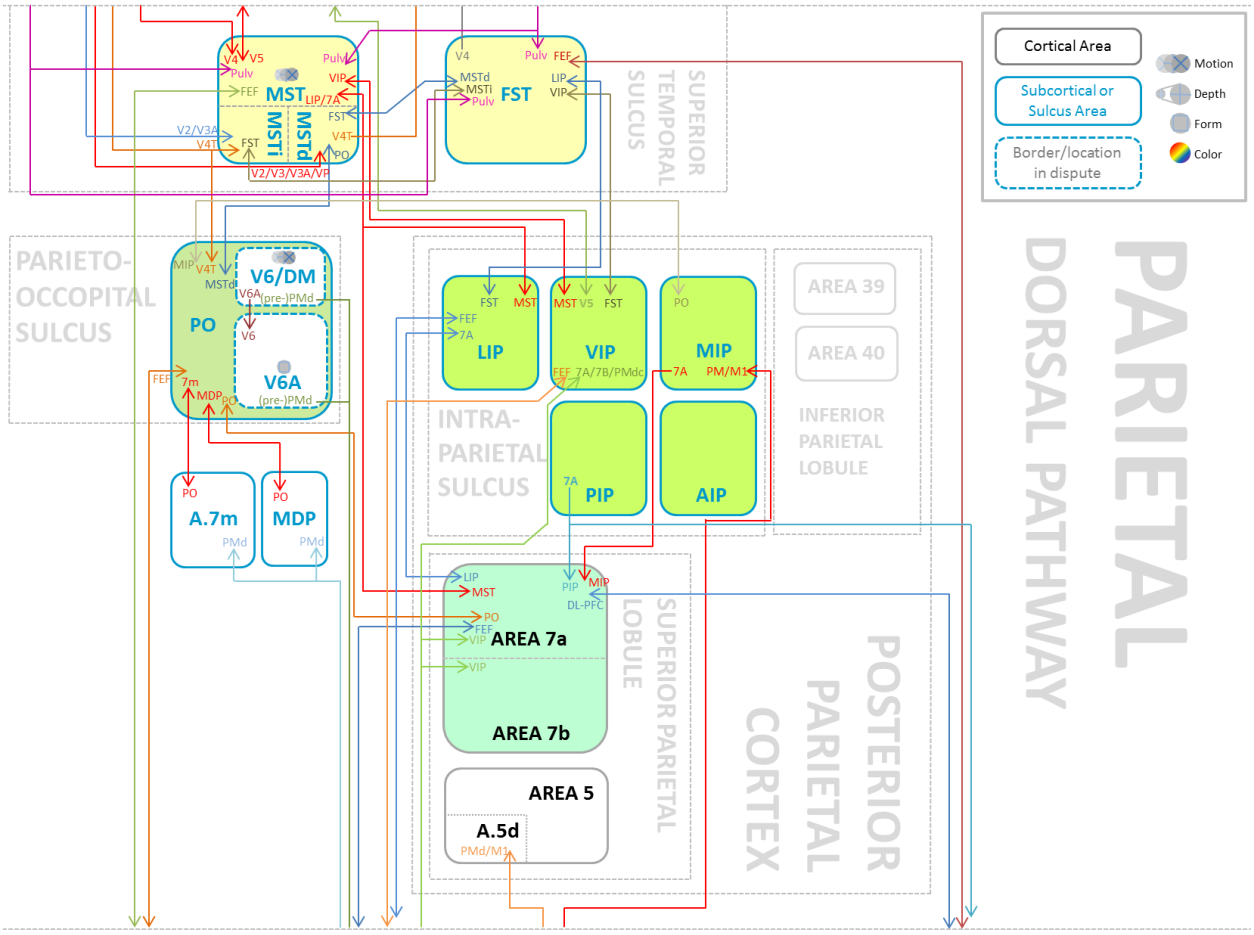

Figure 1.5: Structural connectivity map: *structures in the sulci and beyond*. Abbreviations: MST = Medial Superior Temporal Area; MSTi = Inferior Medial Superior Temporal Area; MSTd = Dorsal Medial Superior Temporal Area; FST = Fundal Superior Temporal Area; PO = Parieto-Occipital Area; V6/DM = Visual Area 6/Dorsomedial Area; V6A = V6 Accessory Area; LIP = Lateral Intraparietal Area; VIP = Ventral Intraparietal Area; MIP = Medial Intraparietal Area; PIP = Posterior Intraparietal Area; AIP = Anterior Intraparietal Area; MDP = Medial Dorsal Parietal Area. The color codes of pathways are arbitrary, but consistent between figures.

Area PO is located in the parieto-occipital sulcus (POS) and may be further distinguished into the dorsomedial area (DM) or V6 (Galetti et al. 1996), and V6A, which is responsive during finger pointing and reaching movements of a monkey (Galetti 1999; Pizalis et al. 2013). Both are directly connected to MST, regions in the IPS, and the PMd. In a review, Cohen & Andersen (2002) describe areas in the PPC and its involvement in transforming sensory stimuli to guide movements, with the express goal to outline how an eye-centered reference frame is modulated by vestibular, eye, body, and limb position signals. With this idea of higher-level cognitive functions in mind, the parietal reach region (PRR; proposed in Andersen & Buneo 2002), including MIP and V6A, would be associated with reach specialization, AIP with grasp, LIP with saccadic eye movements, and the combination of PRR and LIP with movement planning (Cohen & Andersen 2002; Kaas et al. 2011). These have been important steps in elucidating the functional role of the PPC in sensorimotor integration. Just dorsal to LIP, on the cortical surface, lies area 7a, thought to be important for spatial perception and modulated by saccadic activity, visually guided arm movements, memory tasks, visual memory and attention, and movement planning (Andersen et al. 1990; Barash et al. 1991; Steinmetz 1994; Snyder et al. 1997). This area is densely connected to regions in all three sulci discussed above (POS, IPS and STS) and the FEF and PMd in the frontal cortex.

1.4.4 Motor Output: The Frontal Eye Fields

Electrical stimulation in the frontal eye field (FEF) elicits eye movements, a result found nearly 70 years ago by Rasmussen & Penfield (1948). It has since then been postulated to be one of the principal regions involved in oculomotor control and visuo-spatial cognition, with a considerably distributed connectivity profile. These regions include the supplementary eye fields (SEF), areas in the prefrontal cortex, areas in the IPS and the parietal eye field (PEF), as well as the subcortical area SC and caudate nucleus (CN; Vernet et al. 2014). Interestingly, FEF is completely disconnected from the classical motor cortices M1 and PM, sharing only indirect connections, and receiving the same downstream information from the aforementioned cortical and subcortical areas. The oculomotor system only requires the coordination of 12 muscles to move the two eyes, controlling the position of the fovea in six different ways: 1) fixation to keep the fovea on target; 2) saccades to move the fovea rapidly between objects; 3) smooth pursuit to track a moving object; 4) vestibular and 5) optokinetic movements, both to keep the eye still in space when the head or the environment move; and

6) vergence to adjust the angles of each eye in order to keep an object at a certain depth in focus (Kendal et al. 2005). The neural mechanisms underlying the two major types of eye movements, saccades and smooth pursuit, were investigated by studying the different areas which were connected to the FEF (Ferraina et al. 2002). In relation to saccades, the SC receives direct excitatory inputs from the FEF and LIP, modulated by the CN and substantia nigra. At the same time the FEF is modulated by areas in the parietal cortex, involved in visual attention, and the SEF, involved in specific aspects of saccadic control. The SC sends a command to the brain stem saccade generator to activate the muscle. FEF is also involved in smooth pursuit initiation, while areas MT and MST use incoming visual information from V1 to calculate updated smooth pursuit movement speed and trajectory to match those of the target. FEF, MT and MST project to the descending pathways via the midbrain and drive the smooth pursuit action of the eyes (Paus 1996; Kendal et al. 2005; Parton et al. 2007; Mustari et al. 2009).

1.4.5 Motor Areas: M1, PM, and the Descending Pathways

In parallel to FEF receiving information from areas in the parietal occipital cortex and the intrapratietal sulcus, another motor system also receives many of these inputs, starting with the supplementary motor area (SMA) located in the medial wall of the frontal cortex, and the premotor cortex (PM) located in its lateral wall. The SMA has a substantial connectivity contribution to the corticospinal tract (Hutchins et al. 1988; Lemon 2008) and evidence of direct connections with motor neurons in the spinal cord (Dum & Strick 1996; Rathelot & Strick 2006), which makes it directly related to motor output together with PM and M1. In contrast, pre-SMA predominantly projects to the prefrontal cortex, the same as its neighbor SEF, and is postulated to play an important role in exerting cognitive control over voluntary actions (Nachev et al. 2007; 2008). The PM covers a relatively large area of the frontal lobe, and can be further divided into dorsal/ventral and rostral/caudal areas, with a functionally diverse profile, covering motor planning, rule-based response learning, sensorimotor integration for reach guidance and grasping behavior (Matelli et al. 1985; see Figure 1.6). Briefly put, the dorsal premotor cortex (PMd) is active during reaching movements and the preparation of learned motor programs, whereas the ventral premotor cortex (PMv) is more involved with the spatial location of the target to be reached (Hoshi et al. 2004, Chouinard 2006). The PMd in particular receives a lot of visual input via direct connections with the superior parietal lobule (SPL) suggesting that it is part of a fronto-parietal network that

functions as a visuomotor controller, using sensory and attentional information to prepare, select and execute movements (Wise et al. 1997). Several studies have tried to elucidate the connection between the manual motor system that controls hand movements and the visual information it needs to guide their actions. This topic remains hotly debated today.

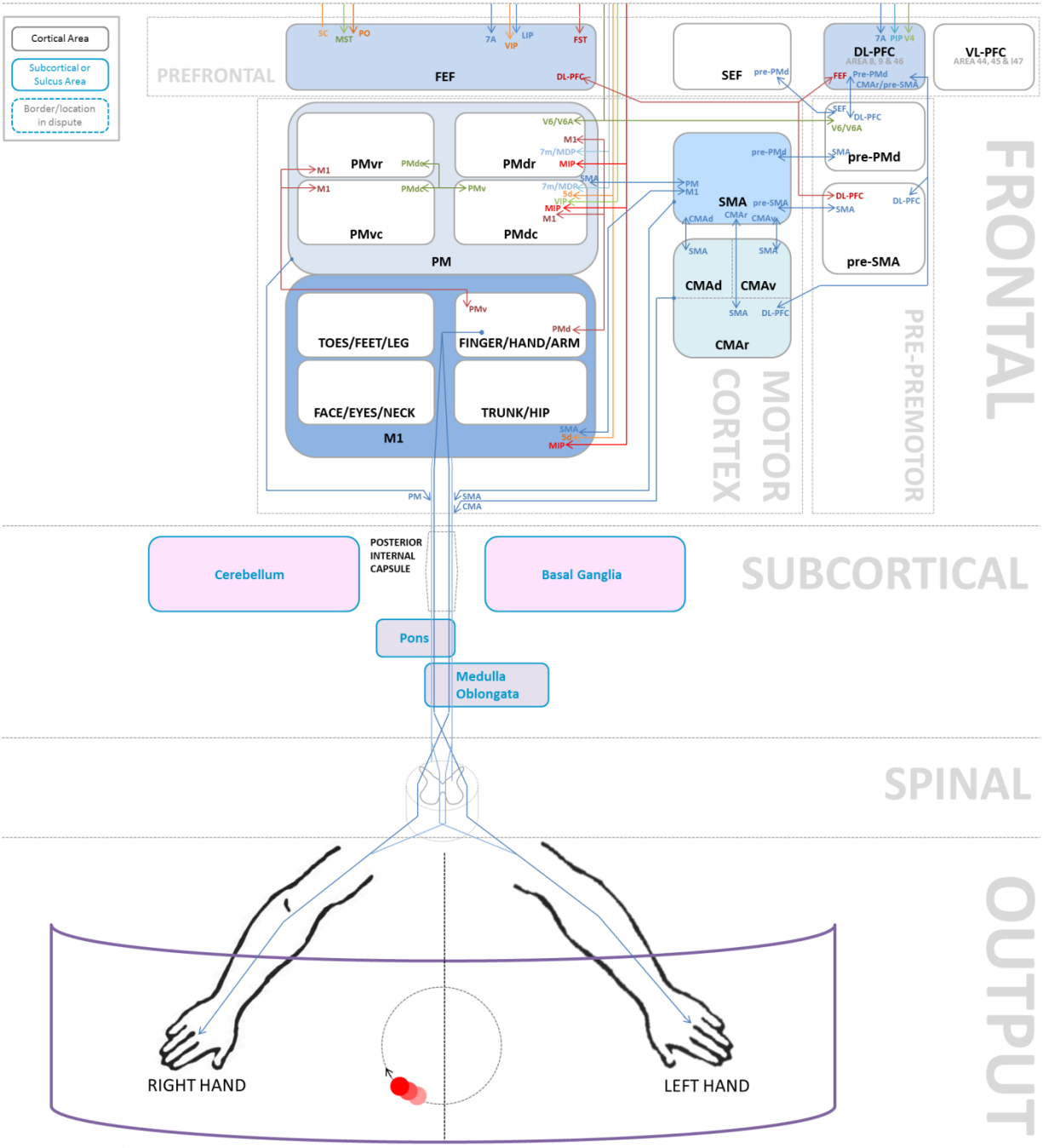

Figure 1.6: Structural connectivity map: *motor areas.* Abbreviations: FEF = Frontal Eye Fields; SEF = Supplementary Eye Fields; DL-PFC = Dorsolateral Prefrontal Cortex; VL-PFC = Ventrolateral Prefrontal Cortex; CMAd = Dorsal Cingulate Motor Area; CMAv = Ventral Cingulate Motor Area; CMAr = Rostral Cingulate Motor Area; SMA = Supplementary Motor Area; Pre-SMA = Pre-Supplementary Motor Area; PM = Premotor Cortex; PMvr = Rostral part of Ventral Premotor Cortex; PMvc = Caudal part of Ventral Premotor

Cortex; PMdr = Rostral part of Dorsal Premotor Cortex; PMdc = Caudal part of Dorsal Premotor Cortex; Pre-PMd = Pre-Dorsal Premotor Cortex; M1 = Primary Motor Cortex. The color codes of pathways are arbitrary, but consistent between figures.

A review by Galetti et al. (2004) examines the most direct visual pathway to the frontal cortex through several tracing and electrophysiological studies showing how visual input starting at V1 projects to the SPL, splitting into V6A or MIP, and subsequently end in the PMd (Colby et al. 1988; Johnson et al. 1993; Tanné et al. 1995; Shipp et al. 1998; Galetti et al. 2001). Besides receiving this broad set of sensory information from several sources, the PMd strongly and reciprocally projects to the primary motor cortex (M1) and outputs to the spinal cord (Kendal et al. 2005). M1 has been considered to be the final, common path for motor command signals to the spinal cord, but it is in fact more likely to be a parallel organization of cortical output to the spinal cord. M1 is involved in generating the neural impulses that control movement execution, and receives inputs from the somatosensory cortex and the posterior parietal cortex according to a somatotopic organization, which follows a correspondence between areas of the body with the areas in the motor cortex. However, this somatotopic organization in M1 is not precise or fixed, as often depicted incorrectly by the homunculus, and can be altered during motor learning and following injury, with generally a lot of overlap between different body parts (Donoghue et al. 1990). Together, SMA, PM and M1 give rise to most of the fibers in the corticospinal tract, a motor pathway that runs through the midbrain, pons and medulla oblongata and ends on motor neurons or interneurons, which ultimately elicit control on muscles in the limbs and trunk (Chouinard & Paus 2006; Lemon 2008). The rest of the corticospinal connections come from distributed areas, which include the somatosensory cortex and the parietal cortex. The subcortical movement circuits, which cover the thalamus, cerebellum and multiple nuclei of the basal ganglia (caudate nucleas, putamen, globus pallidus) are instrumental in the learning and selecting the best appropriate motor programs and mediating voluntary movements (Graybiel et al. 1994; Kendal et al. 2005). Continuous changes in sensorimotor input from these cortical and subcortical areas modulate the motor information carried over the corticospinal tract, which affect the final outgoing movements which subserves the goal-directed behavior.

The areas discussed in this chapter represent a crude map of all the possible functional and anatomical connections that are in play when we exhibit visually-guided motor behavior. It does, however, give the reader a good overall view of principal areas that are involved in even the simplest eye-hand coordinated behavior, in a sequential feedforward manner. In reality

many areas form parallel functional loops between many brain regions, with numerous feedback connections integral to adaptive motor behavior. However, it is beyond the scope of this thesis to collect and scrutinize every functional and anatomical detail from the existing literature, but forms an attempt to change our perspective so that we consider all of the contributing brain regions to a certain sensorimotor behavior, rather than focusing on the contribution to this behavior one system at a time.

1.5 Eye-Hand Coordination

There are vast parallel neuronal mechanisms behind different components of goal-directed behavior that merit closer examination, but considering the scope of my thesis and the emphasis on coordination between sensorimotor areas, it is useful to regard studies of eye-hand coordination. In a review by Crawford et al. (2003) the topic of eye-hand coordination has only recently endeavored to become a distinctive field of study, requiring a synthesis of spatial vision, eye movements, cognition and neurophysiology, and muscular control of arm and hand movements. The topic can be approached in a multitude of ways, by studying the coordination of eye and hand movements (Khan et al. 2011), or pondering whether the allocation of attention to targets is independent of either movement (Jonikaitis & Deubel 2011), as examples. Fundamental to any of these approaches is a clear definition of the processes that underlie the use of vision to guide hand movements (Herman et al. 1981; Biguer et al. 1982; Crawford et al. 2003; 2004). The long-term goal of our vision-for-action project is to elucidate the influence of natural eye movements on hand movement control by means of electrophysiological investigations. We aim at deciphering the underlying feedforward transformations in the brain that link visual stimuli to coordinated eye and hand movements, and the impact of feedback onto the visual input. The first link, from visual stimuli to eye movements, transforms the retinal representation of an object into a spatial representation that can be used by the oculomotor system. This relatively simple motor system rapidly responds with a saccadic eye movement to the object, bringing the stimulus into the fovea, and securing a useful flow of visual information that can be used downstream to guide body/limb movements (Andersen et al. 1985). This requires determining the spatial location of the object with respect to the eye position, but also with respect to the position of the head, the body, the limb, and finally the hand. With this important questions arise: do all these body segments have their own spatial transformation map, or is it a combinatorial map, built-up by the position of all body segments relative to each other and the target? Or perhaps

certain transformations only occur when a specific body segment is recruited to contribute to a response, i.e. a body or limb movement towards an object. Multiple sensory and motor areas, each endowed with a specific geometry and organization, must somehow reconcile their activity to a single spatial map at the level of the central nervous system (Lacquaniti & Caminiti 1998), but its nature remains elusive. Early reports of brain lesions in the sulci of the posterior parietal cortex caused misreaching to visual goals (optic ataxia) and hinted at a possible location where sensorimotor transformations occur (for a review: Andersen et al. 2014). It has been shown that key areas in the intraparietal sulcus (IPS) project to the reach-related zone of the PMd, making these locations early candidates to explore their potential role in transforming visual input into pointing and reaching movements (Mountcastle et al. 1975; Johnson et al. 1993; 1996; Goodale & Milner 2006; Tanné et al. 1995). This drove further investigations of neuronal activity of areas along the IPS during visually guided reaching movements, and showed that certain neurons were indeed modulated by different spatial variables, such as target location on the retina, eye position in the orbit, position and orientation of the arm, and preparation of combined eye-hand movements (Ferraina et al. 1997, Kalaska et al. 1997, Caminiti et al. 1998; Grefkes & Fink 2005). Interestingly, besides areas such as MIP, V6A, PRR, and other posterior parietal regions, reach-related activity in frontal area PM was also found to be modulated by the position of the eye in the orbit (Andersen et al. 1990). Another study showed the existence of gaze-related discharge modulation in PMd during controlled fixation, and tried to see whether such modulation is present during brief fixations during natural behavior (Boussaoud et al. 1993, 1998). Cisek & Kalaska (2002) set up an experiment to elucidate whether discharge modulation in monkey PMd can be related to gaze during a reaching task with unrestrained eye behavior. A modest effect was found in PMd, whose activity was mostly modulated by planning and execution of arm movements, but a striking influence of gaze was found in area 5 of the superior parietal cortex, a neighboring area to V6A. Neuronal responses in this area were influenced by both gaze and arm related modulation, suggesting that the arm and eye reference frames are both present in areas more associated with visuomotor integration, i.e. regions of the posterior parietal cortex. Breveglieri et al. (2016) pursued quantifying the range of a mixed representation of either reference frame in area V6A and found prevalent mixed encoding of target position, with eye-centered and spatiotopic representations differently balanced in the activity of the same neurons. In contrast, findings from an inactivation study in PRR, which includes V6A, suggested that the PRR is in fact not involved in eye-hand coordination (Yttri

et al. 2014). Indeed, inactivation of PRR did not induce any effect on the saccadic eye movements and no visual attention deficits could be detected. Reach reaction time was affected, however, suggesting this is a limb-specific area which influences reach planning occurring upstream from mechanisms involved in eye-hand coordination. In the same year, Hwang et al. (2014) showed that PRR inactivation caused shortened reach and saccade amplitudes when both hand and eyes moved together (though with only a weak correlation between saccadic and arm movement reaction times), yet they only observed this shortened amplitude for reaching movements and not for eye movements when the effectors were decoupled.

These and other studies in this field are finding mixed and sometimes contradictory results, but collectively push our understanding into multi-systemic sensorimotor coordination forwards, utilizing a myriad of recording techniques in both human and monkey participants expressing sensorimotor behavior. It remains a broad and daunting topic to study, with many avenues of investigation. In the next two sections I will: 1) evaluate literature directed at the modulatory influence of eye position and orientation on neuronal processes in different brain regions, and 2) outline some of the limitations of studying natural behaviors in an artificial experimental environment and discuss the influence of spatial decoupling of coordinated eye-hand movements.

1.5.1 Positional Influence on Neuronal Activity

Early neurophysiology studies used individual electrodes to record single cell activity and were predominantly concerned with categorizing neurons functionally into groups with a specific response pattern associated to a stimulus or behavior. In an early example of such a study the activity of single units was recorded in area 7 during a task that required macaque monkeys to fixate on stationary visual targets, track targets which moved slowly, and make saccadic eye movements to targets that jumped from one place to another (Lynch et al. 1977). The authors determined different types of visually responding, eye movement-related and reaching/hand manipulation neurons within the same area, which were rarely visual-only, and would often respond to selective attention. This was repeated in a study focusing on space perception in area 7a neurons, concluding there were a large variety of visual neurons responding to different spatial aspects (Sakata et al. 1985). Around the same time it was also shown that the activity of posterior parietal neurons increased during attentive fixation, with a strong influence from the gaze angle, depending solely on the position of the eye in the orbit

in about one-half of the neuronal population (Andersen & Mountcastle 1983). This initiated further investigation of different postural influences (eye, hand, head, body orientation and position) on the functional properties of neurons in different brain regions. This led to the introduction of the notion of 'gain-field' modulation. Early gain-field studies showed that the visual responses of neurons (spiking activity) in the parietal areas were non-linearly modulated by the position of the eye in the orbit (Andersen et al. 1983; 1985; 1993; Brotchie et al. 1995; Salinas & Sejnowski 2001, Cohen & Andersen 2002). Since then it has been proposed that processes in any area receiving an eye position signal may be affected, such as the early visual areas, the aforementioned parietal areas, and frontal areas. Indeed, studies utilizing functional magnetic resonance imaging (fMRI) have predominantly been used to assess the gaze dependent effects on multiple areas throughout the human brain, and found that static gaze orientation affects movement-related brain activation in frontal and parietal areas, and in subcortical areas such as the cerebellum and putamen (Bédard et al. 2008). The effect on the primary motor cortex is still in contention, however, as gaze modulated movement-related processing was not found by DeSouza et al. (2000), yet it was found by Baker et al. (1999).

The difficulty with functional whole brain analysis using the blood-oxygen level dependent (BOLD) signal is its limited temporal resolution, forcing participants to remain stationary in their gaze to correctly assess its effect on neuronal activity. The dynamic changes in unrestrained natural eye movements over time during a visually-guided pointing task would cause a significant bias in the interpretation of BOLD signal changes, especially considering that the average brain activity within a single voxel (3D volumetric pixel) encompasses roughly 630.000 cortical neurons (Lent et al. 2011). In order to explore the influence of unrestrained natural eye movements on hand motor control at the level of individual neurons with the highest temporal resolution, one must return to the classic technique of extracellular recording. This technique still yields vital discoveries, such as measuring the influence of horizontal, vertical, and depth eye-position signals on different visual neurons (Rosenbluth & Allaman 2002), yet has an obvious limitation that imaging techniques do not have: the total volume of neuronal tissue that can be recorded from simultaneously. With the advent of chronic high-density multielectrode arrays, however, investigations of the neural mechanisms of parallel processing architectures in the cortex reached a milestone when recording capabilities approached 100 microelectrodes in the 1990s (Campbell et al. 1991; Nordhausen et al. 1996). Since then, extracellular recording technologies have continued to expand,

covering larger cortical surfaces (multielectrode arrays: MEAs) and multiple layers (laminar recordings) with greater spatial resolution and sustainable recording quality (Nicolelis et al 1997; Cheung 2007; Kelly et al 2007; Crist and Lebedev 2008; Charvet et al 2010; Chase et al 2012; Fernández et al. 2014). A substantial amount of research groups use these recording technologies to explore the responses of neurons in a specific brain region to behavioral events (Riehle et al. 2013; McFarland et al. 2015; Best et al. 2016), but are not so much utilized when it comes to parallel recordings in *multiple* areas of the brain, relying rather on distributed single electrodes to sample neuron responses from different regions, or imaging techniques to get averaged responses over larger cortical and subcortical areas. In recent years studies have started to implant multiple multielectrode arrays (MEAs) in several cortical areas of the monkey brain in parallel (Poort et al. 2012; Michaels et al. 2015; Takahashi et al. 2015), but have so far seen limited application of these technologies in their exploration of dynamic gaze changes influences on brain network dynamics and visuomotor transformation processes (Lehmann & Scherberger 2013). The development of our experimental setup is built around the premise of exploiting current recording technology fully, which means implanting multiple high-density electrode arrays in targeted areas of a macaque monkey brain. These massively parallel electrophysiological recordings would yield an abundance of scientific data from just a single monkey engaged in a simple task. The connectivity map presented in section 1.4 served to outline and target the most relevant and accessible brain regions that 1) are involved with processing visual input, visuomotor transformation and motor output, 2) are integral to coordinated visually guided goal-directed behavior (eye-hand coordination in particular), and 3) have been shown to be modulated by eye position and orientation or body/limb position and orientation, or a combination of both. Before developing an appropriate experimental setup and a good behavioral task that engages these areas appropriately, we first scrutinized the potential influences of experimental conditions and task parameters on participant behaviors and electrophysiological responses.

1.5.2 Natural Behavior in Artificial Environments

Implanting MEAs can already be considered as an extraordinary condition for a macaque monkey to undergo, as is wearing a cap with EEG electrodes for humans (though not quite as invasive). Developments that accompany deep brain stimulation devices, brain-machine interfaces and next generation technology such as wireless recording implants bring us closer to having invisible recording devices (Gardner 2013; Brunner et al. 2015; Lebedev &

Nicolelis 2017; Kim et al. 2017), but we are not there yet. Therefore, experimentalists have to structure their recording methods in such a way that they do not interfere with the participant's behavior. Additionally, the requirements of the task and the scope of the experimental system also contribute to how much the participant is perturbed. In the case of recording stimulus-evoked responses of an anesthetized animal this is of little concern (Hubel & Wiesel 1959), but for a fully awake participant every moving body segment increases the chances of bias. A researcher interested in movement must therefore strike a balance between the extent of natural movement behavior, the reproducibility of task-dependent behavior, and the analyzability of the recorded behavior. Even when our actions are goal-directed with single trajectory hand movements to a simple target, the unconscious posture changes of different body segments in time (drift) and the variability in 3D hand movements towards the target make it difficult to disentangle influences from different sources and almost certainly complicate further analyses. Therefore, in many studies undesirable movements are often eliminated by locking them down, so that only movements pertinent to the research questions are considered and measured during the experiment (Vercher et al. 1994; Boussaoud et al. 1997; Van Donkelaar 1997; Pelz et al. 2001; Neggers and Bekkering 2001; Fraser et al 2011; Lee et al. 2013). It must be noted that these restrictions on movement behavior will implicitly bring a level of bias to findings, as they interfere with the natural range of movements. A particular example of these movement studies comes from Reina & Schwartz (2003), which inspired the early content formation of this Vision-for-Action project. In their study they present findings on coupling behavior between unrestrained eye movements and visually guided hand movements of a macaque monkey, while simultaneously recording extracellular activity in the PMvc (see also: Schwartz et al. 2004). This required the monkey to be seated in a chair to restrain body movement, to have his left hand remain stationary, and to have his head fixed, leaving only eye movements and right handed movements to be performed and measured during a visually guided motor task. Their findings revealed specific gaze strategies during the hand movements, which changed as a function of tracking speed: smooth pursuit eye movement followed slow tracing movements of the hand, and clustered saccadic eye behavior occurred when tracing at normal speeds, indicating 'gaze anchoring' (Neggers & Bekkering 2001). An important behavioral consideration was met with this experimental design, by having the arm interact with a visual stimulus that was directly viewed by the participant, eye and hand movements were coupled in the same space and time as the visual stimulus. For sensorimotor transformations that underlie such spatially congruent guidance of

the eyes, limbs, and body toward targets in visual space, the term standard mapping is used, as opposed to non-standard mapping mechanisms that require different cognitive processes (Wise et al. 1996). These terms were briefly introduced in section 1.2, and are not always considered by researchers designing their experimental setups. In a task with non-standard mapping conditions, the eye and hand are dissociated to some degree, for example, when the hand manipulates a mouse to interact with a target on a monitor through a curser, while the eyes are focused on the target and cursor interaction and not on the hand. In a study by Hawkins et al. (2013) the difference of influence was measured between standard mapping and non-standard mapping conditions on neuronal activity in the superior parietal lobule (SPL) when a macaque monkey had to employ different visuomotor rules into their reaching behavior to perform the task. Buneo & Andersen (2006) described the SPL as being involved in spatial orientation, reach planning and execution, and deemed this area critical for sensorimotor integration. They found that more SPL neurons had a higher tuning strength during a standard reaching behavior than when the eye-hand behavior was dissociated. In fact, they observed significant suppression in activity during dissociated conditions, suggesting that neurons in areas involved in visuomotor transformation and reach preparation/execution may inhibit habitual networks for eye-hand coupled reaching when visual and reach targets are in different spatial planes. A follow-up study by Sayegh et al. (2014) presented similar findings, and the authors concluded that the weight of proprioceptive feedback and online monitoring was altered as a result from decoupling the actions of the eyes from the actions of the hand. Behaviorally, they did not see a significant difference in movement time and reaction time in either condition. This shows how the same task yields the same behavior, yet will have a different neuronal activity profile relative to the level of sensorimotor dissociation. These findings were carefully considered when creating our own experimental setup to study naturalistic behavior and responses within an artificial environment.

1.6 The Multi-systemic Approach

In the previous sections I presented behavioral and electrophysiological aspects of visually-guided goal directed behavior, and gave a perspective on how visual processing evolved from primitive reactive behavior of simple organism to a two-stream interconnected model that subserves visual behavior in primates, such as tracking objects that enter the retinal image, classifying what they are, and act upon them via down-stream motor structures. I presented classic and current ideas on how the visual input on the retina travels in parallel through a

multitude of brain areas, experiencing several stages of reference frame transformation, in order to control motor output of the hand. I presented this in a sequential feedforward manner in order to simplify the connectivity between subcortical and cortical regions, with the explicit caveat that there are in fact multiple feedback loops present between these brain areas. In the final section I make a brief attempt in explaining the complexity of studying different systems that must coordinate their neuronal activity to successfully express behavior, as it is the case in eye-hand coordination. Each brain region that has an eye/head/hand/body signal present potentially experiences a modulatory influence when the gaze or a body segment changes position. However, the dynamic changes in neuronal activity in brain structures caused by the eye movements are difficult to capture when we lack the temporal resolution (fMRI imaging) or spatial extent (single electrode extracellular recording) to do so. We finished this section by considering how even slight dissociations between eye and hand behavior can have far-reaching consequences on the neuronal responses, by reporting on literature exploring the influence of decoupled eye-hand movements versus coupled movements.

These aspects combined form the starting principles that our setup must adhere to. The goal of the setup in a broader sense is to allow a researcher to study large-scale cortical network dynamics in different areas of the brain during the naturalistic performance of a complex visuomotor task, including visual and/or motor perturbations, in both monkeys and humans. Since there were no single integrated experimental systems available which met all of the experimental requirements, the Real-time Integrated Visuomotor Behavior and Electrophysiology Recording (RIVER) setup for use with human and monkey participants was developed, and presented in chapter 2 with some stringent conditions:

1. Both eye and hand movements must be recorded continuously.
2. Both eye and hand movements must correspond to the same spatial reference frame as the targets (eye-hand coupled condition involving ‘standard mapping’).
3. Influences from movements of other body segments must be reduced to a point that they do not introduce additional bias in the recorded data.
4. Access to the cranium for MEA implantation in the monkey setup and for an EEG cap in the human setup must be available, while causing minimum interference to the participant.

5. Adding a range of options for real-time manipulations of eye and hand movements, such as load changes and perturbations of the hand, allows quick and flexible development of novel experiments suitable for different research questions.

6. For the sake of reproducibility and compatibility between the monkey and the human version of this setup, a common software platform is used, including in-house produced data treatment software, similar hardware architecture, and similar behavioral recording techniques.

7. Data output should follow the same structure and logic between setups, and should be analyzable with the same tools, containing circumstantial information in the form of metadata, e.g. task parameters, participant details, session observations, and the like.

2 THE RIVER SETUP

From submitted work: ***Real-time visuomotor behavior and electrophysiology recording setup for use with humans and monkeys*.** Marcel J. de Haan, Thomas Brochier, Sonja Grün, Alexa Riehle, Frédéric V. Barthélemy (under revision in Journal of Neurophysiology).

2.1 Introduction

Within my PhD project I was given the opportunity to develop an experimental setup that would utilize and integrate the latest behavior tracking and electrophysiology technology, and synthesize a flexible real-time task environment for two types of participant: human and macaque monkey. The aim of this setup is to thoroughly explore the coordination between cortical areas along the vision-for-action pathway of both species during continuous visually-guided motor behavior in a standard mapping condition. A specific avenue of investigation, mentioned in chapter 1, was to study the static and dynamic influence of natural eye position/movement on hand motor control, by analyzing neuronal response modulation in several brain regions, including occipital, parietal and frontal areas. In monkeys, we will record electrophysiological signals with multiple chronically implanted multi-electrode arrays (MEAs), which allow us to capture single neuron and local field potential (LFP) signals. In humans we will use high-density EEG recordings. To achieve these goals the experimental setup had to fulfill the constraints of a highly precise on-line control of eye and hand movements performed in the same spatial coordinate system in normal or perturbed conditions. These constraints have to be identical in monkeys and humans with respect to the requested behavior and the requirements for recording the behavior. For this reason, and for the purpose of cross-species comparison, we aimed to build two setups that employ similar hardware architectures to accommodate the technical demands, and run principally identical software relevant for task development, control of behavior, eye calibration, and online data processing. Since there was no single integrated system available which met all of our behavioral and electrophysiological requirements, we decided to integrate several commercial systems to construct the two setups. For both monkey and human setups we selected the KINARM exoskeleton robot because of its ability to record continuous and precise arm/hand movements in the horizontal plane, with the possibility to perturb the movement and/or its visual feedback (KINARM Exoskeleton Lab, BKIN Technologies; www.bkintechnologies.com). For measuring eye movements, the EyeLink system was

selected for infrared non-invasive eye movement recordings (SR-Research; www.sr-research.com; EyeLink 1000 in case of monkeys, EyeLink II in case of humans). However, these systems come with their own proprietary software and specific hardware features, and were designed as independent platforms. In order to develop an integrated experimental setup we had to establish a clear hierarchy between these systems. We selected the hand tracking system as the master component of the setup in order to take advantage of its real-time management ability. This component controls task behavior and timing, motor perturbations and load changes, effector calibration and feedback, visual stimuli, and output of behavioral data. The eye tracking system and the data acquisition (DAQ) system (Monkey: Cerebus, Blackrock Microsystems; www.blackrockmicro.com. Human: in parallel, both ADwin Keithley EMG; http://uk.tek.com/keithley, and Biosemi EEG; www.biosemi.com) were integrated as slave components in the setups. This way, both eye and hand movements can be processed synchronously in real-time. Finally, we developed a computationally light-weight eye-calibration method for both setups to express the eye positions in the same (horizontal) coordinate system as the hand positions.

In this chapter I present in detail the complete integration of the eye tracking system into the hand tracking system for each setup in parallel. In chapter 2.2 (Materials & Methods) a common solution for each aspect of integration is proposed, and minor setup-specific adaptations are pointed out when they were necessary. Chapter 2.3 (Results) presents the results of extensive tests that were designed to assess the reliability of the eye-calibration method. The performances of a human participant in the human setup during our tests and the ones of a servo-controlled artificial camera eye in the monkey setup are presented in parallel in this chapter. Once we validated the methods in both setups, we implemented them in real experimental conditions with human and monkey participants engaged in a sequential reaching task (chapter 3).

2.2 Materials & Methods

2.2.1 Hand/Eye Movement Control Systems

Both human and monkey setup configurations were built around the KINARM Exoskeleton Lab (BKIN Technologies). The motorized KINARM exoskeleton was fixed to a chair, with the upper arm and forearm of the participant placed in arm supports at shoulder height enabling the arm to move in a 2D horizontal space. The positions of the joints (shoulder and elbow) were recorded continuously in real-time, with two torque-motors capable of applying

mechanical loads at each joint independently. This chair/exoskeleton module was then fixed to the virtual reality (VR) display, which provided to the participant the visual feedback for executing the motor task. The VR display consisted of a horizontal computer screen facing downward, with its image reflected on a horizontal semi-transparent mirror. The VR display allowed preventing direct vision of the hand while projecting visual targets and feedback of the hand movements on the mirror through the computer screen. The hand feedback represented in the VR environment was coupled to the exoskeleton end-effector and allowed the setup to react according to the behavior of the participant (Figure 2.1A). By adjusting the height of the screen and the mirror appropriately, the reflection of the screen, and in consequence the targets and the hand feedback representation, fell into the plane of the hand position (Scott et al. 1999). To control for the precise timing of the visual stimuli presentation, regardless of the refresh rate of the screen and the display latency, stimuli were accompanied by a change in luminance (e.g., from black to white) of two reference spots on the screen. These two spots (squares, 5 x 5 mm) were located at the top-left and bottom-right corners of the screen and their luminances were measured by means of two photoresistors. The signals recorded by these photoresistors were sampled at 1 kHz and stored in the same data file as the behavior. The screen display latency as well as the spatial and temporal properties of the image refresh rate have been evaluated before the beginning of the recordings. In order to record the participant's eye movements during a visually guided motor task in either setup, several options were considered to optimize the signal quality. In eye tracking configurations requiring high precision, the head of the participant needs to be restrained and the camera to be placed in the center of the visual field. To preserve direct vision of the stimuli, such a mounting uses a 45 degrees angled ‘hot’ mirror (i.e., a mirror that reflects only infrared light) placed in front of the participant and with the camera placed at the side or above (Reina & Shwartz 2003; EyeLink 1000 Tower/Primate Mount, SR-Research). Because of space limitations and the possibility for the monkey to touch the mirror or the camera, we chose to use a direct tracking mode (without a ‘hot’ mirror) and replaced the camera at the back of the VR display (Figure 2.1B). This configuration ensured uninterrupted tracking of the eye movements over the VR display. However when the monkey had to view a target very close to its body, the eyelids covered a crucial part of the cornea, thereby suppressing the contribution of the corneal reflection to the eye tracking and resulted in a signal loss. This problem was accentuated with human participants in whom the absence of a snout allowed for target presentation even closer to the body. Consequently, we chose to equip the human setup

with an EyeLink II system that uses a camera which is mounted close to the eye. In order to preserve the possibility to record EEG in the human setup, access to the head was required; therefore the standard eye-tracker helmet which held the two EyeLink cameras was removed. The cameras were mounted directly onto the VR display frame with a custom-made forehead and chin support (Figure 2.1D).

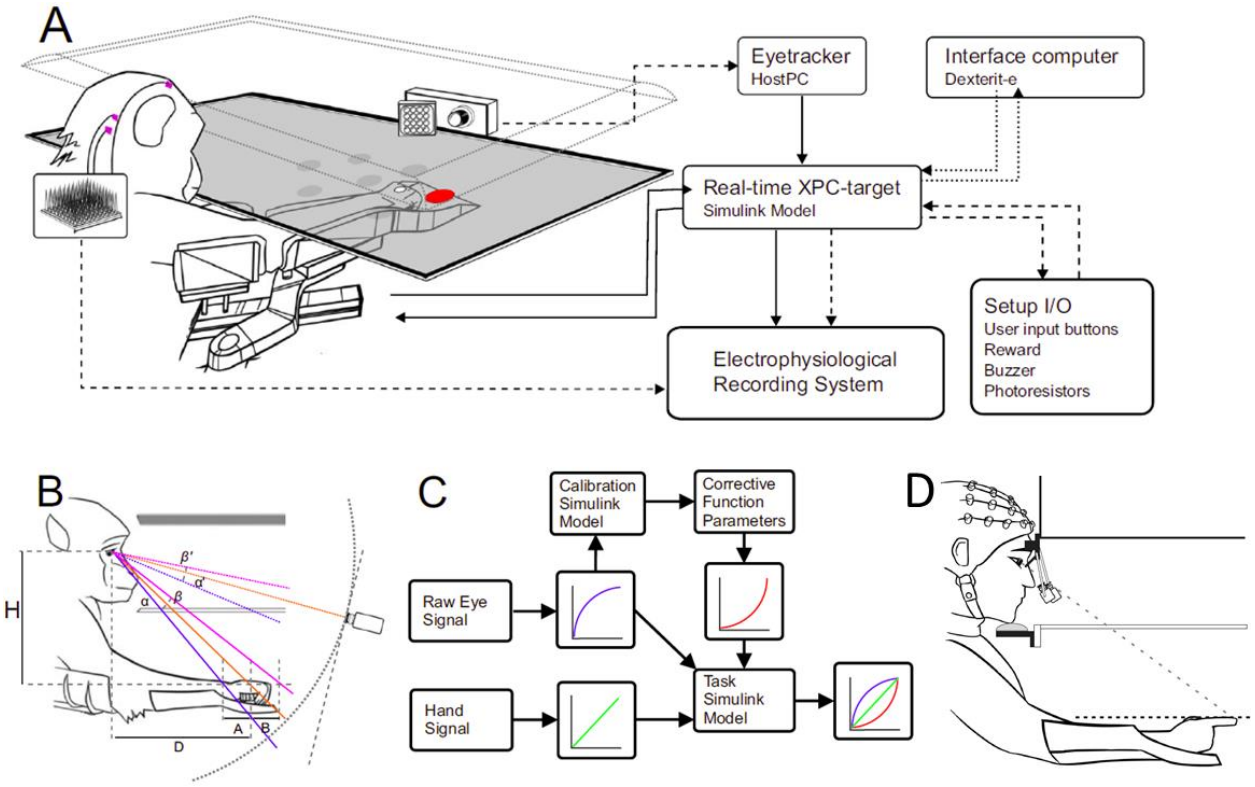

Figure 2.1: Setup overview and non-linearities. A) Organization of the setup with a monkey placed into the exoskeleton, viewing visual stimuli while the camera tracks eye movements. The diagram on the right presents analog (solid lines), digital (dashed lines) and Ethernet/UDP (dotted lines) connections between the different computers. B) Perspective non-linearity. The colored lines are the gaze axes when the subject looks at different locations on the screen. The dashed lines represent the projection of the gaze from the camera perspective for the same locations. C) Eye position correction principle. Setup non-linearities (blue) are compensated by an inverse non-linear function (red) to reconstruct the linear relationship between target space and eye space (green).

The work area of each setup was defined as the overlap of the space the participant could reach with the exoskeleton and the space where the eye tracker was able to reliably retain eye movement recordings. This work area thus defined the spatial parameters of the task, which was scaled so that all stimuli would fall within it, shown in Figure 2.2.

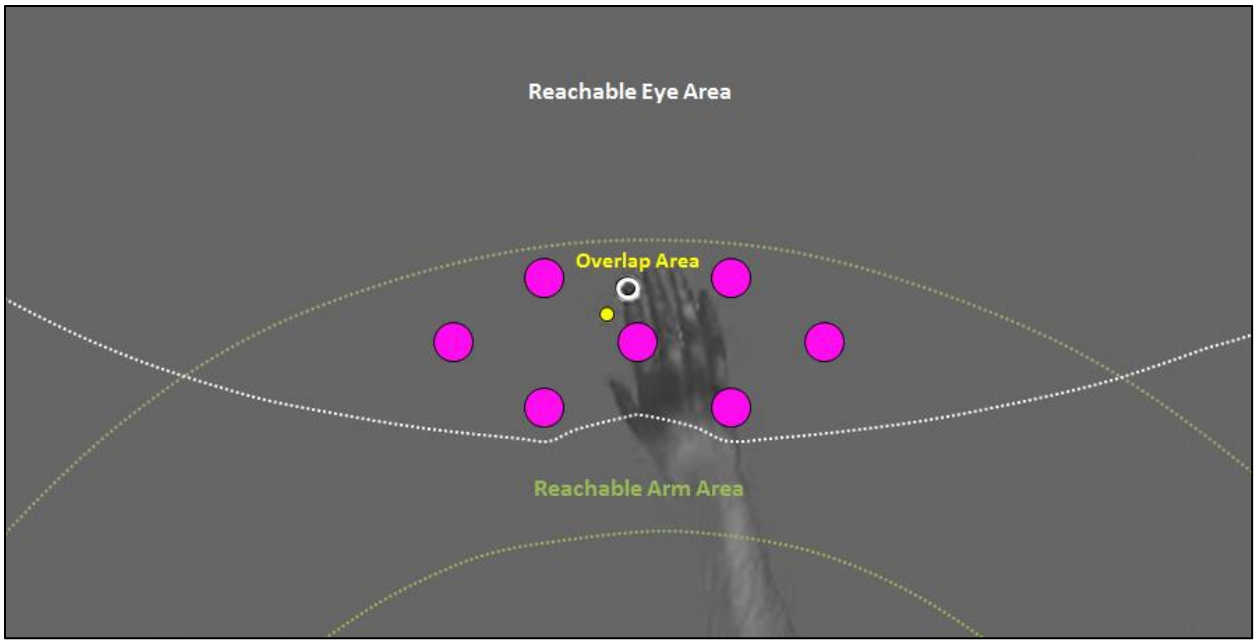

Figure 2.2: The top view of the monkey's work area for any experimental tasks, outlining the overlap between the area which can be reached by the hand, and the area which can be reached by eye without signal loss. The 7 target locations (purple circles, 1 cm diameter) are distributed within the overlap area, and can be used in a pointing task.

2.2.2 System Integration

With the prospect of integrating multiple stand-alone systems into a single setup, a hierarchy needed to be established. In this context, the KINARM was selected to control the experiment and the eye tracker was used as a sensor to provide the eye positions and trajectories. The advantage of such architecture was that the data flow was centralized in the KINARM real-time computer (xPC Target, The MathWorks). An operator controlled the sequence of the experiment and the data collection process with a unique real-time program (Simulink Real-Time, The MathWorks; www.mathworks.com) developed on the KINARM interface computer (Dexterit-E, BKIN Technologies). These programs run on the real-time computer, while an operator monitored eye and hand movements and visual stimuli on the screen of the interface computer (Figure 2.1A). The voltage corresponding to the position of the eye in the eye tracker image (thereafter referred to as eye position), were collected from two analog outputs of the EyeLink Host PC and sampled in the real-time computer at 1 kHz with an A/D input card (National instruments, PCI-6221). These two analog channels, X_v and Y_v, expressed respectively the horizontal and vertical deviation of the eye in the eye-tracker image. We chose this option over the possible ethernet connection between these two computers to avoid interference with the built-in UDP communication between the real-time computer and the interface computer (Figure 2.1A). Indeed, the UDP protocol does not

guarantee the communication integrity in this situation. In parallel, the raw exoskeleton motor positions were sampled in the real-time computer at 1 kHz with a motion controller card (Delta Tau Data Systems, PMAC-PCI).

These raw data were used to compute the position of the gaze (i.e the location on the screen where the participant is looking at) and the hand, both expressed in the same reference frame as the task. The X_{cm} coordinate describes the position of the gaze (or the target) along the bottom edge of the screen. The Y_{cm} coordinate describes the position of the gaze in depth. The unique real-time program controlled the interactive components of the task for participants by directly reacting to inputs from the eye tracker and the KINARM exoskeleton. In parallel, the program sent behavioral data continuously to the interface computer for storage in C3D format, together with task parameters. Additionally, the gaze and hand positions were also outputted at 1 kHz with a D/A output card (National Instruments, PD2-AO-16x16) to the electrophysiology DAQ system. Even though our system was designed to be compatible with any DAQ system equipped with enough analog and digital channels, here we have chosen the ones already used in our laboratory: electrophysiology DAQ system from Blackrock Microsystems in the monkey (Riehle et al. 2013; Milekovic et al. 2015), and a combination of the KINARM with EEG recordings in humans (Torrecillos et al. 2015). In both setups, digital events linked to the task sequence (e.g. target onset) and participant's behavior (e.g. hand reach to the target) were sent by the real-time computer to setup-specific DAQ systems to ensure the synchronization of the data-files and to provide time markers for future analysis. Finally, a direct copy of the raw eye and hand movement data was sent to the setup-specific DAQ systems. The integration of the different systems required a complex connectivity. Both movement control and DAQ systems required multidirectional connections. A custom-made hub was created to regulate communication between these systems, which included multidirectional routed connections and allowed direct operator access to all input/output channels via a front panel with BNC connectors. This hub ensured connections between systems for direct and split signals, with adequate shielding to maintain signal integrity. Figure 2.4 depicts a simplified connectivity diagram of the experimental apparatus in the training room (KINARM exoskeleton + chair, VR display, EyeLink Camera, Reward system) and computer systems in the control room (EyeLink Host PC, KINARM Windows PC, KINARM Real-time PC, Cerebus 1 & 2 PC, Neural Signal Processor 1 & 2). Figure 2.3 shows what the configuration of the monkey training and control room looks like.

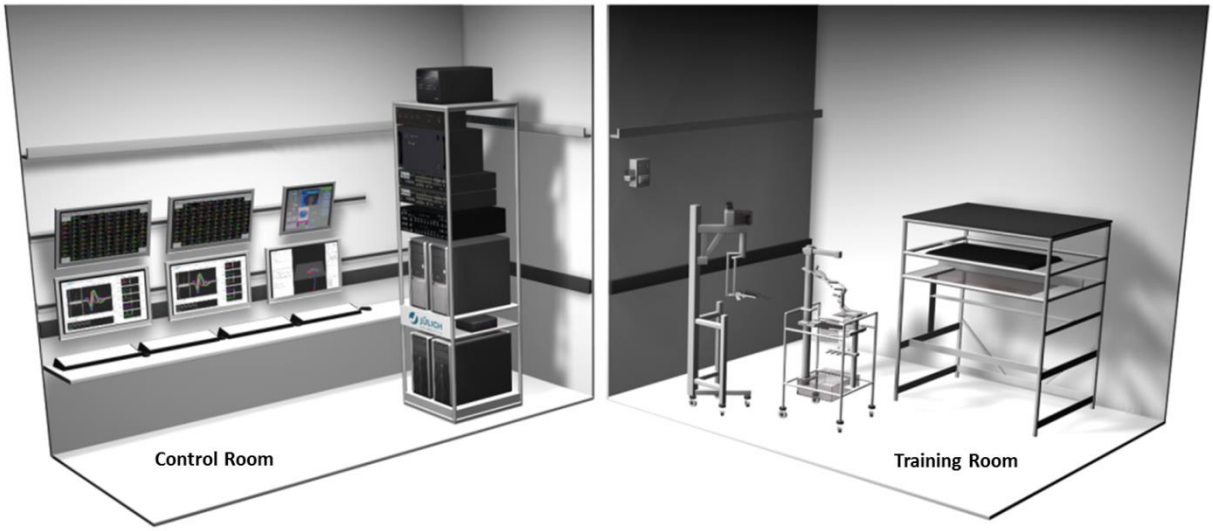

Figure 2.3: Control room adjacent to the monkey training room. 3D CAD design of the actual control and training room at the INT, deconstructed in Figure 2.4 into system components situated in both areas, featuring hardware connectivity and dataflow.

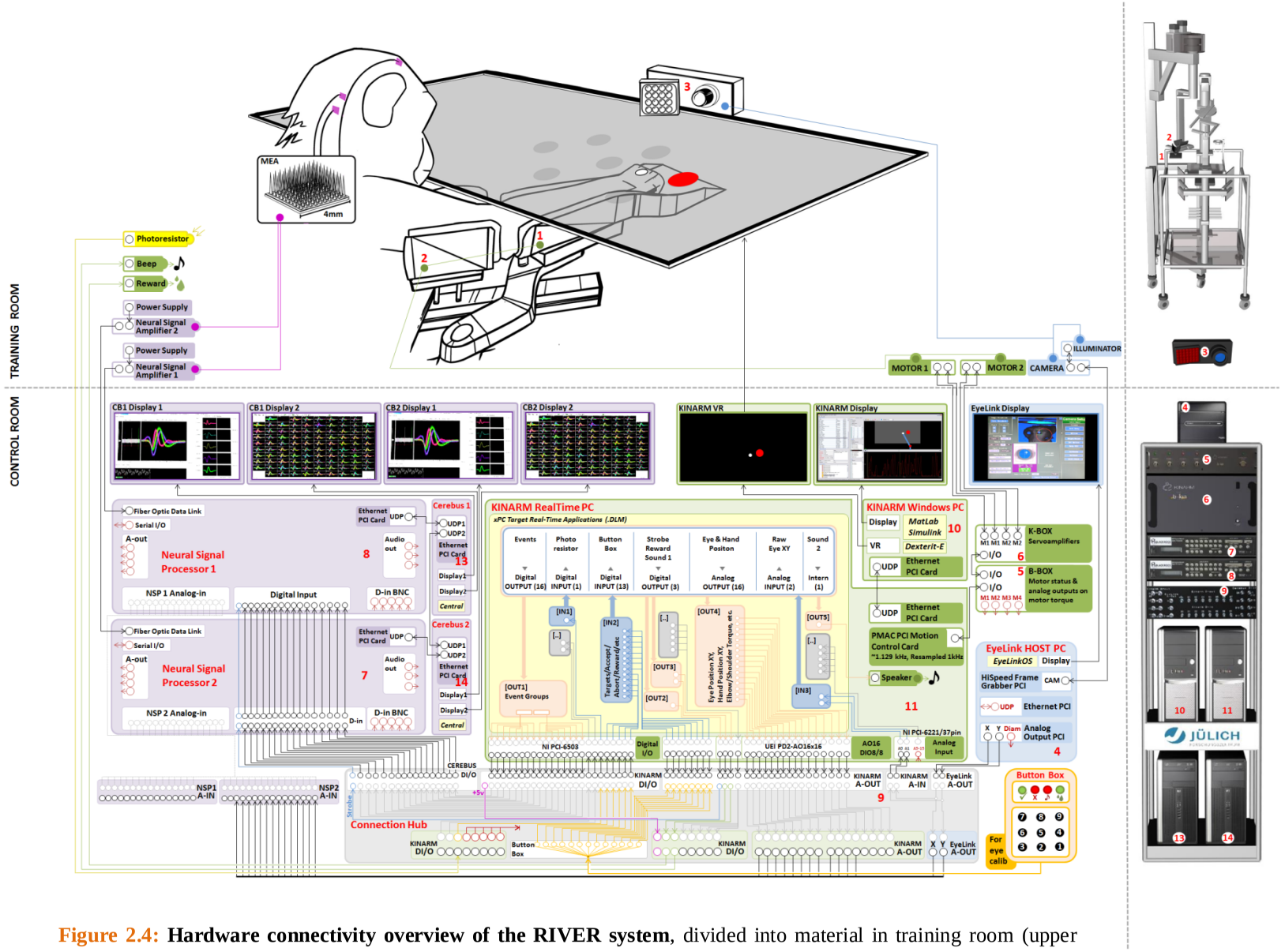

Figure 2.4: Hardware connectivity overview of the RIVER system, divided into material in training room (upper figure) and control room (lower figure). The lower figure outlines the connectivity between the EyeLink 1000 system (blue boxes), the KINARM lab (green boxes), and Cerebus DAQ system (purple boxes).

2.2.3 Eye Calibration

In order to analyze temporal and spatial features of eye and hand behavior in the context of a visually guided arm movement task, all components needed to be expressed in the same reference frame. In the KINARM system, target positions are natively expressed in the hand reference frame, which in turn is dependent on the exoskeleton hardware settings. This system offers an integrated virtual reality task environment with high-resolution control of the entire arm; it was therefore deemed simpler to convert the eye tracker signal to fit the hand reference frame than bringing all the KINARM features into the EyeLink system. However, this required a custom eye calibration method that was able to accurately express gaze location in the KINARM task environment and compensate for non-linearities introduced by the setup architecture (Figure 2.1C). We developed an empirical calibration procedure which was self-adapting to the participant's size and position and to the different setup dimensions, and accurately converted EyeLink *eye position* signals in volts to KINARM compatible *gaze position* in centimeters.

For each participant, the recording limit of the *eye position* on the virtual reality display was set by adjusting the eye tracker gain and offset. This ensured that the eye tracker was able to measure the *eye position* wherever the participant was looking within the work area, with optimal resolution and without saturation. In the monkey setup, this was done by directly adjusting the Eyelink 1000 in-built settings. However, for the EyeLink II of the human setup, we had to build a custom analog interface to control these adjustments. After these adjustments, the calibration procedure involved the recording of the *eye position* signal of the eyelink along the X and Y axes during 100ms, while the subject fixated each of 25 targets (0.2cm radius) presented in a random sequence on the virtual reality display. These recordings were repeated at least three times to ensure that a sufficient amount of data was collected at each target for accurate position estimation.

We designed a calibration GUI in Matlab (MathWorks) to visualize the recorded eye positions and remove deficient trials, such as blinks, saccades. Following this preprocessing step, we computed the average voltages recorded at each of the 25 reference points. The goal of the calibration is to establish the transform functions that should compensate for spatial distortions by linking the eye position voltages and the corresponding position of the targets on the screen. One typical example of *eye position* recordings is presented Figure 2.5A (black dots), scaled to the range of the targets (circles) to facilitate the visualization. It clearly shows

that the X_v channel amplitude varies as a function of target position along X_{cm} and Y_{cm}. This dependency on the X_{cm} and Y_{cm} couple is even more pronounced for the Y_v amplitude. In consequence, when computing the opposite transformation, we have to consider the *gaze position* along each screen axis as a function of X_v and Y_v. Figure 2.5B represents the relationship between the X_v and Y_v eye position recordings and one screen axis (X_{cm}) as a set of points in three dimensions, each point corresponding to one target. Figure 2.5C shows the same for the other screen axis. Because of the dependency of the eye position to X_{cm} and Y_{cm}, the points are sparsely distributed in the voltage space. Therefore, we reconstructed regularly distributed data by adjusting a grid to each dataset using a biharmonic spline interpolation (Matlab function *griddata*, using V4 method; Sandwell 1987). The results are two 3D matrices that link eye positions to gaze position in two look-up tables (one for X_{cm} and one for Y_{cm}).

In order to transfer the conversion rules into the Simulink model used during the experiments with a limited number of parameters, we fit a 4th order two-dimensional polynomial function to these grids.

$$X_{cm} = a + bX_v + cY_v + dX_v^2 + e\,X_vY_v + fY_v^2 + gX_v^3 + hX_v^2Y_v + i\,X_vY_v^2 + jY_v^3 + kX_v^4 + lX_v^3Y_v + m\,X_v^2Y_v^2 + n\,X_vY_v^3 + o\,Y_v^4$$

$$Y_{cm} = a' + b'X_v + c'Y_v + d'X_v^2 + e'X_vY_v + f'Y_v^2 + g'X_v^3 + h'X_v^2Y_v + i'X_vY_v^2 + j'Y_v^3 + k'X_v^4 + l'X_v^3Y_v + m'\,X_v^2Y_v^2 + n'\,X_vY_v^3 + o'\,Y_v^4$$

This allowed us to obtain two optimal parameter sets (a to o; a' to o') to express gaze position in the hand coordinate system as a function of the two EyeLink output voltages. These optimal parameters were subsequently injected into the Simulink task program to define the parameters of its online eye position conversion module. Due to the non-linear correction of the calibration model, a change in head position during task execution would have a significant impact on the input signal. Rerunning a complete calibration task because of small unconscious movements of the participant would be time consuming, and detrimental when training a monkey. A drift correction module was therefore developed allowing the operator to easily assess and adjust small offset shifts between trials. This module can be inserted into any current and future real-time program. Its functioning is illustrated in the chapter 2.3.2.3, on drift correction.

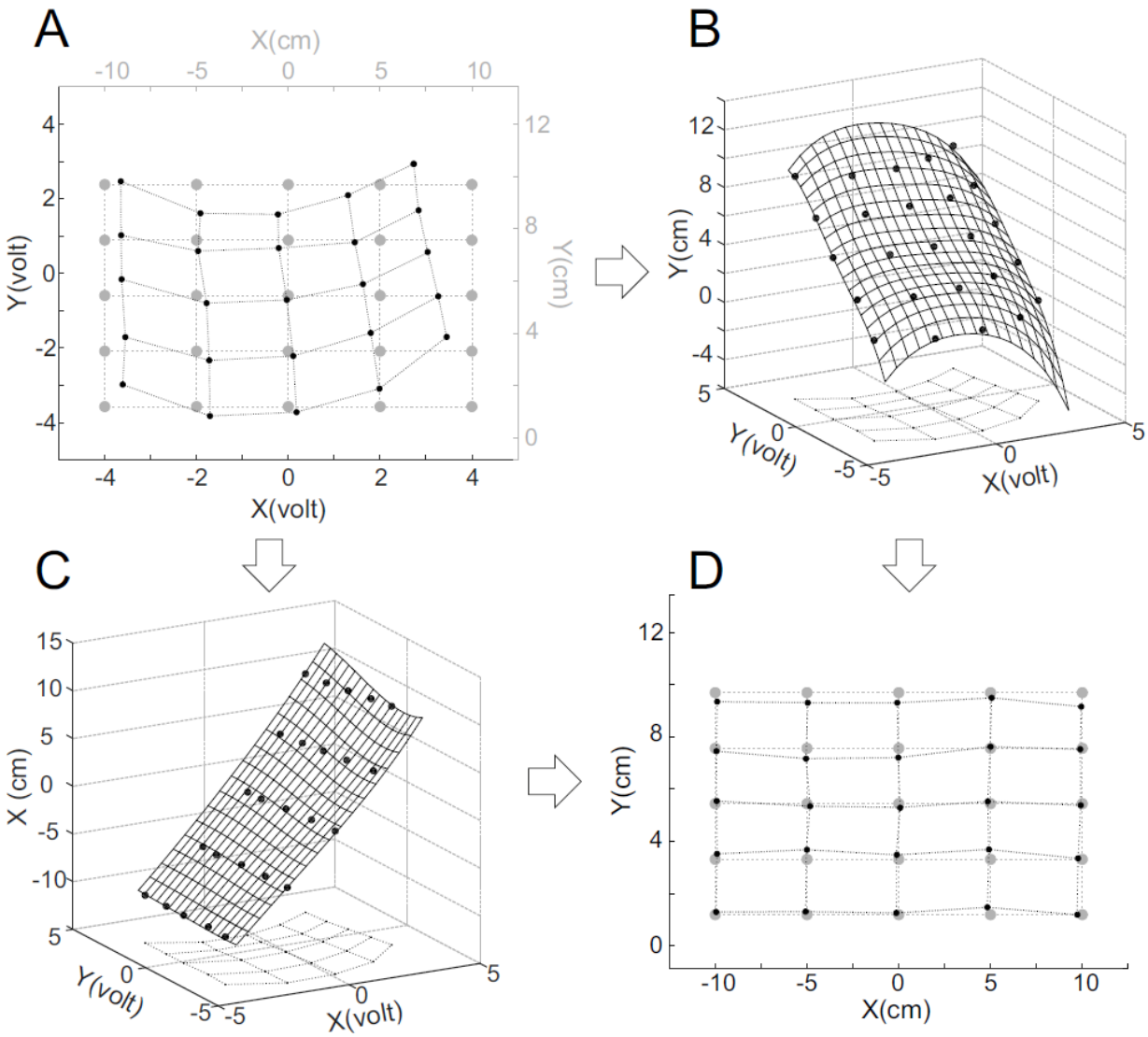

Figure 2.5: Eye calibration. (A) Average raw eye position voltages (black dots) at 25 target locations (gray dots). (B) 3D representation of the target position along the Y axis of the screen as a function of recorded voltages. The 3D grid is the surface obtained by a bi-harmonic spline interpolation. (C) The same as (B) for the X axis of the screen. (D) Gaze position on the screen (black dots) reconstructed for fixations on 25 target locations (gray dots).

2.2.4 Task Participants

Before applying our novel eye calibration methods to monkeys and humans, they were first tested and validated using a custom-made servo-controlled artificial eye. This robot eye was animated by two small brushless motors, via a wireless microcontroller (EZ-B v4 Wi-Fi Robot Controller, EZ-Robot; www.ez-robot.com), producing independent horizontal and vertical movements. It was held by a support that fitted in the monkey chair and was secured to it to prevent any movement. The design of the robot included an artificial pupil that could

be tracked consisting in a micro-camera in the middle of a white plastic disc, with the lens mimicking a pupil (Figure 2.6D & 2.6E). This allowed the EyeLink to provide an eye position signal wherever the robot was looking at within the work area. The robot eye was dimensioned to make sure its eye was at the same location as the monkey's eye to allow for conservation of hardware settings. Since the camera and the plastic disk were not reflective, we could not track the corneal reflection with this robot. However, its position stability allowed us to switch from the EyeLink "pupil + corneal" to "pupil-only" tracking mode. The micro-camera transmitted in real-time a wireless video signal at 20 frames per second and in a 640x480 pixels resolution to a nearby laptop, which allowed the operator to adjust the camera position and align it with the calibration targets (Figure 2.6D, inset).

A first version of the robot eye was created to test different spatial configurations of the EyeLink camera and the light source in the setup and to measure its impact on the signal (Figure 2.6A & 2.6B). Two human participants (authors MdH and FB) were tested in the human KINARM system with the EyeLink II option (Figure 2.6C). They were seated with their right arm in the exoskeleton, and their head was stabilized by means of a headrest and chinrest.

One male rhesus monkey (Macaca mulatta) was trained in a sequential pointing task; monkey Y (6 years, 8.5kg). A second male rhesus monkey (R; 7 years, 12.5kg) and a third female rhesus monkey (E; 7 years, 6.5kg) were also trained to fulfill rudimentary pointing behavior, and are currently still in training. All data, behavior and findings relating to monkey performances in the following sections come from monkey Y. All animal procedures were approved by the local ethical committee (authorization A3/10/12) and conformed to the European and French government regulations. Monkey Y was trained to sit in a modular chair ("Arms Free" monkey chair, BKIN Technologies) by sliding his nylon collar (Primate Products) into a slightly angled neck plate, and to accept left arm restraining with an L-shaped armlet. The right arm was placed in the exoskeleton. To reduce large head-movements, the monkey was trained to position his head within a custom made plastic mask (Figure 2.6F). Monkey Y was naïve to behavioral training procedures prior to this project and did not yet receive any form of electrophysiological implantation, and was kept in a colony of 3-4 monkeys in a modular housing pen (Allentown), with access to a central play area.

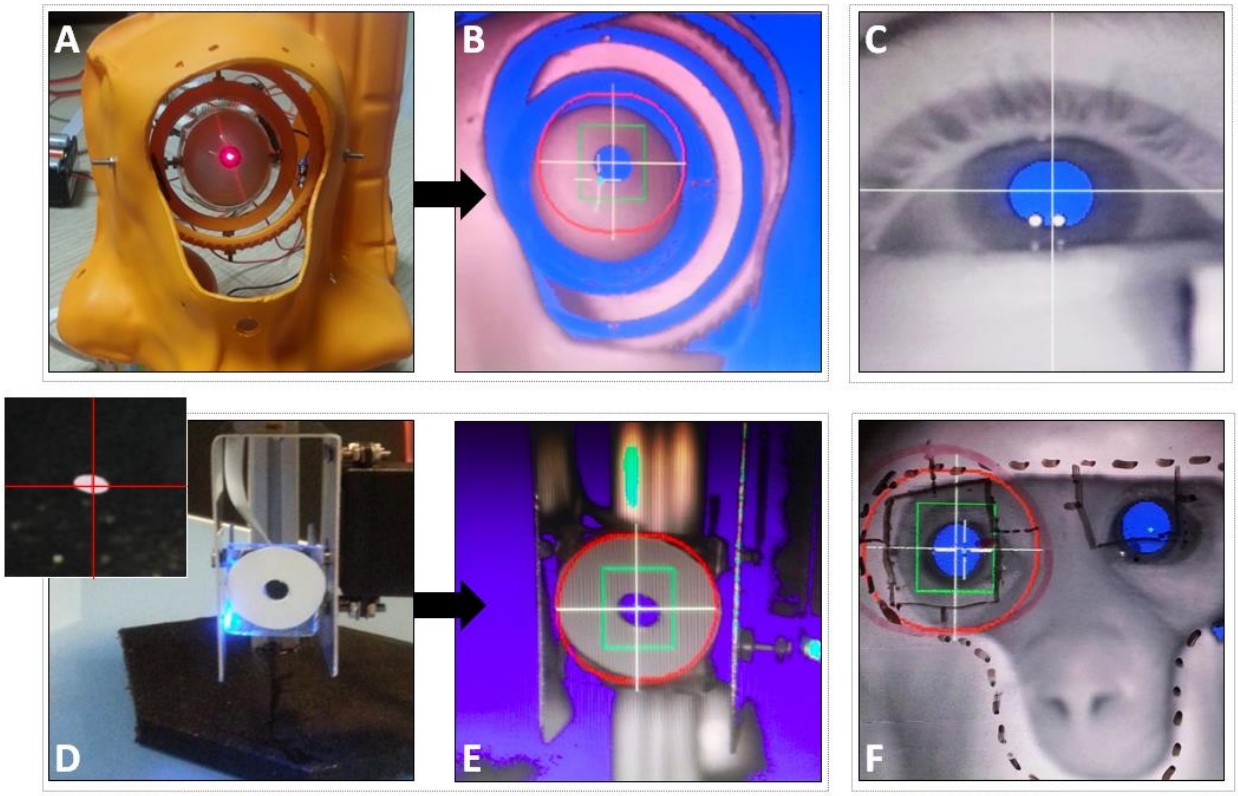

Figure 2.6: Eye calibration robots and EyeLink feedback. A) The robot eye used for illuminator placement testing consists of a laser mounted on a 2-axis (XY) robotized frame. D) The robot eye used for calibration consists of a camera mounted on a 2-axis (XY) robotized frame. The inset shows the feedback used by the operator to fixate on the targets. EyeLink tracking video output is shown of robot eye 1 (B), robot eye 2 (E), human eye (C), and monkey eye (F).

2.3 Results

We designed an integrated recording and interacting system that expresses the hand and the eye positions in the same reference frame, to be used in humans and monkeys. To assess the limits of our eye calibration method and the reliability of both setups we made several tests using a robot eye in the monkey setup, and a human participant in the human setup. Each test started with a calibration of the eye position, followed by multiple validation experiments where the participants were asked to fixate at individual targets. For each trial, eye position was computed as the average of the samples recorded during 100ms (100 sample points). To compare the performance of our setup with the industry standard for eye tracking, we determined the noise in the gaze position estimation using the methods employed by SR-research or Tobii Technology, for example, and described extensively in Holmqvist et al. (2011). This measure was achieved by calculating the root mean square (RMS) of the inter-sample distances during a single fixation trial. In our system, the noise was 0.065cm in the human setup and 0.002cm in the monkey setup. These values are comparable to the eye-

tracking system standards. Despite their capacity to report a recording system noise level, these measures are far less interesting when it comes to evaluate the performance of our setup in the context of experiments.

In order to describe i) the distance between the corrected gaze position and the actual target position, and ii) the reproducibility of the measures, we computed two non-parametric statistical indices: *accuracy* and *precision*. The choice of non-parametric statistics was made for conservative reasons and because the normality of the data was not proven.

Accuracy is the median fixation error, computed over the distribution of the Euclidean distances between the eye positions and the target center position across trials. This corresponds to a standard measure reported by eye tracker developers. *Precision* is the inter-quartile-interval of the eye position distribution across trials. This measure shows the variability of eye positions during an experiment. Both measures are independent from each other, which can lead to accurate yet imprecise eye positions, or inaccurate yet precise eye positions. To express these measures in the context of the setup VR display, we will indicate their values in cm on the screen. However, the relationship between the eye position and the gaze will be influenced by the target position along the X and Y axes. Therefore we will also express the accuracy and precision in degrees of visual angle. In this case, gaze positions and target positions on the screen were used as vector coordinates in a 3 dimensional space centered at the eye position. Precision in degrees of visual angle encompasses the X and Y distance and is therefore expressed as a single value.

2.3.1 Eye Calibration

We used 25 targets (hereafter referred to as calibration targets) located on a 5 x 5 grid whose dimension was adapted to the size of the participant's work area. The work area was 20 x 9 cm in the monkey setup and 28 x 28 cm in the human setup; this difference was mainly due to the longer arm-reach of human participants. All tests were done in darkened rooms, with only visual stimuli on the VR display visible. Human and monkey participants were required to fixate at each calibration target. With the robot eye, the operator manipulated the X and Y axis servomechanisms to find the best possible alignment between the micro-camera crosshair (i.e. fovea) and the target centers (Figure 2.6A, inset). Once the fixation was correct, the eye position was sampled. The average voltages recorded at the different calibration targets were used to deduce the signal non-linearity. The estimated parameters of the corrective non-linear

functions were subsequently calculated by our custom calibration GUI, inserted into the control software of the interface computer (Dexterit-E, BKIN Technologies), and used by the real-time program for online correction of the eye position during the validation tests.

2.3.2 Eye Validation

In the first two validation tests, we recorded the computed positions of the gaze in the VR display when participants were fixating at multiple targets (hereafter referred to as validation targets). In the first test, the validation targets were at the same location as the calibration target. In the second validation test, the targets were randomly distributed across the entire calibrated area to assess the model generalization to the entire work area. In the third validation test, three targets were fixated multiple times to assess local accuracy and precision. We then tested how well drift correction was able to compensate for unstable head position, and finally challenged the output of the calibration method during a sequential pointing task with human and monkey participants.

2.3.2.1 Accuracy & Precision

The goal of the first test was to evaluate the capacity of the model to accurately compute the gaze position from the EyeLink eye position signal. Black dots in the inset of Figure 2.7A show the average position recorded with the robot camera eye during fixations of each the 25 validation targets in 3 trials (Figure 2.7A, inset, gray dots). The relationship between target position and gaze position appears linear, suggesting that our corrective functions compensated for the setup non-linearities. To quantify the compensation, we aligned the gaze positions made at different target locations to a single target position by subtracting the target coordinates from the gaze coordinates. The resulting distribution of gaze positions presented in Figure 2.7A was centered on the target, with a larger variability on the Y axis than on the X axis. For the robot eye, the measured accuracy was 0.97 degrees (0.27 cm) with a precision of 0.49 degrees (X axis: 0.11 cm. Y axis: 0.19 cm). Similar results were obtained with a human participant: accuracy was 0.88 degrees (0.81 cm), with a precision of 0.43 degrees (X axis: 0.31 cm, Y axis: 0.59 cm). The reconstructed gaze positions were either inside or within close proximity of the actual target. The measures obtained with robot and human fell in the same range but differed in one important way. The robot showed better accuracy and precision in cm, but lower performances in degrees than the human participant.

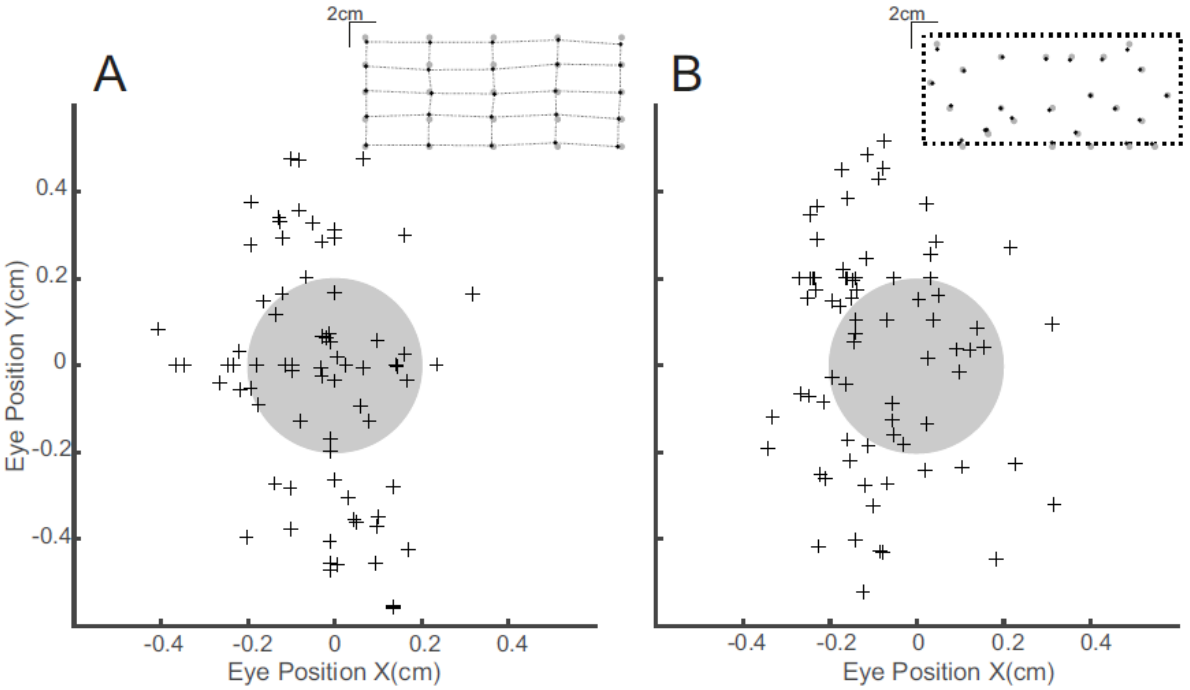

Figure 2.7: Eye correction validation. In (A) all eye positions (crosses) relative to the center of a target during the fixation period are shown, sampled across 25 different locations. The inset shows the gaze position on the display (black dots) together with the targets used to test the correction validity (gray dots). This is repeated in (B), but with the 25 locations being randomly distributed within the calibrated area (dotted rectangle).

This can be explained by the larger work area in the human setup, especially along the Y axis. In a second test, validation targets were randomly located in the work area to evaluate the model generalization capacity. Figure 2.7B and its inset represent the recordings in the same format and with the same symbol code as Figure 2.7A. As in the previous test, the reconstructed gaze positions were all close to or within the target limits. For the robot eye, this yielded an accuracy of 0.99 degrees (0.26 cm) and a precision of 0.63 degrees (X axis: 0.10 cm. Y axis: 0.16 cm). For the human participant, this yielded an accuracy of 0.72 degrees (0.71 cm) and a precision of 0.32 degrees (X axis: 0.28 cm. Y axis: 0.57 cm). For human and robot, these values were similar to the ones obtained in the first test, indicating that the model generalized accurately to the entire work area.

2.3.2.2 Signal Variability

In the first two tests, we observed, even in ideal conditions of stability, a small but systematic variability of the robot fixation position (Figure 2.7A & 2.7B). The origin of this variability lay in the raw signal inconsistency, but its amplitude could be altered by the eye correction model. To estimate the respective contributions of these two possible sources of the overall variability, we compared the raw eye tracker voltage signal with the reconstructed gaze

position on the screen. In detail, the inputs (raw eye tracker voltage) and outputs (reconstructed gaze position on the screen) of the model were compared at three validation targets located at three different positions within the work area. Targets were presented 75 times in the same sequence, requiring a manipulation of the two servo-controllers of the artificial eye horizontally and vertically between each fixation.

Figure 2.8 shows the continuous recording of the input (raw voltage, Figure 2.8A) and output (eye position, Figure 2.8B) as gray traces over the entire session for Target 1, indicated by the arrow in the insets. The input and output traces show a similar pattern of parallel paths, which cluster in bands. This was a consequence of the minimal discrete positions of the servo-controllers, leading to discrete positions of the robot camera. This was responsible of the clustering of the fixations (represented by the crosses) selected by the operator, and strongly indicated the source of the variability in the input signal.

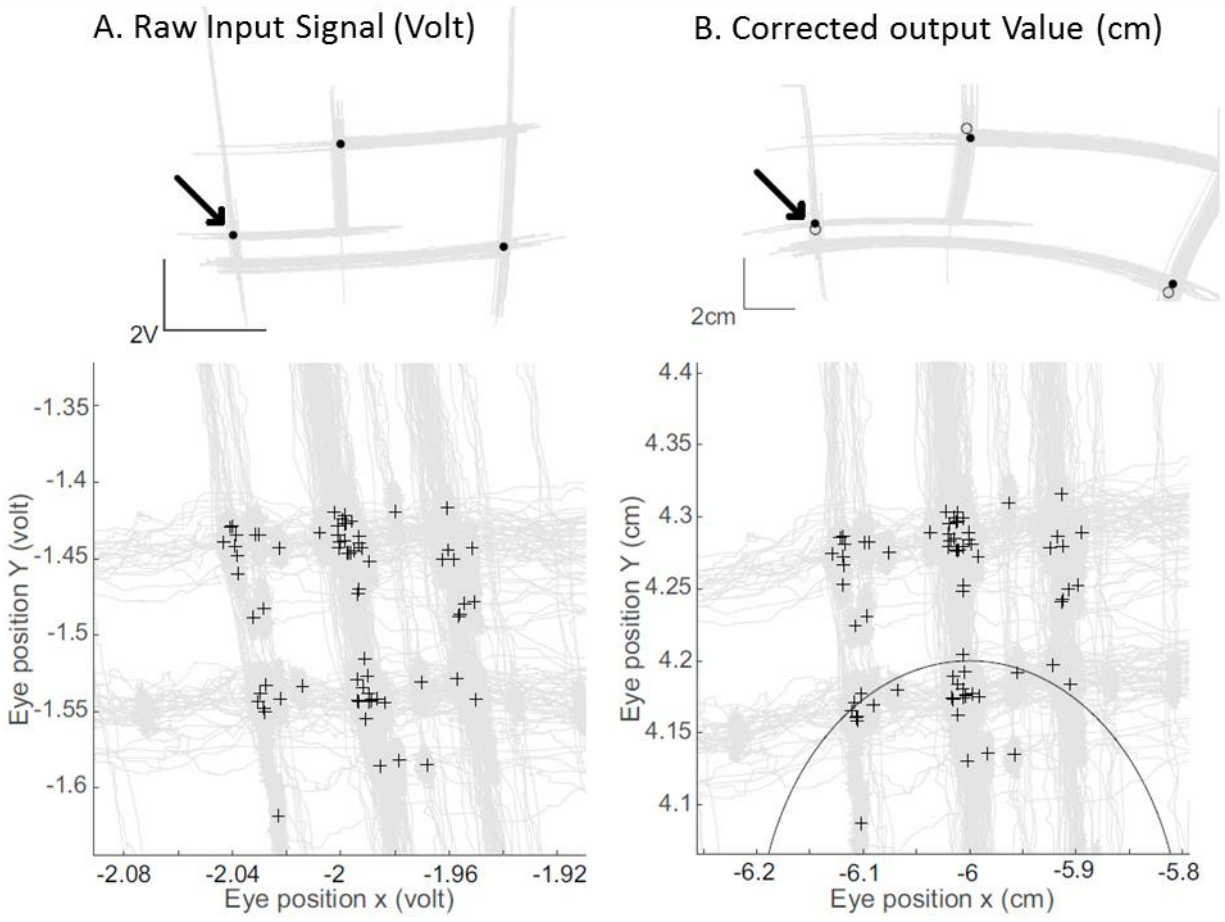

Figure 2.8: Clustered eye position samples. The gray traces are the robot eye movements in XY space, whereas the crosses are eye position samples taken by the operator during fixation on the target (indicated by an arrow in the inset). The traces and eye position in (A) are the raw signals, before the model correction. The traces and eye position in (B) are the corrected signals, after the model correction. The circle shows the target edge.

However, it was necessary to check if our model did not introduce more variability into the signal. A Wilcoxon signed-rank test was used to compare the normalized raw eye tracker voltages and the normalized reconstructed gaze positions on the screen. The results showed no significant difference between the two distributions on Target 1 (X: $p = 0.35$; Y: $p = 0.27$; $n = 74$; 1 outlier was removed due to an incorrect fixation), indicating that variability observed after implementation of the corrective model was already present in the input signal. Similar results were obtained for Target 2 (X: $p = 0.78$; Y: $p = 0.91$; $n = 75$) and Target 3 (X: $p = 0.18$; Y: $p = 0.99$; $n = 70$; 5 outliers were removed because fixations were outside of the calibrated area). Therefore, the corrective process in our model did not introduce any supplementary variability in the signal. However, the model did not compensate for the input variability. As a consequence, the quality and the stability of the input signal are essential for the accurate and precise estimation of gaze location.

2.3.2.3 Head stabilization

We have shown that the eye positions were aligned to the 25 reference points under stable conditions, with both the robot eye and a human participant (Figure 2.7). However, since our corrective model consisted of the application of a non-linear function applied to the raw eye tracker voltage, we showed that the output values of the model varied as function of the input signal, being different for the same target from trial to trial. This is particularly important in situations where the head is not fixed with a stable head-restrain system. Indeed, a drift in the head position will lead to a change in the participant's eye position in the eye tracker image, causing a global offset in the voltage signal. This offset may cause errors in the reconstruction of the gaze position, through the alteration of the spatial relationship between the signal non-linearity and the correction parameters. A solution to this problem is the use of a drift correction, which will correct for the offset of the raw eye tracker voltage by defining and applying a compensatory shift. With the constraint that the selected solution must be simple and quick enough to minimize interruption of the actual task, we developed a drift correction module that could be easily integrated into human or monkey experiments and run between trials.

To test the efficacy of our drift correction, we compared the reconstructed gaze positions of robot and human participant's during the fixation periods in three consecutive tasks. For each task, the participant had to fixate 25 validation targets located at the same coordinates as the calibration targets. In the first task the participant had to actively maintain the head in a fixed

position. (Validation: Figure 2.9A & 2.9B, square symbols). The participant subsequently changed head position (for the robot, its support was moved before again recording the gaze positions during the second task), and then repeated the same eye fixations (drift: Figure 2.9A & 2.9B, inset). Before the third task the participant and robot had first to fixate on a target located at the same coordinates and then the center of the calibration grid. The calibration model calculated the difference between the voltage recorded during this fixation and the one recorded for the central target during calibration.

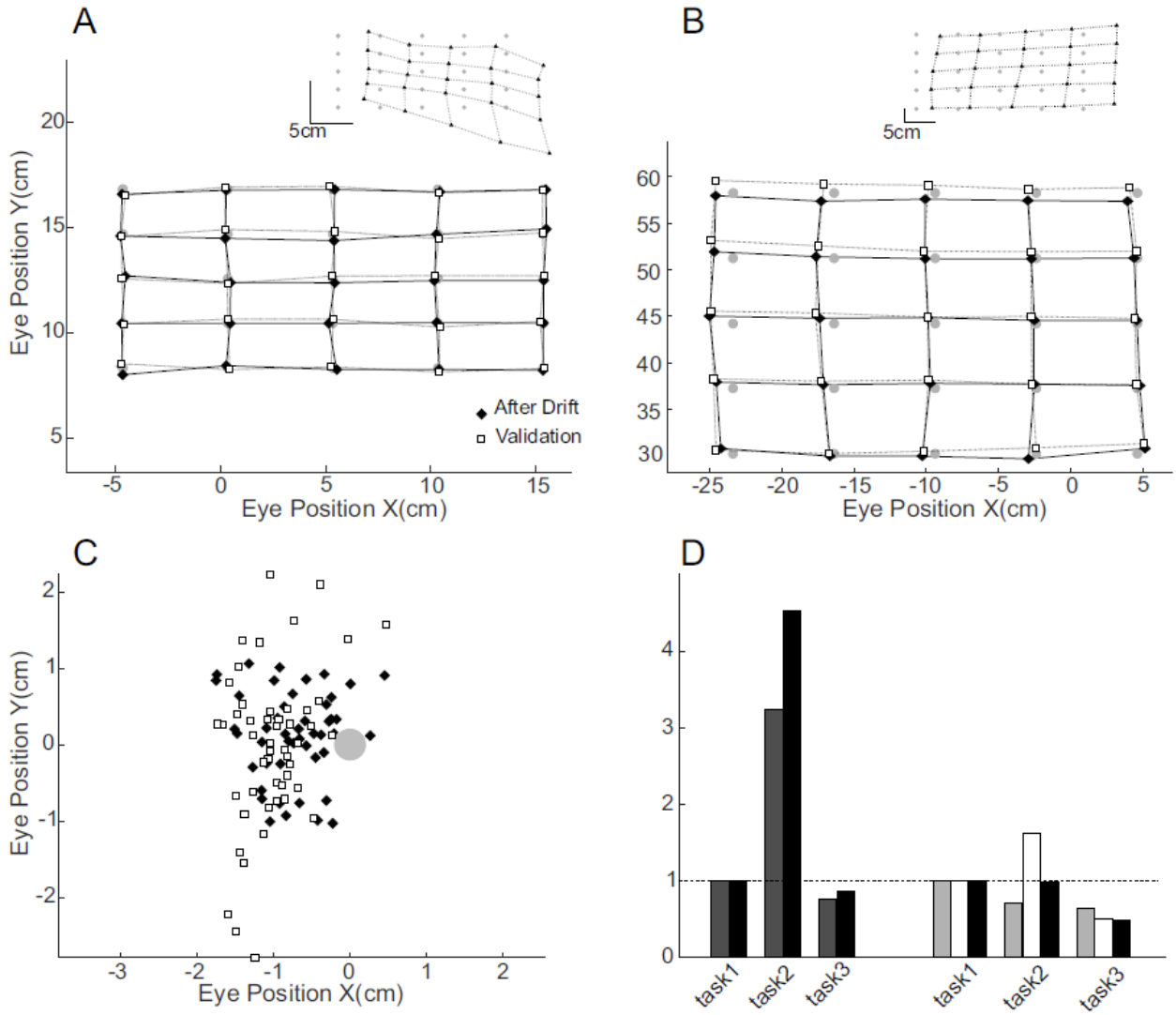

Figure 2.9: Drift correction. Positions of robot eye (A) and human eye (B) before head movement (open squares) and after compensatory drift correction (filled diamonds), gray circles indicate target positions; insets: Eye position after head movement. C) Human fixation positions aligned to the target (gray dot) with same symbols as in A and B. D) Left: ratio between values for the different tasks and task1 for accuracy in cm (dark gray) and in degrees (black). Right: the same for precision ratio in cm along X axis (light gray), in cm along Y axis (white) and degrees (black).

This difference was used as an offset value to shift the voltage input back to the range of voltages recorded during calibration (drift correction: Figure 2.9A & 2.9B, diamond symbols). We subsequently compared the accuracy and precision of the distribution of gaze positions recorded in task 1 (before drift, Figure 2.9C, square symbols), task 2 (after head movement) and task 3 (drift corrected, Figure 2.9C, diamond symbols) to establish whether the head movement in task 2 was fully compensated. To assess the distributions of the spatial location of the eye position, we also compared their medians. The three measures are shown in Figure 2.9D and are expressed as a fraction of the corresponding measure in task 1.

2.4 Discussion

The primary goal of this work was to develop a system for use in humans and monkeys to provide rigorous hand and eye movement control through non-invasive means with a high spatial and temporal resolution. To fulfill this goal, we integrated an eye-tracking system and a hand-tracking system together into two unified setups. These setups realize a common processing of the data stream coming from different systems and ensure the synchronization of the signals. They conserve all features available for hand movement control and make them applicable also to the eye signal. With the choice of the KINARM and the Simulink model as the core system of our setups, we were also able to implement most of the functionalities required for online analysis of eye movements (e.g. saccade or blink detection). Moreover, the setups provide an on-line conversion of the eye positions into the same reference frame as the hand and the task environment. This conversion extends the reactivity of the setup to eye and hand movements, leading to a strong control over eye-hand coordination in the context of the task. For example, in the perspective of future studies, we will be able to observe the impact of perturbations, applied at many levels, from visual stimuli to movement execution, on eye-hand coordination.

In this chapter, we presented the results of multiple tests designed to estimate the quality of our reconstructed eye position signal. The recordings made in an ideal situation with an artificial eye or with a human subject showed that our conversion system is very efficient in terms of accuracy and precision. Indeed, our results are comparable with the native accuracy and precision given for commercially available eye-tracking solutions in humans (specifications at www.bkintechnologies.com/bkin-products/kinarm-exoskeleton-lab).

However, our results also indicate that the correction model is not able to compensate for fluctuations in the input signal, for example in the case of large head movements. A predictive model could be more efficient to compensate automatically for changes in the signal, but would limit the possibilities for unrestrained eye movements. In the recordings we made during a reaching task, we showed that arm movements did not perturb the signal stability within a trial. Consequently, the periodic drift assessment and correction should be efficient enough to compensate for head movement in normal recording conditions in humans. This drift correction, together with the flexibility of the non-linearity compensation model, allows for the use of a mask rather than a head post. With monkeys, the use of a mask as a non-invasive solution to stabilize the head was reported sporadically over the last decade (Fairhall et al. 2006; Slater et al. 2016). These solutions present many advantages over the classical implantation of a head post, the first being the reduction of surgical risks. In the context of multi-electrodes array implantation, the absence of a head post saves space on the animal skull for connectors.

With the ability to record eye and hand behavior synchronously with massive parallel electrophysiological data, our setup appears to be an efficient tool to study the neuronal mechanisms underlying standard and non-standard visuomotor mapping (Wise et al. 1996; Battaglia-Mayer et al. 2001). The efficient on-line treatment provided by the setup and its flexibility in terms of input/output connectivity makes it a serious candidate to link with brain machine interface. Furthermore, the development of this setup for both human and monkey opens promising perspectives for translational approaches connecting monkey models and multiple fields of human research including study on eye-hand coordination development, clinical or aging research.

3 TASK DEVELOPMENT & MONKEY TRAINING

3.1 Introduction

Prior to the setup development for human participants, all techniques and solutions presented in chapter 2 were first tested during the development of the monkey setup. This prototyping stage occurred in parallel to the task development and the training of monkey Y (Figure 3.1). Therefore, developments and findings presented in this chapter will only concern the monkey setup and monkey Y, unless otherwise stated. In this chapter I present a quick overview of the SimuLink and StateFlow task program development which run the experiment, and outline how data flow into a single time-synchronized format, together with a reference to experimental conditions as metadata. Access to this metadata will allow researchers to revisit data easily, and greatly aids collaboration and the fluid exchange of data between laboratories. Our data acquisition (DAQ) practices have therefore followed a workflow favoring a common representation of the core data, compatible with the data format "Neo" (Garcia et al. 2014) and the "open metaData Markup Language" (odML) for collecting and exchanging metadata (Grewe et al. 2011). In particular, the coding logic behind experimental conditions and behavioral/task-related events follows good metadata practices presented in Zehl et al. (2016). Additionally, I will show the features of two custom Matlab-based tools developed by Frédéric V. Barthélemy that allows the user to transform the raw eye signal into a corrected signal and to use it during a task (see chapter 2.2.3), and an eye/hand event marking tool which can be used to index data for off-line analysis of saccade onset/offset, hand movement onset/offset, and other events related to eye-hand behavior. I will subsequently describe monkey Y's behavioral performance through progressively difficult training sessions in the chair, with the exoskeleton, and novel movement restriction measures, culminating in the development of a final sequential pointing task protocol with the eye calibration/drift correction component used in both monkey and human setups. This is followed by spatiotemporal analyses of the eye-hand behavior of the monkey in this task. The results of these data are discussed in conjunction with the literature featuring specific behavioral aspects, concerning in particular the notion of 'gaze anchoring'. The final section is dedicated to describe the choice of chronic implantation sites of multiple MEAs on the cortical surface areas of monkey Y, with a discussion of the surgical procedures and outcome.

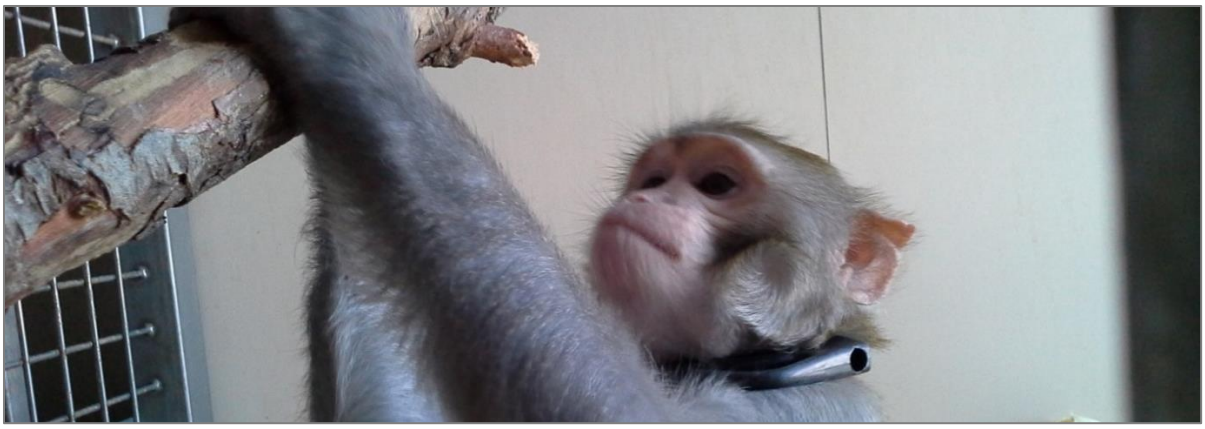

Figure 3.1: **Rhesus Monkey Y (Macaca mulatta).**

3.2 Experimental Task Programming

As described in chapter 2 we use the task development environment of BKIN Technology's KINARM exoskeleton lab. This includes their proprietary control software, Dexterit-E, which communicates with the real-time computer running xPC target (MathWorks). Dexterit-E allows the user to control features of a task program, such as reward time, target onset, arm-movement perturbations, visual feedback, and gives the user direct insight on movement behavior and performance during a task. This task behavior comes from a Simulink model which is uploaded to the real-time computer via Dexterit-E and controls all the hardware and software components of the experimental environment. This model is created in a graphical programming environment that uses a block diagram tool as a primary interface, with block libraries from MathWorks, BKIN Technology, and built in-house. These blocks predominantly control visual feedback output, treatment of input/output of digital/analog signals, control of motor torque of the KINARM exoskeleton, and other hardware features. These blocks are event-driven by a Stateflow chart, which uses parallel and sequential decision logic based on state machines and flow charts to control task behavior and parameters. A significant portion of my thesis was spent building model attributes that allow us for custom block functions, alterations of existing block libraries, and event/signal processing within Embedded Matlab, which is a subset of the MATLAB language used by Simulink for efficient code generation, but with some limitations (e.g. excluding command/function duality and dynamic variables). In the following section I will outline the basic structure of a Simulink model, featuring block libraries and a Stateflow chart, as well as our own signal processing transformation code and other customizations (for a detailed use of graphical block programming and modeling in Simulink, please visit the MathWorks website, www.mathworks.com).

3.2.1 Model Development & Task Programs

Before we can control combinatorial processes of the setup, we must first identify all components that provide input/output signals, and couple them to appropriate driver blocks. This includes the proprietary block library for Dexterit-E which is essential for the correct functioning and communication between the computer running Dexterit-E software and the real-time computer. This library controls several DAQ cards that 1) drive KINARM exoskeleton motors and receive down-sampled signals at 1 kHz, 2) receive raw eye signals of eye positions (in voltage values) at 1 kHz via the analog output card of the EyeLink HOST PC, and 3) output behavioral, eye/hand kinematic, task-related, and digital event data to Cerebus Multi-Channel DAQ system. Data output is also sent back to the Dexterit-E control computer, for task performance feedback on the user screen and behavioral/task data storage in a motion analysis C3D file format (Visual 3D) upon task completion in parallel to Cerebus DAQ data storage (for details of cards and hardware connectivity, see Figure 2.3).

The control of these DAQ cards, output/input signals from various sources, visual feedback communication to the VR display, eye signal transformation, and data logging are visualized in Figure 3.2 with various blocks (color) and a Stateflow Chart block (pale) that controls Dexterit-E interface and task behavior/protocol/parameters. This model is compiled and uploaded to the xPC Target platform on the real-time computer by Dexterit-E, ready for use with a participant. The blocks in Figure 3.2 have a variety of functions and attributes, with brown blocks controlling aspects of the Dexterit-E interface and the visual environment of the VR display, including the eye/hand feedback on the screen (yellow box). The gray blocks control different conditional load values affecting the motor torque of the exoskeleton, as well as receiving hand position feedback relative to target. The green box contains the 'Task Wide Parameter' box, a table with task parameter definitions accessible and alterable by the user in the Dexterit-E environment. This box is external and therefore not connected with arrows within the Simulink model, which is also the case with the blue 'Eye Signal Transform' box. These user-defined values are then introduced as attributes to the Stateflow chart via the orange block, affecting task behavior according to the user's wishes. A small piece of code of the Stateflow chart is enlarged at the bottom to show how a trial is initiated outside the 'MainTrial' chart after a 50ms delay (on the left, indicated as *100 e_clk* because the model has a clock speed of 2 kHz on the real-time computer in order to process 1 kHz signals).

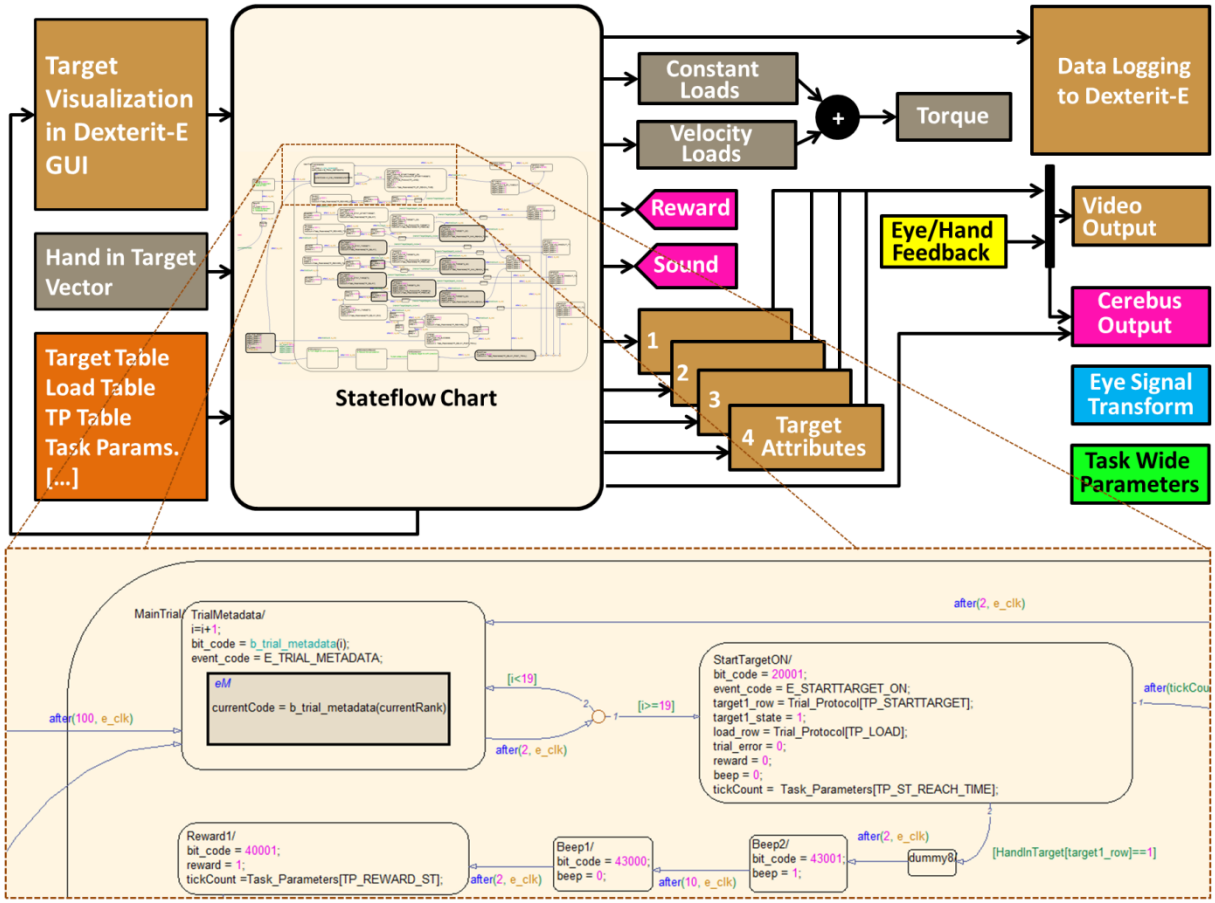

Figure 3.2: Example of a Simulink Model with block programming and a central Stateflow chart.

Inside the 'TrialMetaData' chart metadata of the upcoming trial is collected before the trial starts, and sent in 16-bit code to the digital output card. After 19 metadata values are sent to an external DAQ system, the trial starts with the 'StartTargetON' chart, which simultaneously outputs a 16-bit identifier (bit_code = 2001) externally and an event code (E_STARTTARGET_ON) to Dexterit-E, selects the trial protocol (TP_STARTTARGET = location, color, size) and the state of the target (0 = OFF, 1 = ON), drives external devices, such as reward and beep (0 = OFF, 1 = ON), and defines the time limit for the hand to reach the target (TP_ST_REACH_TIME). If the hand reaches the target on time, the state flows towards the lower charts, giving an audio feedback and a reward (depending on training). If the hand does not reach the target in time, the event is logged as a failure, and the trial restarts.

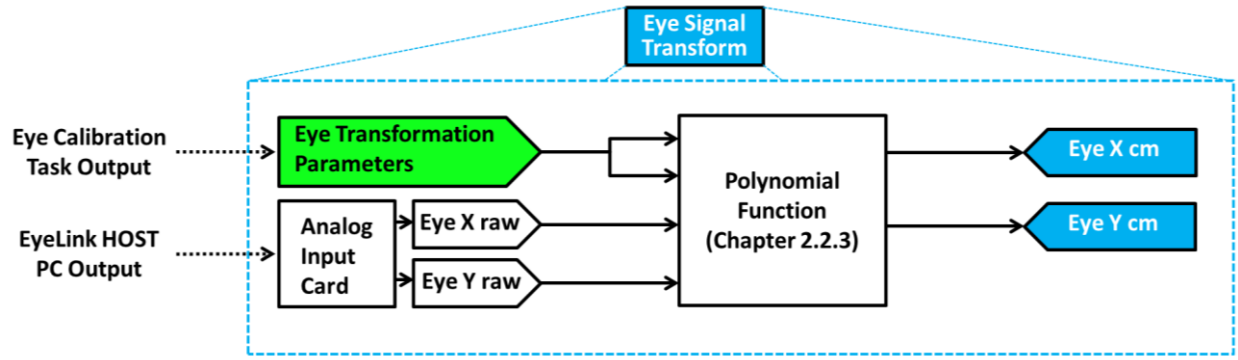

Figure 3.3: Custom block function of raw eye signal transformation.

In the 'Eye Signal Transform' block parameters from the eye calibration task are automatically placed into the task wide parameters block visualized in Figure 3.2. The parameters are used by the polynomial function to transform the raw eye signals to the latest available calibration data Figure 3.3. This eye signal is subsequently used as eye feedback on the Dexterit-E display, to give the user a hand and eye position visualization in the same target reference frame (see Figure 2.2 in chapter 2.2.1). In parallel, it is sent to the external DAQ system Cerebus, alongside KINARM and task-related analog/digital outputs.

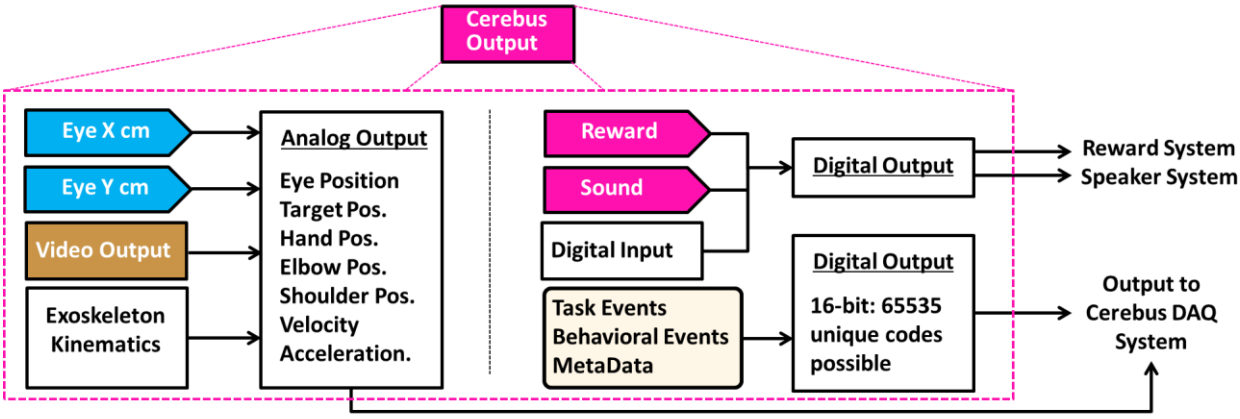

Figure 3.4: Custom block function for analog and digital signal processing.

All analog and digital signals are processed in order to output them to the Cerebus DAQ system, as seen in Figure 3.4. It must be noted that the Cerebus system is for the monkey setup only, and not used in the human setup. The human setup stores the same output signals from the KINARM and EyeLink locally as a C3D file, with a synchronization output to the EEG/EMG recording systems for off-line temporal alignment of different formats.

3.2.2 Event Coding & MetaData Output

The Vision-for-Action project is a collaboration between two research groups in different countries, the experimental Cognitive Motor Control (CoMCo) group at the INT (Institut de Neurosciences de la Timone) of the CNRS and Aix-Marseille University in Marseille, France, and the theoretical Statistical Neuroscience (SN) group at the INM-6 (Institute for Neuroscience and Medicine 6, Computational and Systems Neuroscience) of the Jülich Research Centre in Germany. A common hindrance scientists encounter when sharing data between institutes with different workflow approaches is the extent of proper and thorough documentation of experimental conditions, such that the circumstances that led to data acquisition is understandable and uniform between both research groups. This is important so that data may be revisited and (re-)analyzed at a later stage, without relying on the expertise of the researcher(s) who conducted the experiments (a comprehensive case describing the importance of data and metadata management is made in the PhD dissertation of Lyuba Zehl, April 2017). We have therefore endeavored to automatize the output of task parameters and experimental conditions as metadata alongside data. Every state change in the Stateflow chart, from hand position inside a target to the audio feedback that accompanies it, has a unique 16-bit identifier. This means every behavioral and task-related event that occurs is digitally coded alongside analog recordings of eye/hand/target position in time. Each session starts with a stream of metadata being sent from the KINARM system to the Cerebus, and contains basic information about the software versions, task wide parameters, task protocol definitions, color/size/shape of targets and feedbacks, which arm is used and load parameters for the exoskeleton. Table 3.1 provides an example of how event coding is used in our task programs to output behavioral/task events and metadata information for each session and trial. Simple event occurrences are single coded or ON/OFF coded, whereas those with variable parameters are flanked by START/END codes, with a 16-bit code to indicate value of parameters. Each category is divided by the first number (1xxxx, etc.), and within these categories the ON/OFF or START/END parameter is coded with a 1 or 0 at the end, respectively.

This leaves 999 possible unique identifiers (553 for 6xxxx) for each category, making it robust for future additions. Once coded, these events should remain unaltered over time to benefit from experimental continuity, though additional codes can be added of course. With this we output the maximum possible channels relating to eye/hand/target behavior (16 analog channels), and consistent task/behavior/metadata event codes (16-bit digital signal) to the Cerebus DAQ system, which are processed and stored locally in a C3D file format and

externally in NEV and NSx Blackrock Microsystems data files. In parallel to this behavioral data, the massively parallel electrophysiological recordings from chronically implanted MEAs of the monkey are stored in the same NEV and NSx files.

Table 3.1: Example of digital event coding definitions.

Experiment MetaData	*Trial MetaData*	*Screen Related*	*Exoskeleton Related*	*Other*	*Behavior Related*	*Error*
0xxxx	**1xxxx**	**2xxxx**	**3xxxx**	**4xxxx**	**5xxxx**	**6xxxx**
00011/00010	**10011/10010**	**20001/20000**	**30001/30000**	**40001/40000**	**50001/50000**	**60001**
Session Start/End	Trial Start/End	Start Target	Load	Reward	Hand	Time-Out
00101/00100	**00101/00100**	ON/OFF	ON/OFF	ON/OFF	IN/OUT	**61001**
Metadata Start/End	Metadata Start/End	**20011/20010**	**31001/31000**	**42001/42000**	**51001/51000**	Hand-Out
01011	**11001/11000**	Target 1 ON/OFF	Perturb	Manual	Eye IN/OUT	**62011**
Target Features GO	Block No. ON/OFF	**20021/20020**	ON/OFF	ON/OFF	**53001**	Signal
00201	**11011/11010**	Target 2 ON/OFF	**32001/32000**	**43001/43000**	Hand	Loss
Feedback Color	Trial in Block	**20031/20030**	Velocity	Beep ON/OFF	Velocity	**63001**
00301	ON/OFF	Target 3 ON/OFF	ON/OFF	**46001**	**54001**	Drift
Load Table GO	**11021/11020**	**21001/21000**		Abort Button	Eye Velocity	
00501	Block in Set ON/OFF	Visual Cue ON/OFF		**47001**	**55002**	
Task Protocol GO	**11031/11030**	**22001/22000**		Accept Button	Saccade	
[…]	Trial Number	Target Move	[…]		PEAK	
	ON/OFF	ON/OFF			**56001**	[…]
	[…]	[…]		[…]	Blink	
					[…]	

3.2.3 Head Fixation & Eye Calibration Tool

With the hardware connectivity between the systems in place (Figure 2.3 in chapter 2.2.2), and the correct dataflow and storage functions available (Figure 3.2), the monkey setup was ready to run user-defined visually guided motor tasks. Before any training or recording session, we needed to calibrate both eye and hand movement systems such that both effectors are correctly aligned in space with the visual feedback and targets. For the KINARM exoskeleton this was done via Dexterit-E's own calibration routine, but for the eye tracker we had to create a Simulink model to output transformation parameters. An important complication had to be overcome with this technique: the variable eye position placement between sessions and a non-surgical method to compensate for head movements (briefly mentioned in chapter 2.3.2.3). In order to implant multiple MEAs into the visual and motor cortical tissue of the monkey, two connector pedestals would need to be fixed to the cranium

in order to connect the MEAs via specific head stages to the Cerebus DAQ system. These would populate the occipital and frontal skull, leaving a limited amount of space left for a surgical head fixation. These fixations are generally quite large, complicating the placement of connectors and MEAs. Additionally, having both fixation and MEAs implanted would require multiple surgeries, which would bring significant health risks to the monkey. To promote refinement for the benefit of animal welfare (the 3 R's, i.e. Replacement-Reduction-Refinement, NC3Rs, https://www.nc3rs.org.uk; European Directive 2010/63/EU), the decision was therefore made early to make a sincere attempt to include a non-surgical head fixation, a mask, to restrict head movements, together with some restrictions which would limit the movement of the left arm and the legs (Figure 3.5). Once habituated to the restrictions, the monkey engaged in an eye calibration task, performing multiple fixations, which were sampled and corrected by the user with our custom eye calibration tool (see chapter 2.2.3). This tool visualizes data from the eye calibration task and allows the user to flag and remove outliers. The remaining fixation points are then averaged per target, and used to match the average position measured in voltage to the corresponding target position measured in cm through fit functions described in chapter 2.2.3. An example of this process is shown in Figure 3.6. Both X and Y traces are visually inspected, flagged, resulting in a uniform yet non-linear grid pattern (Figure 3.6A). When we then fit functions, we get a sense of how well the model corrects for the non-linearity (Figure 3.6B). If deemed acceptable, the output parameters are saved to the task wide parameter table of a particular Simulink model used by Dexterit-E, which will give a transformed, calibrated eye position when the task is loaded (Figure 3.6C). Three extended calibration sessions were run on three consecutive days with the same offset/gain values between days to get an impression of how stable the head within the mask was, and whether basic parameter values needed to be recalibrated before each session. Whereas in a regular calibration session the 25 target grid pattern was repeated 3 times, in these extended calibration sessions they were repeated 30 times, culminating in 750 eye position samples.

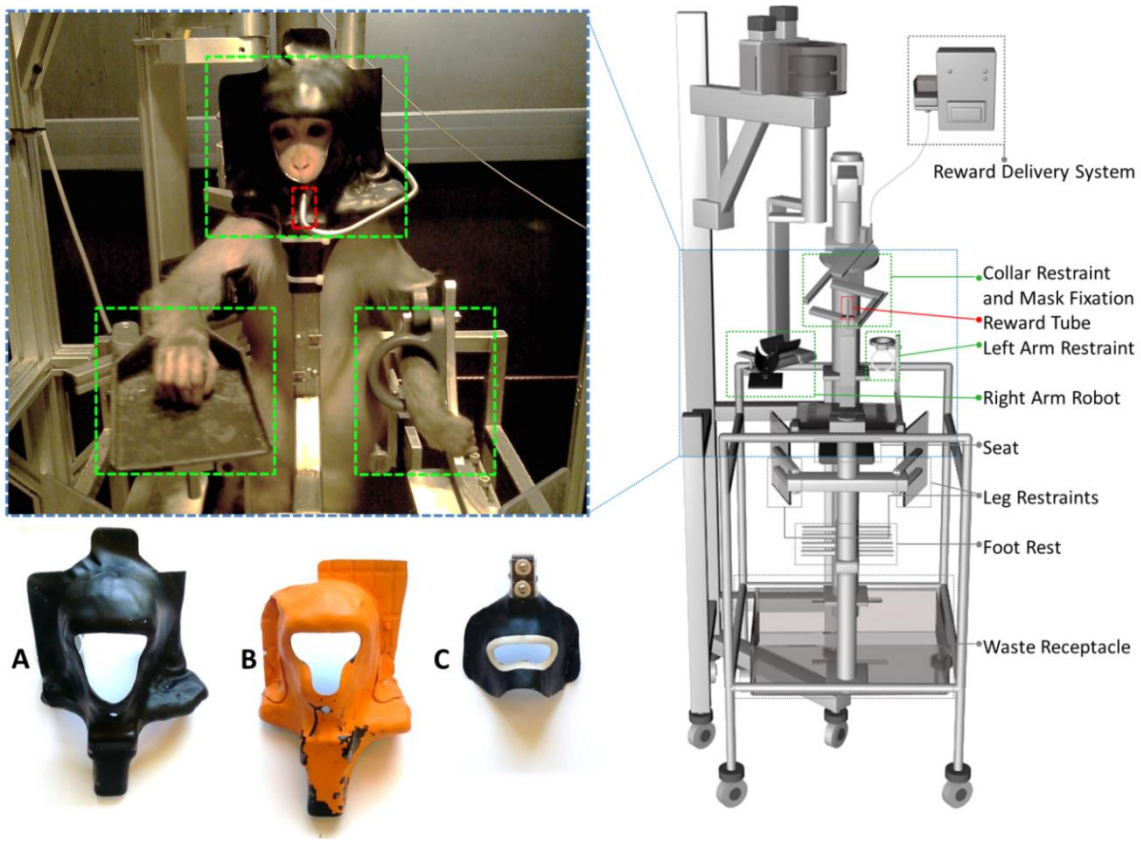

Figure 3.5: Monkey in chair. Right: KINARM Monkey chair + reward delivery system. Top Left: Monkey Y is seated in the chair, with his right arm in the KINARM exoskeleton. Mask B was the mask most used during training monkey Y.

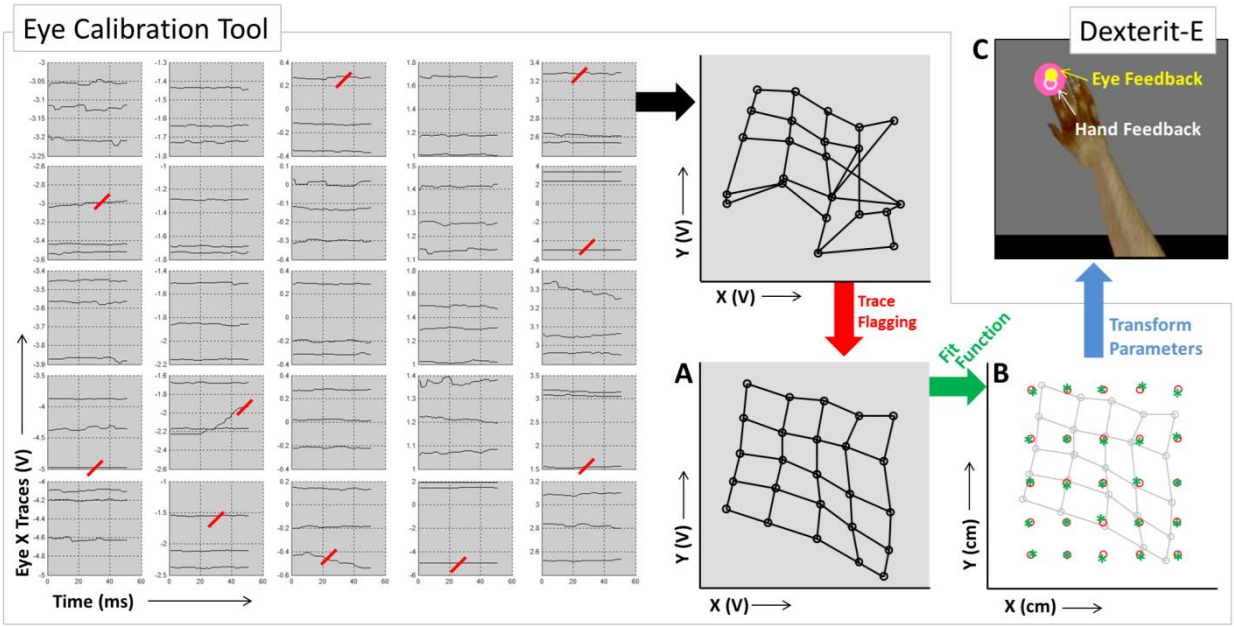

Figure 3.6: Eye calibration GUI interface for A) eye fixation flagging, B) model fitting, and C) transformation parameter output on Dexterit-E.

In Figure 3.7A we see the averaged raw voltage value at each calibration point of the three sessions with unaltered offset/gain parameters. When we align the three sessions in Figure 3.7B, the overall shape of the eye calibration grid seems to be coherent across sessions. This indicates that the gain is not affected between sessions, but there are minor offset shifts between sessions, which nevertheless fall comfortably within the voltage signal range. From this we cannot comment on the within-session variability, however. During the task, a small head movement, or drift, can occur which slowly misaligns the eye signal. This is compensated for by running frequent drift correction protocols throughout the experiment, which realign the raw eye signal. However, if these head movements exceed the capability of the protocol to correct misaligned eye signals, a recalibration is required. Eye calibrations with an unwilling monkey that is easily distracted are complicated and time-consuming, so the calibration was developed with the clear intention to minimize the calibration time for the monkey prior to the actual task, so that it does not significantly influence his task performance. This is also the case for drift correction; it is a fast solution between trials to shift the signal back into alignment. Human participants will also benefit from this speedy calibration process, though their ability to follow instructions will undoubtedly contribute to the procedure.

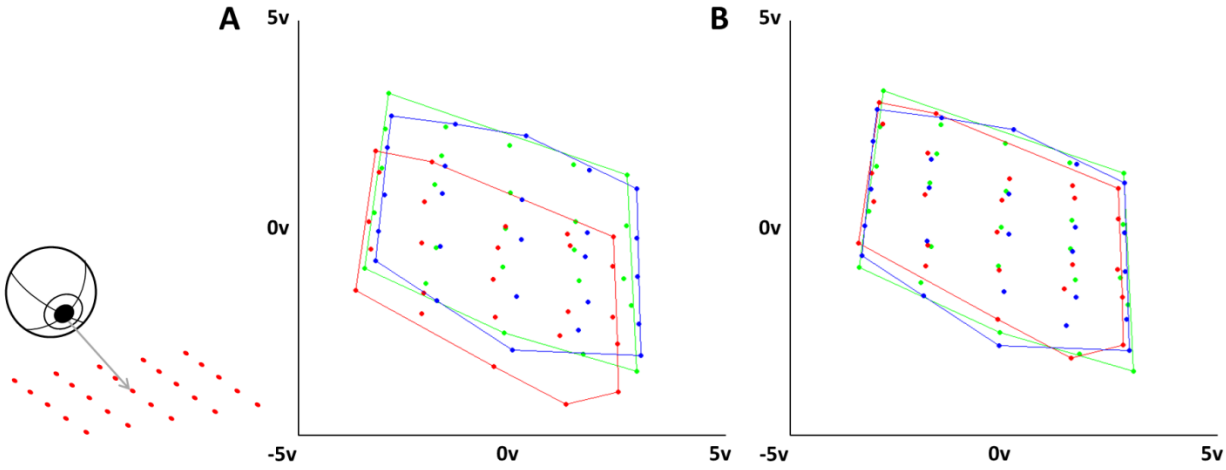

Figure 3.7: Dense eye calibration sessions. A) Average eye position of Monkey Y during 30 calibration task repetitions (in volt) across 3 days (green, red, and blue). B) Grids aligned to the first calibration session (green), offset correction of session 2 (red) required a shift of 0.2V on X axis and 1.1V on Y axis, for sessions 3 (blue) this was -0.2V on X axis and 0.1V on Y axis.

3.3 Monkey Training

In parallel to finding hardware and software solutions for integrating the hand and eye tracking systems and creating an experimental environment that suits our scientific needs,

habituation and early training sessions were performed with monkey Y. This was to teach him basic behavioral traits, such as presenting his collar in the cage to connect it to the guiding rod, and teaching him the best way to move from the cage to the KINARM chair (see Figure 3.8A). Additionally, I had to learn how to interact and handle macaque monkeys, making sure our interactions were calm and pleasant, benefitting us both. During experiments this would be in the form of a sweet reward for the monkey, and a certain learned behavioral response of the monkey to a stimulus for me. Once the monkey showed a clear understanding of what was expected from him, I proceeded to the next phase. Over the course of several weeks/months the monkey would learn to present his collar, move from the cage to the chair, slide his collar into the holding frame, stay seated with his legs comfortably placed, allow his left arm to be placed in an L-shaped arm restraint, and his right arm to be placed in the KINARM exoskeleton (Figure 3.8B).

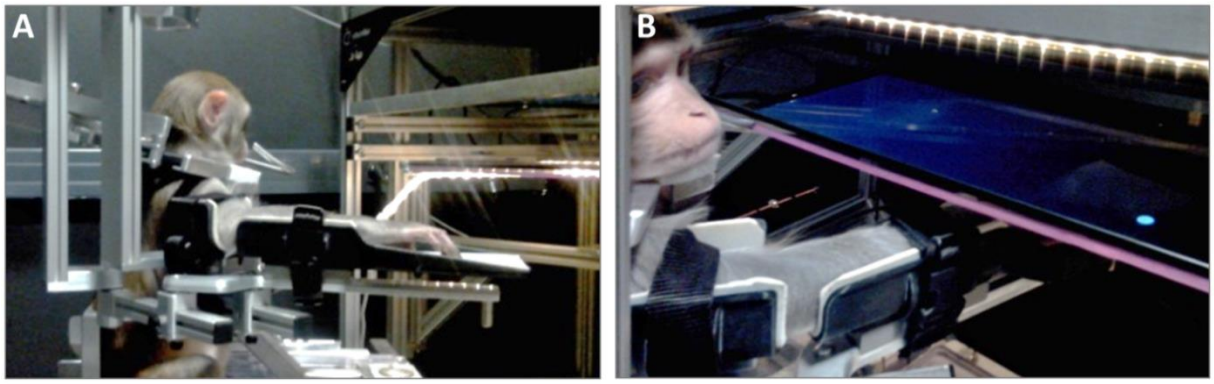

Figure 3.8: Monkey entering a task. A) Monkey in KINARM chair being moved to VR display. B) Hand feedback of the right hand on the semi-transparent mirror.

I then proceeded training him, by using a reward system, to keep his head in a transparent mask, which was eventually be replaced by an orange mask (see Figure 3.5B). The color was chosen because the transparent mask confused the corneal reflection routine of the EyeLink, and the black mask would be confused as a pupil by the EyeLink. Once the mask was accepted, the back of the head was locked as well, such that all head and body movements other than eye and right hand were precluded. We also developed a 'click' mask (Figure 3.5C) to allow the monkey to position his head into the mask connected to a switch, initiating the task once activated. If the head moved, the switch was released and the task interrupted until the head returned to the mask. This was a less claustrophobic solution for the monkey, but was never really fully implemented with monkey Y. These were circumstantial experimental conditions the monkey had to get used to before running actual visually guided motor tasks on

the VR display. The first task component monkey Y had to learn was to realize that his hand movements were represented by a continuous hand feedback stimulus on the VR display (Figure 3.8B). He then had to learn that this feedback allowed him to interact with targets on the display, leading to a reward when correctly performed.

3.3.1 Early Training

There were two major training requirements to fulfill before we continued to our final task configuration. The first requirement was to perform a simple pointing task routine, in which the monkey had to move his hand, and by extension the hand feedback on the VR display through the exoskeleton, into a visual stimulus presented as a circular purple target on that same VR display. The diameter of the target decreased between sessions as a function of performance. Once the hand feedback was in the target, and the monkey maintained his hand in there for at least 250ms, he received an applesauce reward. In later task iterations the monkey had to perform several similar movements in sequence from target to target before getting such a reward. Once the monkey completed 70-80% of the total amount of trials in a session successfully, the difficulty was increased, e.g. the size of the targets was diminished gradually between sessions from a diameter of 4cm to a diameter of 1 cm, the time to move to a target was reduced from unlimited to 900ms, the amount of targets increased progressively from 2 targets until it reached 7 target (See Figure 3.9 for an example of performance-based task change). The second requirement was to perform a simple fixation task for the calibration of eye position measurement, where both hands were locked and the eye had to briefly fixate on multiple small, white targets (diameter: 0.2cm) presented in sequence. The difficulty lay in the understanding of the monkey to react to and fixate on the small white target without moving the hand in order to receive a reward, which was counterintuitive with respect to the pointing task. Additionally, extensive testing with robot eyes showed where the positions of the eyes would be during target fixation, but to insure correct measurements the monkey had to return to the same targets multiple times and remain stationary before the experimenter could sample his eye position reliably. These repetitions may lead to some errors in the sampling data (see flagging feature in Figure 3.6). This was a matter of trial-and-error for both experimenter and monkey, with slow progression initially. Once the monkey was able to differentiate between the pointing task and the eye calibration components, we proceeded to the final task format.

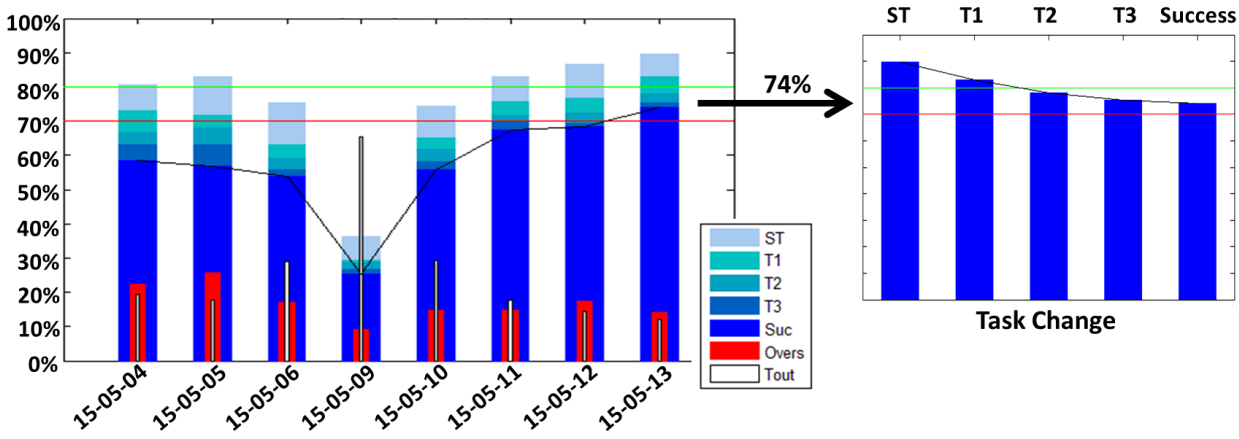

Figure 3.9: Performance during 8 days across 2 weeks (including non-training weekend). The left graph shows the success rate per session for Start Target (ST), Target 1 (T1), Target 2 (T2), and Target 3 (T3) individually, and the overall trial success rate (Suc) that is used as an indicator to adjust the complexity of the task. Overshooting a target is represented by the red bar (Overs), and not reaching a target in time is represented by white bar (Tout). The right graph details the per target performance for a single session, reaching a 74% success rate, which indicated that an increase in task complexity was appropriate.

3.3.2 Sequential Pointing Task

The final version of our sequential pointing task had already been hinted at in Figure 2.2 in chapter 2.2.1. This task contains 6 targets located at the vertices of a hexagon occupying the eye/hand overlap area and one target in the center. The size of the working space ensures that the monkey is able to comfortably reach all targets, and that no eye signal gets lost (see Figure 3.10A). The subtrajectories are differentiated into path types (long/short, horizontal/diagonal) and the angle between two possible locations of subsequent targets that follow within a trial (Figure 3.10B) for later comparative analysis (chapter 3.4). The numbering convention in Figure 3.10 is arbitrary and starts from location 1 at the bottom left and moves counter-clockwise, ending with the Start Target at location 7. The trial starts with the presentation of this Start Target (1 cm radius) at the center of the workspace.

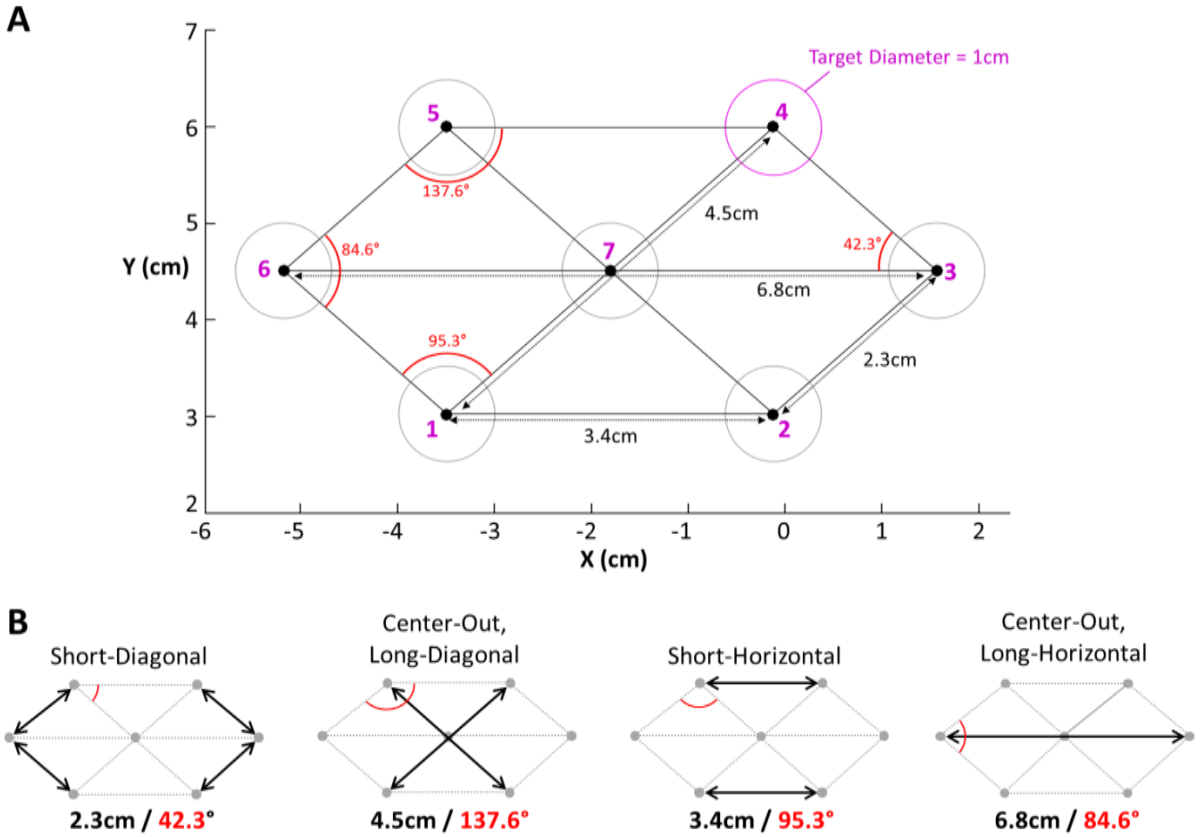

Figure 3.10: A) **Hexagon-shaped sequential pointing task** with 7 targets in XY spatial dimensions. B) Possible paths between targets (long/short, diagonal/horizontal), and the angle between the 2 possible locations of targets that follow. Path lengths and angles between targets are therefore not equidistance and uniform.

The monkey is required to reach this target and to maintain his hand for 250ms inside the target to stabilize the hand position at the beginning of the trial (Figure 3.11A). The Start Target is then extinguished, while a second target of the same size and color was presented: Target 1. Target 1 is randomly located at one of the vertices of the hexagon placed around the Start Target coordinates. The monkey is then required to reach Target 1 within 900ms (Figure 3.11B). After staying in Target 1 for 150ms, Target 2 appears at another vertex of the hexagon, and the process is repeated until a sequence of 3 hand movements (Target 1-3) is completed. After a correct completion of the sequence (Figure 3.11C), a reward is given. The behavioral protocol was designed such that eye and hand movements are performed in the same spatial coordinate system. The smooth performance of the three discrete movements in sequence requires continuous visuomotor processing, transformation and updating to complete the trial within the requested time limit. The fact that eye movements are completely unrestrained and performed naturally allows us to explore their impact and influence on widely distributed cortical activity with respect to hand motor control, such as effector coordination, gaze anchoring, smooth pursuit of the hand feedback, and eye/hand latencies

after target onset. The task can be deconstructed into two task epochs:

1. The center-out component: the hand is located at the Start Target, awaiting Target 1 onset. Target 1 can be located at 1 of 6 possible locations, with pseudo-random occurrence. The monkey must move his hand such that the center of the hand feedback moves over the border of this target to continue the trial (see Figure 3.11A). This component is conceptually different from the subsequent movements, allowing us to explore various aspects of directional tuning in motor control and allowing us to characterize the property of the neurons (Georgopoulos et al. 1982; Kakei et al. 1999).

2. The subsequent 2 targets have the same timing characteristics, with a trajectory that follows a long or short path, which is either diagonally or horizontally oriented. However, there are only 2 possible path directions after the center out component, which never include the Start Target or the same target within a trial (see Figure 3.11B). Eye and hand movements must coordinate at this epoch to complete the task and receive the reward. By adjusting time-of-flight constraints one can move from a step-by-step approach, which consists of a transport phase towards the target followed by a final approach phase under visual guidance, to a strategy in which more than one step is prepared in advance and executed without correction for intervening errors (Bock & Arnold 1993; Badan et al. 2000).

These target sequence possibilities allow for twenty four different trial types. During the trials, eye movements are unrestrained but continuously tracked. Various target positions and paths between targets allow us to address the influence of path orientation and path lengths on eye/hand coordination in space, as well as movement latencies (see Figure 3.10C).

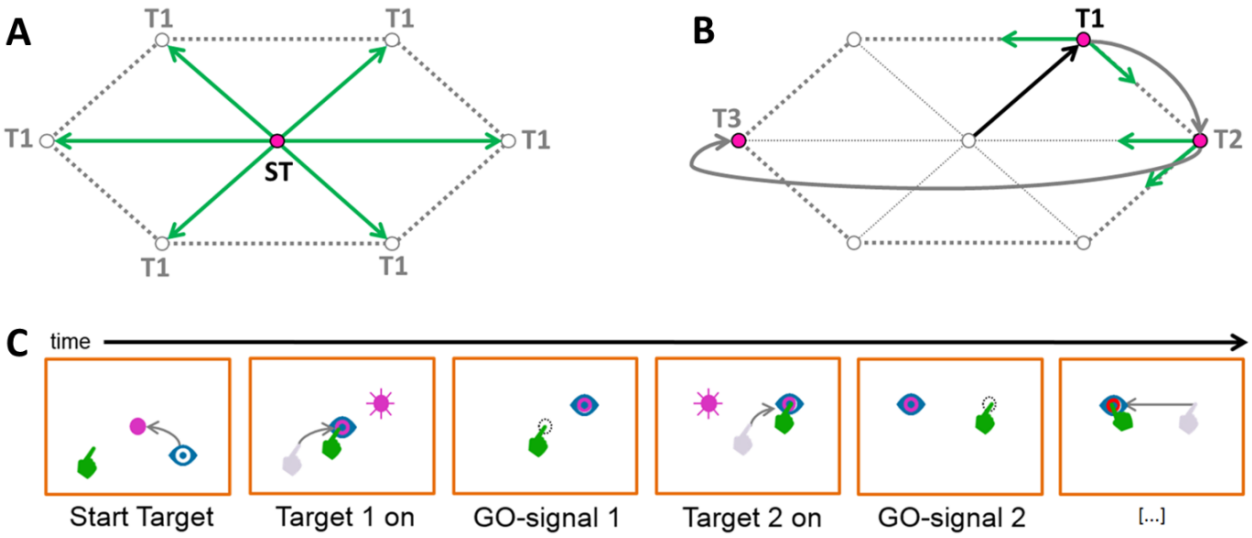

Figure 3.11: Task behavior. A) Center-out component with hand movements from the Start Target (location 7) towards 1 out of 6 potential target locations (1-6). B) The subsequent component of a sequence of two movements, each of which toward two potential target locations different from the preceding movement. C) Task example with eye/hand movements towards targets in time.

In addition, various conditions can easily be layered on top of the basic task design, such as manipulating or removing hand movement feedback, adding mechanical perturbation to hand movements in an expected or unexpected manner, changing the visual environment to bias visual perception, changing temporal limits, changing target behavior, and more. For the training of monkey Y the eye calibration procedure preceded each session and the final version of the sequential pointing task needed to reach a 70-80% success rate before the next phase of the experiment could be prepared: implanting multi-electrode recording arrays (MEAs; chapter 4).

3.4 Analysis Methods & Results

A substantial effort was made towards incorporating the custom eye calibration methods into the task environment and teaching the monkey to cooperate, in parallel to the sequential pointing task. Monkey Y had to learn the rules of two abstract movement tasks, the latter requiring controlled hand movements towards visual stimuli, but leaves the eyes unrestrained, and the former requiring sequential eye fixations on multiple small targets along a grid pattern, but prohibits hand movements. Monkey Y had to complete both tasks successfully under time pressure, with several body and limb restrictions, while accepting a full face mask which immobilized his head. Considering the effort required to introduce these circumstances to other macaque monkeys, I was very fortunate with such a patient and calm monkey. The accuracy and precision measures of eye movements under ideal circumstances with robot and

human participants in both setups were presented in chapter 2.3.3. Figure 3.12A shows the performance during one representative trial of the sequential pointing task, with the recorded hand (green traces) and eye (blue traces) positions for monkey Y. Figure 3.12B shows the horizontal (X) and vertical (Y) components of the eye and hand positions in time for the same trial as that presented in Figure 3.11B.

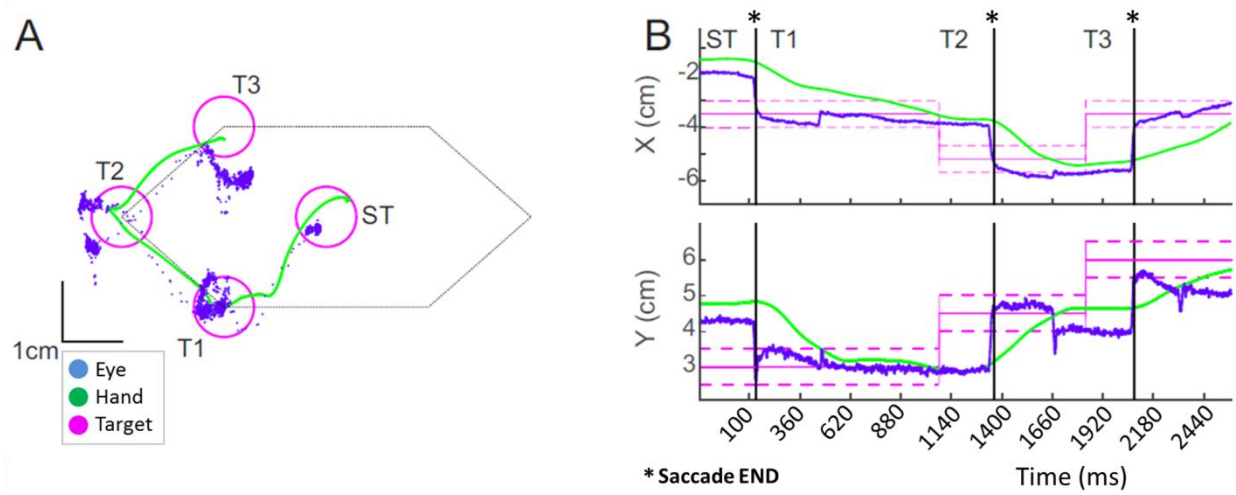

Figure 3.12: Monkey eye/hand traces during one trial. A) Example of eye (blue) and hand (green) XY movements in response to a target (pink) during a single trial with a monkey. B) X and Y axis are differentiated in time.

The coordinates of the target centers and edges are represented in cm with solid and dashed pink lines in Figure 3.12B, at the time they were presented on the VR display. No filtering or alignment of the traces was performed after data collection. All eye traces show clear fixation periods intersected by saccades, which were initiated after target onset, and followed hand movements with timing in agreement with the observations of Prablanc et al. (1979) in humans and Rogal et al. (1985) in monkeys (see chapter 3.4 for latencies). In the gaze position reconstruction, after the saccade, the eye trace terminated within the target boundaries (dashed pink lines). This spatial and temporal coherency, together with the accuracy and precision results presented in chapter 2.3.3, shows the applicability of our method in an experimental task. We repeated the process of eye calibration and the sequential task with a human participant, and found similar recorded traces to monkey Y, strongly indicating that our setups are compatible for cross-species studies (Figure 3.13). The major difference between the monkey and human setups comes from the larger reach of the human participant, which expanded the workspace and allowed us to use a symmetrical hexagon

shaped sequential task. This places targets equidistance from the center target. The human participant is also considerably slower than the monkey.

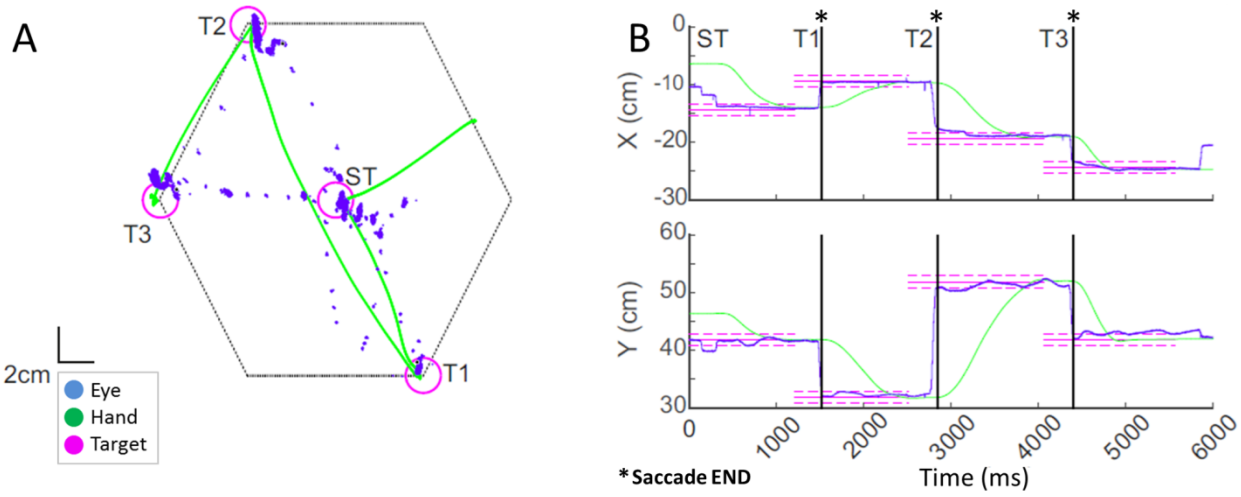

Figure 3.13: Human eye/hand traces during one trial. A) Example of eye (blue) and hand (green) XY movements in response to a target (pink) during a single trial with a human. B) X and Y axis are differentiated in time.

The promising results presented here show the applicability of our method in an experimental task. However, experiments which incorporate human and monkey participants in the same behavioral paradigm are still in the pilot stages at the time of writing this dissertation.

3.4.1 Eye & Hand Movement Latencies

Our automatized temporal markers for specific task-related events, such as target onset, trial error, hand-IN-target, and hand-OUT-target, give us insight into the progression of each trial in time. However, it does not give us insight into movement events, such as continuous eye and hand movements and movement onset. Therefore a visual marker tool was created to indicate such movement events by visual inspection (see Figure 3.14A for description). We use monkey Y's final behavioral dataset before MEA implantation in order to explore spatiotemporal features during the sequential pointing task, and analyze behavioral strategies observed in a number of trials.

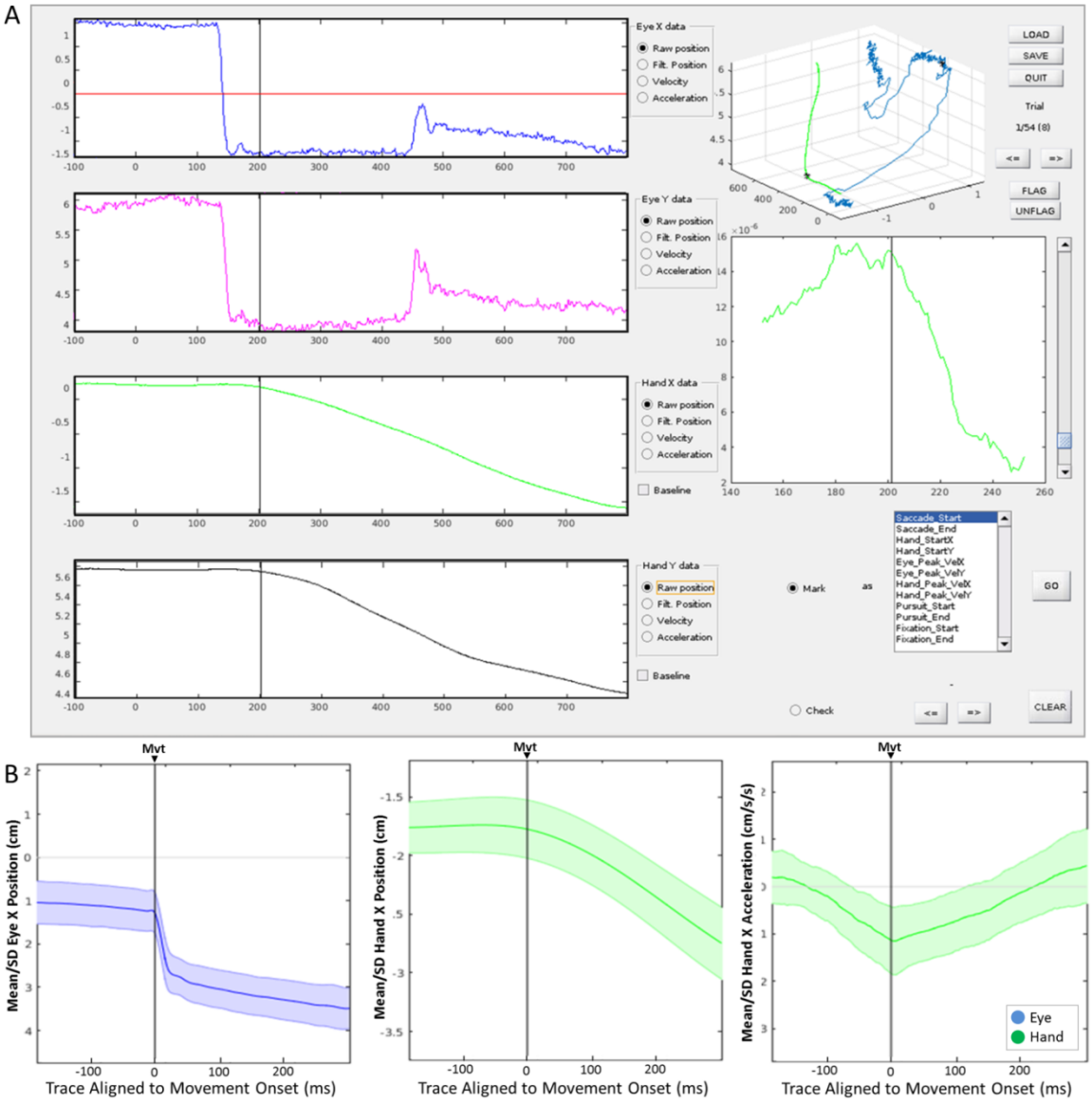

Figure 3.14: A) **The Visual Marker Tool** takes subtrajectory data and plots eye and hand (filtered) position, velocity or acceleration in X and Y space (cm) against time (ms), starting at the Target Onset event and ending at the Hand-In-Target event. By clicking in any of the 4 windows on the left side, a single black line appears to indicate a time marker, which may be labeled using the list of event names on the bottom right panel, such as 'SaccadeX_Onset' or 'HandX_Onset'. By pressing button 'GO' the time point is stored with the corresponding label and a new time point can be selected with a different event name. The middle right panel zooms in 100ms around the selected window and time point, so the user may be more precise in selecting a time point. The upper right panel shows the relationship between the eye and hand in 3D space, with X and Y in space (cm) and Z in time (ms). B) After marking the events with the labels 'SaccadeX_Onset' and 'HandX_Onset', we align each subtrajectory to the events, and average across them for eye (blue trace, panel 1), hand movements (green trace, panel 2), and hand acceleration (green trace, panel 3) to assess marking coherency across subtrajectories. The solid middle line is the average, the lighter colored space above and below is the standard deviation of each respective measure.

The dataset contains 484 trials from the same session, yet each trial could be divided further into 3 subtrajectories according to their chronological rank within the trial: rank 1 is the period between ST and T1, rank 2 is the period between T1 and T2, and rank 3 is the period

between T2 and T3. This allowed us to include subtrajectories from unsuccessful trials in which rank 1 and 2, or just rank 1, was completed, giving us a total of 827 successful ranked subtrajectories. To mark the moment of eye movement onset/offset, a sudden change in position indicating a saccade was used (Figure 3.14A, first left trace), and to mark the moment of hand movement onset two measures were used because of the somewhat slow and subtle movement onset, the changes in position (Figure 3.14A, third left trace) and acceleration. To reiterate, all latencies discussed in this chapter are relative to the target onset. With this tool we explored the relationship between eye and hand movement in time during a sequential pointing task, allowing us to assess coherency by aligning to saccade onset, hand movement onset, and hand acceleration across subtrajectories (Figure 3.14B). We calculated a linear correlation (Pearson's *r*) between saccadic and hand reaction times (RT), i.e. the times between target onset and saccadic or hand movement onsets, and found that these behavioral measures were significantly correlated ($r = 0.33$, $p < 0.01$, $n = 827$; Figure 3.15A). This means there is a positive linear relationship between the onset of the eye and hand movements.

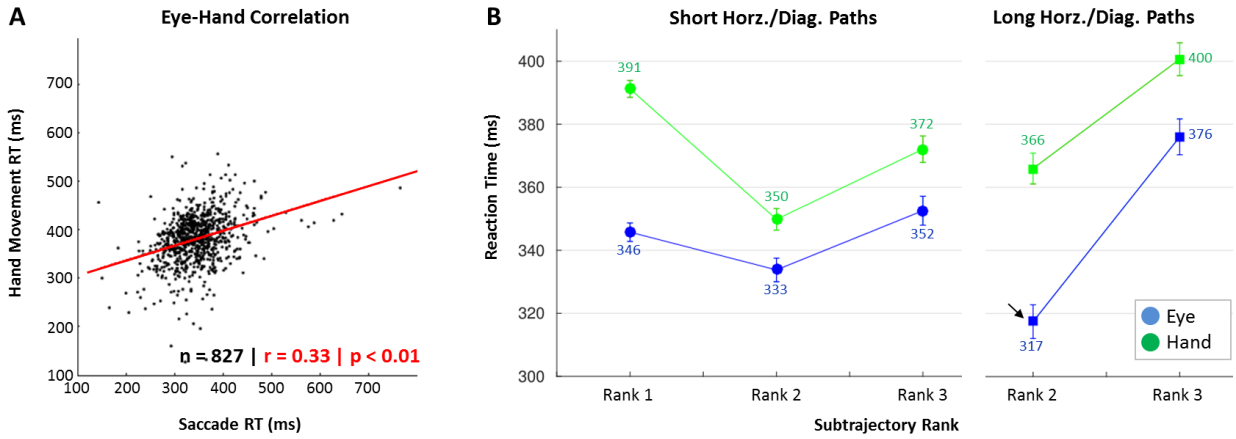

Figure 3.15: Relationship between eye and hand movements. A) The positive correlation between the hand movement onset (reaction time, RT) and eye movement onset is represented by the red regression line ($r = 0.33$, $p < 0.01$). B) Average latencies of horizontal and diagonal saccade and hand movements for three subtrajectories in a single trial (ranks 1 - 3), which are further differentiated by path length (short/long) in rank 2 & 3. Eye and hand latencies are represented by blue and green lines, respectively, with the means near the corresponding markers.

Ranking the subtrajectories 1 to 3 allowed us to assess whether average latencies (RTs) for eye and hand movement onset differed with respect to the rank, by using a one-way analysis of variance (ANOVA; Matlab function: *anova1*) and a multiple comparison test of population marginal means with a Tukey's honestly significant difference (HSD) procedure (Matlab functions: multcompare with 'hsd' procedure; McHugh 2011).

For eye movements in rank 1 saccade onset latency was 346±50ms (mean±SD; n = 320), which was slower than that in rank 2 (328±47ms; n = 292), but faster than in rank 3 (362±62ms; n = 215). The hand movement started after saccade onset in all ranks, with a delay that decreased with rank, being 45ms, 32ms and 20ms in rank 1-3, respectively. The group averages per rank were significantly different from each other, for both eye and hand movements ($p < 0.01$). This result indicates that data cannot be pooled across ranks, raising the following question: why do we observe different behavioral latencies between sequential components (ranks) with near identical behavior requirements? We differentiated the dataset further to include path length and ran the same tests (Figure 3.15B). This did not affect latencies in rank 1 as it only contained *short* horizontal (3.4cm) and diagonal (2.3cm) path subtrajectories (see cm and angles for each path in Figure 3.10), due to its center-out movements from the Start Target to 1 out of 6 possible locations (ST to T1). Also, there are only 2 possible target locations following rank 2 and 3. To restate, the first rank allows us to characterize the neurons, and the two subsequent movements (rank 2 and 3) reflects ongoing eye/hand coordination dynamics, which makes them conceptually different from rank 1 and the focus of analyses moving on. Eye movement latencies for *short* horizontal and diagonal path subtrajectories in rank 2 (333±45ms) and rank 3 (352±48ms) both differed ~20ms from hand movement latencies (rank 2: 350±52ms; rank 3: 372±43ms). However, in the *long* horizontal (6.8cm) and diagonal (4.5cm) path subtrajectories we see an average difference between eye and hand latencies in rank 2 of 49ms (indicated by black arrow marker in Figure 3.15B).

We therefore explored another dimension that had the potential to impact performance: movement direction per subtrajectory. Each movement direction is expressed as a vector between two target locations, i.e vector 43 is a short, diagonal movement between target location 4 and 3 (Figure 3.10 for locations 1-7). In Figure 3.16 vector 43 can be found in the inset of the 'Rank 2 Short' panel (marked with *), which corresponds to a directional vector in the upper figure (also marked with *). The length of the vector 43 in this figure represents the mean saccade latency in case of the blue line/marker (359ms) and mean hand movement latency for the green marker (376ms) in a range of 200-500ms. The same is expressed with other vectors in 'Rank 2 Short', and indeed in all panels of Figure 3.16. Vectors with the same orientation but different target locations, e.g. vector 23 and 65, are differentiated by one set of vector markers (blue/green) with a magenta circumference, lacking reaction times for visual clarity.

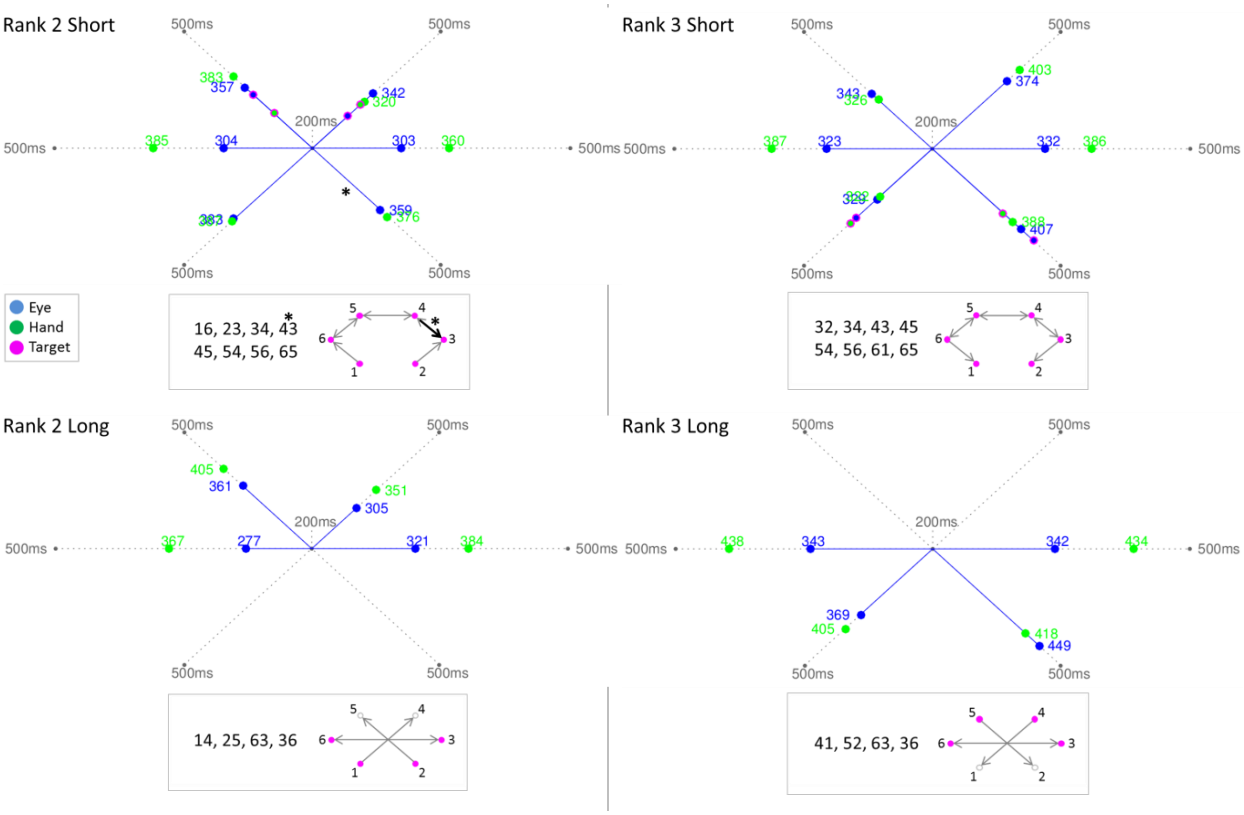

Figure 3.16: Movement latencies and directions. Movement direction is expressed in each panel inset as vectors between two target locations, i.e. vector 43 means movement from target location 4 to location 3. Insets show all possible vectors per rank (2/3) & path length (long/short) for this session. In the main figure, saccade and hand movement RT is represented by a blue/green marker, respectively, with the average RT for each modality placed between 200-500ms.

Superficially, the RTs in all four panels of Figure 3.16 show that an important behavioral expectation, as described by Neggers & Bekkering (2000) to be consistent across trials and subtrajectories, was not met. This was the expectation that saccades always preceded the hand movements, in order to process the visual information of the target location before guiding the hand towards it. Only horizontal movements (vector 36, 63, 54, and 45) fulfill this expectation.

In total, 36 different vectors were possible in our sequential pointing task, but only 30 vectors were used, removing two short horizontal vectors (12, 21) in rank 2 and 3, and four long diagonal vectors (41 and 52 in rank 2, 14 and 25 in rank 3). These vectors were present in two later sessions, which, across three days, covered all 36 possible vectors in all ranks. This was consciously done to maximize sample size per vector without sacrificing the pseudo-random target location per rank (six possibilities in rank 1, two possibilities in rank 2 and 3). However, this bias directly impacts the averages presented in the *long* paths of rank 2 and 3 in Figure 3.15B (expressed as individual vectors in Figure 3.16 'Rank 2 Long' and 'Rank 3 Long'). Rank 2 only has horizontal and diagonally *upward* movements, and rank 3 only has

horizontal and diagonally *downward* movements. As a consequence, the data in rank 2 and 3 were pooled (n = 507) and grouped into horizontal, diagonally upward and diagonally downward movements to explore whether mean response times were significantly different across movement direction, rather than rank (Matlab functions: *anova1* & *multcompare*, ctype:hsd). The results are presented in Figure 3.17. Reaction times differed significantly from each other ($p < 0.01$), with horizontal eye movement onset being the fastest (mean±SD = 317±37ms, n = 190), followed closely by the RT for diagonally upward movements (mean±SD = 337±48ms, n = 174), and a 66ms/46ms slower RT, respectively, for diagonally downward movements (mean±SD = 383±65ms, n = 143). In contrast, RT was the slowest for horizontal hand movements (mean±SD = 391±41ms), with diagonal upward movements starting earliest (348±58ms), and diagonally downwards movements having the same average onset time as the saccade (383±48ms). We discuss the possible causes behind these varied findings in the discussion (chapter 3.5).

A second behavioral expectation outlined in Neggers & Bekkering (2000) was that the eye remained fixed on the target until the hand reaches this target, a phenomenon known as 'gaze anchoring'. However, we cannot address gaze anchoring with temporal events, it requires a comparison of spatial derivatives of eye and hand movements, which is presented in the next section (chapter 3.4.2).

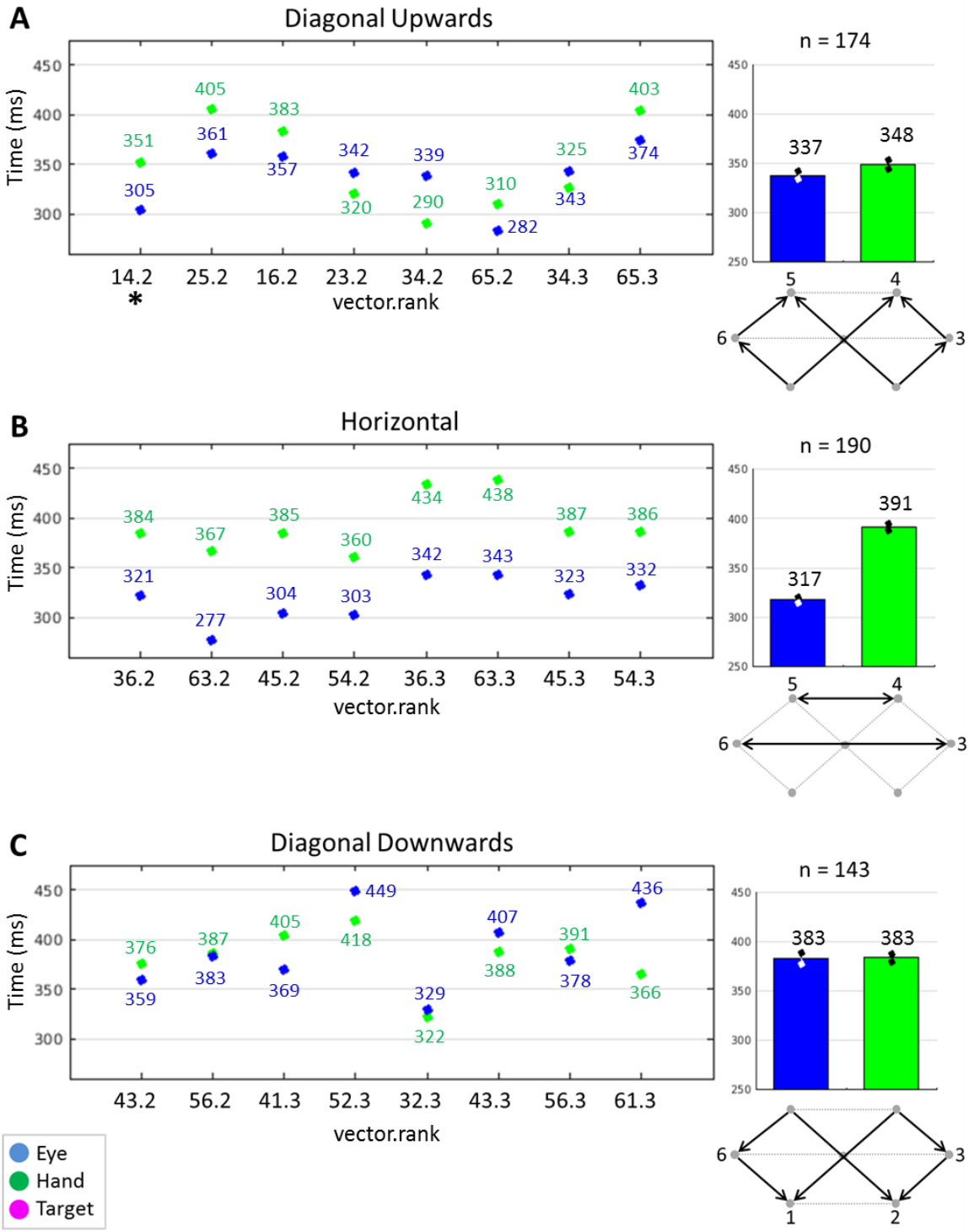

Figure 3.17: Latencies in three groups. In the scatter plots, saccade (blue marker) and hand movement (green marker) RTs are represented for each movement direction per rank, or vector.rank, e.g. a movement between target location 1 and 4 in rank 2 gives the ranked vector 14.2 (marked with * in panel A). The bar plots on the right represent average saccade and hand movement RTs (in ms, including standard error) for diagonally upward (A), horizontal (B) and diagonal downward (C). The vectors in XY space are represented by the black arrows in the inset of each panel.

3.4.2 Eye & Hand Velocity Matching

The homing-in of the hand to a target is presumed to require spatial on-line movement control, which ties visual attention to the fixated region and blocking the possible shift of attentional focus to another target. In the premotor theory of attention introduced by Rizzolatti et al. (1987) it is assumed that visual attention needs to be shifted in order to prepare a saccade, which underlines the inability for saccade preparation while the hand is still in flight, and attention is still at the target. This is reflected in the experiments by Neggers & Bekkering (2000) where human participants were asked to move their hand towards a target. The hand was visible and not represented by a hand feedback stimulus. No requirements were made for the eye, but they were recorded continuously. As soon as the participant reached a certain hand movement velocity, a second target appeared, which had to be reached as soon as possible, but only after the hand reached the first target. The authors observed that participants kept their gaze fixed on the target while the hand was moving towards the target, regardless of the second target's RT, position or distance relative to the first target or hand location. In our experiment we do not have two targets at any given time, but we do have two visual stimuli during a trial: one is the target (a pink circle, 1cm diameter) and one is the hand feedback stimulus (a white circle, 0.2cm diameter).

Following the literature discussed above, we expected that for each subtrajectory a saccade would occur towards the target after a relatively stable latency, followed by a gaze fixation period on the target until the hand entered the target. Once the target was extinguished, the gaze was released. The next target appeared, shifting the visual attention to the new target location and reinitializing a saccade and fixation period, followed by a hand movement, which was repeated until all conditions of the trial were met and a reward was given. However, of the 827 successful subtrajectories in our dataset, 674 subtrajectories (~82%) show a second saccade occurrence near the end of the hand movement, just before the hand enters the target, shown in Figure 3.18 (black arrow marker). On the surface, it seems that the eye makes a saccade (blue trace) back to the hand feedback (green trace) and tracks its position in time as the hand enters the target (time period after black arrow marker).

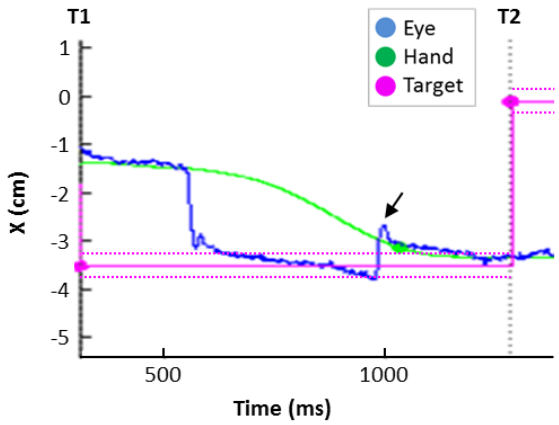

Figure 3.18: Example of a second saccade indicated by the black arrow marker, during the second subtrajectory of a trial (specifically vector 42, rank 2). The filled magenta circles indicate target onset and its location on the X-axis, the solid line represents the target center, and the two dashed lines represent target diameter (1cm). The green and blue traces represent X-axis hand and eye movements in time, respectively.

This indicated that the second saccade shifted the eye from fixating on the target to a smooth pursuit behavior on the hand feedback as it approached the target. In order to measure whether the eye was indeed engaged in smooth pursuit of the hand feedback in all 674 trials with second saccade observations, we compared average eye velocity (m/s) with the average hand velocity (m/s) across all subtrajectories around the time of the second saccade onset. If the velocities match for hand and eye movements, a smooth pursuit is in effect. In Figure 3.19A & B we see a 300ms window for the average XY eye/hand velocity profiles for vector 25, across 26 trials, in blue and green solid lines, respectively (SD is the lighter colored space above and below each respective line). The second saccade velocity was aligned to 150ms after saccade offset. This was done because 1) we were interested in the velocity of the eye *after* the second saccade has occurred, in order to assess whether it matched with hand movement velocity (vector 25 example: Figure 3.19D & G), and 2) we were interested in the velocity of the eye *before* the second saccade has occurred, in order to assess whether the eye was fixated at a target location or was already engaged in a smooth pursuit of the hand movement feedback (vector 25 example: Figure 3.19C & F). This gives us four windows comprising two axes and two time periods (before/after). For all 30 vectors, we subtracted the hand velocity values from the eye velocity values of both XY axes in the before and after periods (vector 25 example in Figure 3.19E & H), and ran a one-sample *t*-test on the absolute eye/hand velocity difference in each window. For vector 16 and 25, a significant difference in velocity between eye and hand movements was found in the period before the second saccade ($p = 0.04/0.04$ for both vectors), while the velocity profiles matched in the period after the second saccade ($p = 0.21/0.22$ for vector 25, $p = 0.07/0.08$ for vector 16).

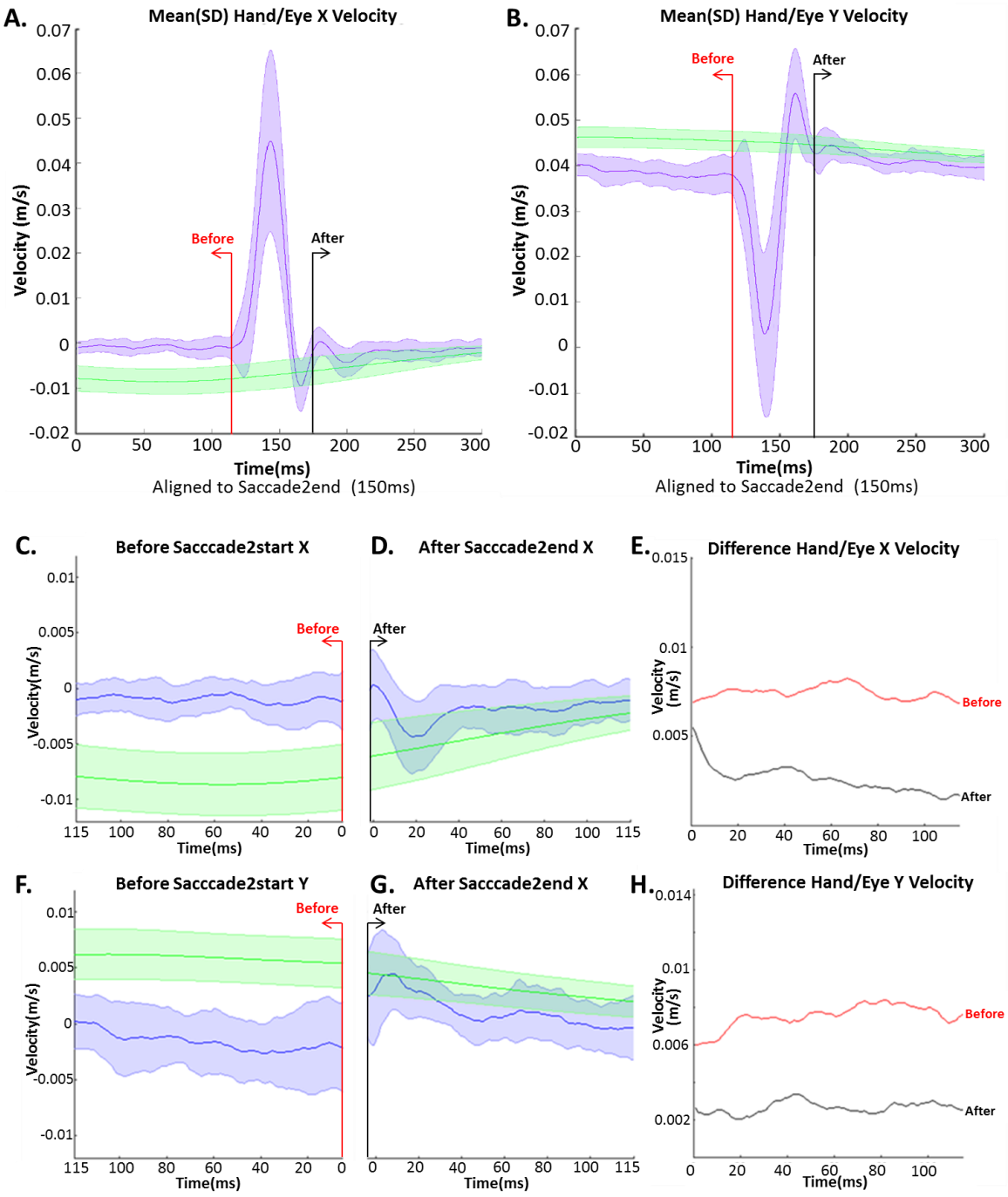

Figure 3.19: Velocity matching: A/B) The hand/eye X/Y velocity profiles in a 300ms window, aligned to saccade 2 end (150ms); C/D/F/G) Windows are divided in two 115ms periods, 35ms before and after saccade end, for the X and Y axes; E/H) Mean XY velocity differences of the eye relative to hand velocity in the periods before and after second saccade end.

This means that in vector 16 and 25 the eye was fixated on the target until the second saccade, at which point it was in smooth pursuit of the hand feedback. However, in 72% of the vectors there was no significant difference between the eye velocity profile and the hand velocity before or after the second saccade. In the remaining 18% the eye and hand velocity matched in the period before the second saccade, but not after.

3.5 Discussion

We endeavored to explore the relationship between hand and eye movements of a trained monkey during a sequential pointing task within the final training session, before the monkey received chronic microarray implants. A successful trial would yield a reward after the three subtrajectories were completed. Even incomplete trials could have 1 or 2 successful subtrajectories, which were added to the final dataset of 827 subtrajectories. We correlated eye and hand movement reaction times and found a significant positive correlation ($r = 0.34$, $p < 0.01$) between movement onset, in line with previous experiments (Dean et al. 2011: $r = 0.55$, $p < 0.05$; Gribble et al. 2002: Table 2). We compared onset latencies of eye/hand movements within and between trial subtrajectories (ranks), path lengths and movement directions (vectors). These ranked vectors provided insight into the general spatiotemporal strategy of the monkey during this task, with an intermediate reaction time typically in the first subtrajectory (rank 1), followed by a fast RT in the second subtrajectory (rank 2), finishing in an overall slow RT in the final subtrajectory (rank 3). In particular, the long diagonal movements in rank 2 and 3 had very variable saccade RTs, a difference spanning 59ms. To gain a greater understanding of the causes underlying these timing differences in rank 2 and 3, each possible vector was expressed in Figure 3.16. This figure shows that the task design bias of reducing the amount of possible movement directions (vectors) to bolster sample size leads to grouping unbalanced behavioral data according to rank and path length, making it more difficult to compare. By reviewing the RTs for individual vectors in Figure 3.16 our data suggests a trend in movement directions, rather than rank and path length, for generally long saccade RT towards the lower targets, shorter saccade RT towards the upper targets and the shortest saccade RT towards horizontal targets. To test this, data from rank 2 and 3 ($n = 507$) was categorized into diagonally upward, horizontal, and diagonally downward vectors. The results presented in Figure 3.17 shows that hand movement RTs were consistently longer than eye movement RTs with horizontal vectors (Figure 3.17B, bar plot), and an overall simultaneous eye/hand movement onset for diagonal vectors, although diagonally upward movement RTs were generally shorter than diagonally downward movements RTs (337-348ms to 383ms; Figure 3.17AC, bar plots). Generally, the eye/hand RT relationships between diagonal vectors are more variable than for horizontal vectors, regularly containing hand>eye movement RTs, eye>hand movement RTs and eye=hand movement RTs times. These latency results can be interpreted in several ways. First, the longer response time of the eye movements towards the lower targets may be attributed to the

weak visibility of these targets, as they were located near the lower edge of the overlap area, near the body of the monkey, where the eye and the hand could still be recorded together. Saccade RTs as response to these targets after, or simultaneously with, hand movements suggest the possibility that the monkey memorized the spatial location of the lower targets, which meant that if a target did not appear at the expected time while the trial was ongoing, it served as a go-signal to move to a location of poorly visible targets. This coincides with the finding that some of the eye velocity profiles on certain ranked vectors were engaged in smooth pursuit tracking of the hand feedback prior to the second saccade. Additionally, the predictability in rank 2 and 3 was much higher compared to rank 1, considering there were only two target location possibilities versus six target possibilities in the center-out component of rank 1. As a general rule, shorter RTs are found as the target predictability increases in space and time (Beck et al. 2014). Secondly, the general RTs of hand movements across ranked vectors were not dissimilar, but had a substantial variability of 40-70ms, with a rather slow velocity profile. It became particularly difficult to identify movement onset when position, velocity and acceleration changed extremely gradually over time, in stark contrast to the sudden movement bursts of a saccade. This impeded interpretation of the second saccade, which occurred pervasively throughout the dataset, but only at points when hand velocities were already approaching 0 m/s. From the vector 16 and 25, and several single subtrajectory profiles such as Figure 3.17, the following behavioral strategy was hypothesized: when the eye makes a saccade to a target, the hand follows until it comes within a certain distance of the target. The eye is released from the target when the hand feedback reaches this distance in order to accurately guide the hand into the target and staying there until the target is extinguished and the new target appears in another location (figure 3.19A & B). A saccade-only paper discusses a speed/accuracy trade-off with error-correcting secondary saccades in a similar vein to our findings (Wu et al. 2010). In order to gain rewards rapidly, a monkey primarily exploits the two visual stimuli (hand feedback and target) to complete the task, but this was certainly aided by the memorized spatial location of all possible targets, the predictability of rank 2 and 3, and the fixed timing of events, i.e. target onset, time between targets and between trials. Unfortunately, complete randomization of more vectors decreases the power per vector type and weakens the ability to do statistical comparisons between groups. However, the movement time could be drastically reduced by decreasing the maximum reach time between targets, and coupling target onset to a velocity value of the hand movement. This would mean the monkey would have to move towards a target at a user-

defined velocity, within a limited amount of time. This would make it easier to mark movement onset, and make velocity profiles less ambiguous. The size of the target, however, has to be adjusted in relation to the temporal constraints and accepted error levels: the smaller the target, the higher the accuracy is needed to complete the trial, which requires more time, and vice versa. By using hand and eye movement latencies together with velocity matching, we are able to categorize behavioral components of the monkey during a sequential pointing task as seen in Figure 3.20C.

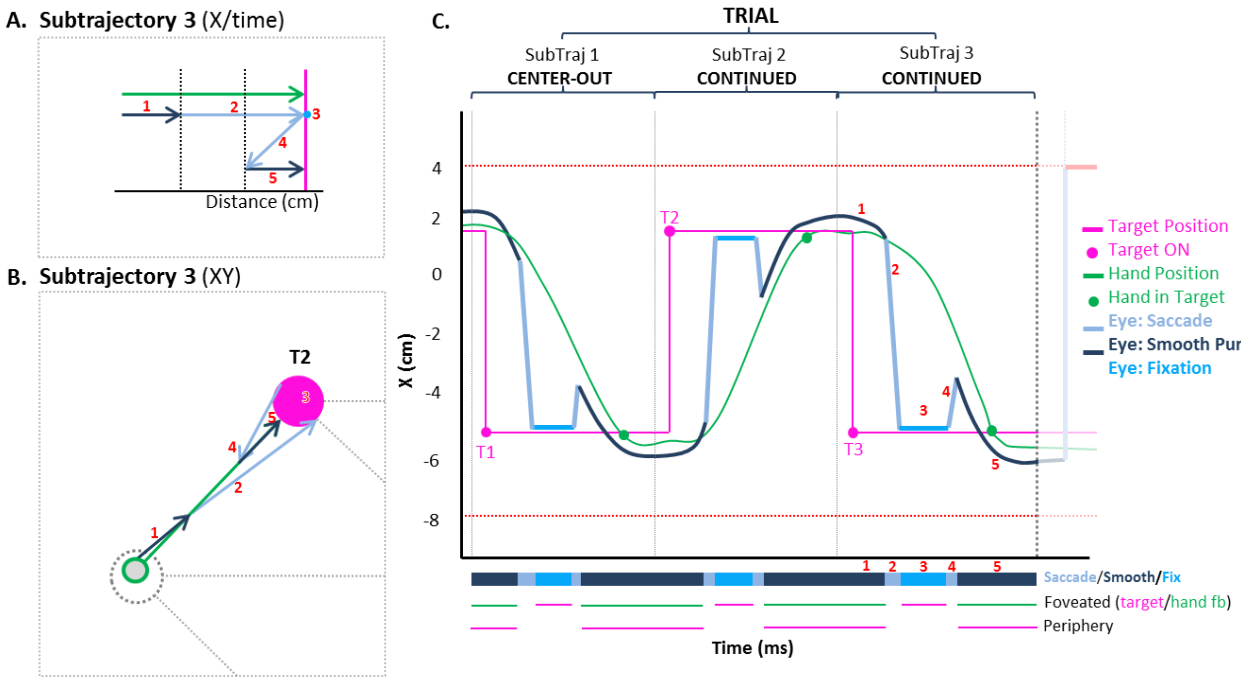

Figure 3.20: Idealized eye/hand strategy during subtrajectory (rank) 3 of a sequential pointing task. A) The hand (green vector) moves towards the target (pink line), while the eye (dark blue) initially tracks the hand feedback before it makes a saccade (light blue) to the target. As the hand moves closer to the target, the second saccade is made towards the incoming hand feedback, in order to guide it into the target. B) Same as A, but in XY space. C) Imagined X traces for eye/hand movements in time (ms) for an entire trial, with alternating eye movement behaviors (saccade/smooth pursuit/fixation) across the subtrajectories to complete the trial and receive a reward.

In this idealized figure, the eye X movements in time are divided into periods of fixation, saccade and smooth pursuit, and indicate periods in which either the hand feedback or the target are in the visual periphery. Switching between systematic gaze attributes in a predictable manner will aid us in exploring the behavioral influences on visual, motor and integrative cortices and the coordination between them.

3.5.1 Gaze Anchoring

As mentioned before, Neggers & Bekkering (2000) hypothesized that saccades do not only

precede pointing movements, but that the gaze is fixed during these pointing movements. In their subsequent publication (Neggers & Bekkering 2001) they extend this hypothesis by exploring how this gaze anchoring is driven. Their findings suggest that three possible mechanisms underlies gaze anchoring:

1) Visual signal, using the retinal image of the moving arm
2) Internally generated efferent signal related to arm movement control
3) Afferent signal carrying information on the dynamic status of the arm (proprioception, muscle)

However, they found that vision of the moving arm was not needed to get the same gaze stabilization, indicating that internal signals related to arm movement control or that proprioception was integrated in the oculomotor system. The contribution of the SC to the organization of ocular behavior was subsequently considered, as this region, in conjunction with FEF and SEF, was involved in saccadic/smooth/fixation related movements. Moreover, the SC reach cells were known to have a direct control over arm movements and/or the interaction of these movements with saccades (Werner et al. 1997). They speculated on the involvement of FEF in anchoring gaze to a target, by delaying the buildup of an oculomotor program for a new saccade until the target is reached. They suggested electrophysiological recordings of these areas during these experiments to characterize the neurophysiological role in gaze anchoring, but this has not occurred yet. In fact, the phenomenon is reported in numerous studies (Hayhoe et al, 2003; Reina & Schwartz, 2003; Sailer et al. 2005), but rarely explored as a stand-alone behavioral feature, except for Rand & Stelmach (2010) who explored gaze anchoring mechanisms and functions as an extension of their eye-hand coordination task. In Rand (2014) this was extended by examining whether subtrajectories are interdependent in saccadic eye movements that accompany hand movements. The circumstances which illicit gaze-anchoring, and the conditions under which it is released prematurely are not fully known, but our very preliminary behavioral results of a monkey engaged in a visually guided pointing task tentatively indicates that accuracy restrictions forces gaze anchoring to be released in order to guide the hand feedback into a target. This hypothesis would require a rigorous repetition of the same experimental task and conditions, across multiple sessions to be accepted, with several of the aforementioned updates to the timing of task events. The inclusion of haptic feedback similar to the task of Bowman et al. (2009) would be well within the technical capabilities of our setup.

4 IMPLANTATION OF MULTIELECTRODE ARRAYS (MEAS)

Monkey Y was the first participant to fully perform successful eye calibration procedures and reach a success rate of 70-80% completed trials in the 3 subtrajectory sequential pointing task paradigm (dataset chapter 3). He was therefore considered ready for implantation of chronic multielectrode arrays in several visuomotor areas. Two connectors would be fixed to the cranial surface, which served as an interface between the next-generation digital headstages, each supporting transmission of up to 128 microelectrode channels (CerePlex E, Blackrock Microsystems), and the data acquisition (DAQ) system (Cerebus NSP, Blackrock Microsystems). These two headstages digitize analog neural signals at the recording site, and send these recordings continuously to the Cerebus DAQ system with a 30 kHz sampling frequency. As mentioned in chapter 2, proprietary Blackrock Microsystem file formats NEV and NSx store these 30 kHz electrophysiological recordings alongside with the 16-bit digital task and behavioral events and 1 kHz analog eye/hand/target position data. A standard 100 electrode 'Utah' MEA (MEA1, 10x10 matrix, 4x4mm surface area, 1.5mm electrode length, and 400µm dirstance between electrodes) was scheduled to be implanted into the motor area (M1 and PMd; Figure 4.1), and a second custom 'Utah' MEA was scheduled to be implanted into the primary and higher visual areas. This latter custom MEA was split into 4 arrays, each containing 36 electrodes, so that multiple areas in primary visual and parietal areas could be recorded (MEA2, 6x6 matrix, 2.4x2.4mm surface area, 1mm electrode length). Due to the shape of visual cortical surfaces, smaller MEAs conformed better.

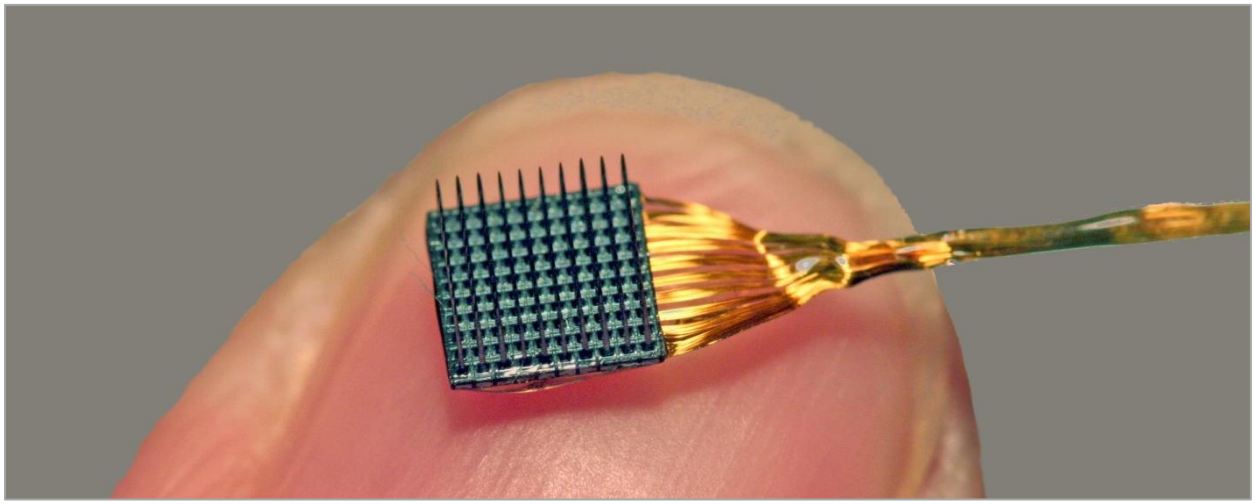

Figure 4.1: A 100 electrode 'Utah' MEA from Blackrock Microsystems (10x10 electrode matrix, 4mm x 4mm).

4.1 Implant Sites

We are interested in recording brain areas that coordinate their activity during a visually guided motor behavior; this includes areas from the motor, visual and parietal (visuomotor transformation/integration) cortices. Considering that the MEAs are generally used to be implanted into the surface of the cortex (with electrodes of 1-1.5mm length), subcortical regions are not considered an option for implantation. To reiterate chapter 1.5.1, the connectivity map presented in Figures 1.2 – 1.5 served to outline and target the most relevant and accessible brain regions that 1) are involved with processing visual input, visuomotor transformation and motor output, 2) are integral to coordinated visually guided goal-directed behavior (eye-hand coordination in particular), and 3) have been shown to be modulated by eye position and orientation or body/limb position and orientation, or a combination of both. With this in mind, the decision was made to implant the MEAs into the following 5 areas:

	Implant	**Area Name**	**Abbrev.**
1.	MEA 1	The motor cortex	M1/PM
2.	MEA 2A	The primary visual cortex (striate)	V1
3.	MEA 2B	Visual area V2 (extrastriate)	V2
4.	MEA 2C	Visual area V4 (extrastriate)	V4
5.	MEA 2D	Parietal area 7a (extrastriate)	Area 7a

The successful placement of MEA 1 in the motor cortex covering part of M1 and PM is the last MEA-accessible cortical area before the motor cortex projects down to the spinal cord. These motor areas are involved with movement planning, anticipation, control, and execution of voluntary movements, and are integral to exploring the cortical dynamics at the level of motor output. For the placement of MEA 2, the decision was made to split into four distinct arrays due to the shape and size of the visual cortical areas. Three arrays (MEA 2A-C) were placed into well studied visual areas V1, V2, and V4, that together process incoming retinal information by stimulus position, orientation and spatial frequency (gratings), direction of stimulus motion, stereoscopic integration, object recognition, spatial vision and attention. It allows us to study the global transformation of visual input in areas with increasing retinotopic complexity; from V1 to V4. The fourth and final array (MEA 2D) was planned for area 7a. This area is considered to be important for spatial perception and is modulated by saccadic activity, visually guided arm movements, memory tasks, visual memory and

attention, and movement planning (Chapter 1.4.3; Andersen et al. 1990; Barash et al. 1991; Steinmetz 1994; Snyder et al. 1996). There are other important candidate structures that are subcortical or lie in the sulci, but considering the limitation that we can only implant in cortical surface areas, we believe our MEAs are placed in the optimal positions to explore visuomotor coordination and cortical network dynamics during a visually guided motor task.

The exact locations were decided upon using the BrainSight neuronavigation system, using MRI data obtained from monkey Y prior to surgery (Figure 4.2).

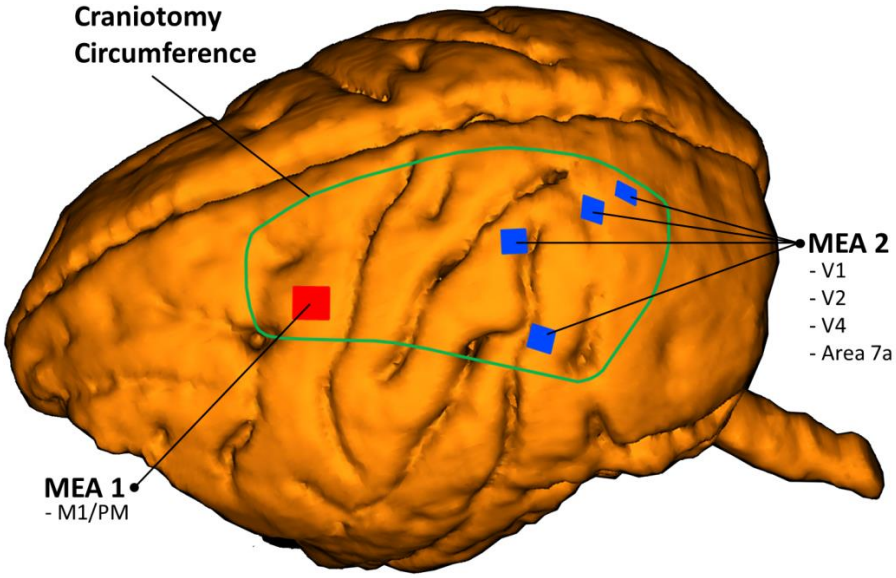

Figure 4.2: BrainSight reconstruction from monkey Y MRI data with MEA 1 and MEA 2 placements and single craniotomy location. From these locations electrophysiological activity at the level of visual input and motor output (M1 and V1), visual information processing (V1, V2, and V4), and visually-guided arm movement and planning (area 7a and PMd) could be recorded.

It should be mentioned that implanting arrays into different visual areas may lead to the receptive fields that do not align. However, at V2 the central visual field is magnified relative to that of the periphery, with receptive fields increasing in size with increasing eccentricity. These receptive fields become even larger in V4 (Figure 4.3) and beyond, with the visual field becoming somewhat disorderly represented due to a variety of different inputs (Gattass et al. 1981; Gattass et al. 1988; Freeman & Simoncelli 2011). These visual areas all have a specific retinotopic organization, but we are interested in a more global effect of coordinated visuomotor behavior, and not so much in the rigorous mapping of visual input from the retina to neurons of ascending visual areas.

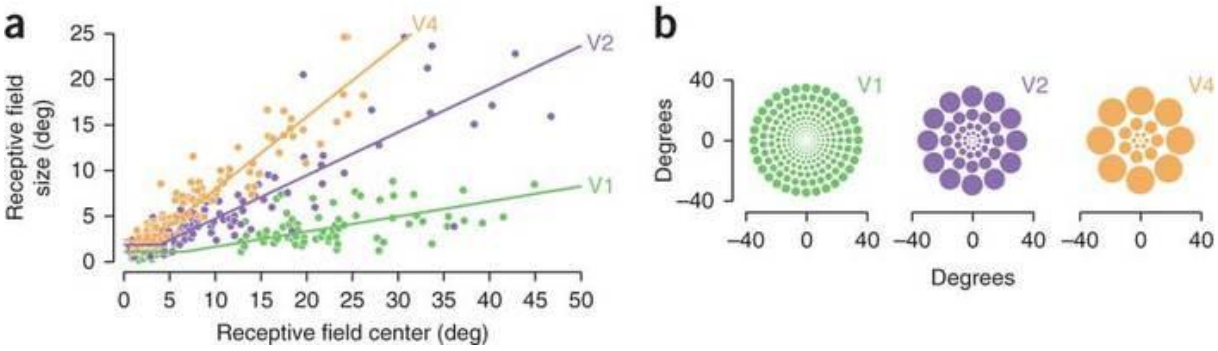

Figure 4.3: Physiological measurements of receptive field size in macaque (From Freeman & Simoncelli 2011). A) Receptive field size (diameter) as a function of receptive field center (eccentricity) for visual areas V1, V2, and V4. B) Cartoon depiction of receptive fields with sizes based on physiological measurements. The center of each array is the fovea. The size of each circle is proportional to its eccentricity, based on the corresponding scaling parameter.

4.2 Surgical Procedures

In order to achieve successful implantation, several surgical stages had to be performed. The surgical staff consisted of a veterinarian surgeon and primate anesthesiologist (from the INT), a consultant pediatric surgeon (from the neighboring university hospital La Timone, two experts in 'Utah' MEA implantation (AR, INT, and Nicholas Hatsopoulos, University of Chicago), and three supporting members providing supplies, assistance, and documenting procedures and progress on paper, photo and video. Medication for starting and maintaining anesthesia was given to the monkey in his home cage, via an injection of the outer thigh (starting with robinul 0.45ml, after 15 minutes followed by ketamine 0.8ml and rompun 0.2ml). The effect of ketamine would last 20-30 minutes, and the monkey was transported to the preparation room, where he was shaved around the relevant areas. The monkey was placed onto a sterile operating environment, with the head into a stereotaxic instrument (David Kopf), providing stability and ensuring precise alignment for the placement of the MEAs. Intubation was performed to ensure gas anesthesia (isoflurane 2-2.5% in 40:60 O^2-air). Monitoring devices for heartrate and CO^2-levels were attached. The skin was incised and the galea aponeurotica (tough, fibrous tissue) and temporal muscles were drawn back until the relevant skull area is exposed. The planned area of the craniotomy (see green circumference in Figure 4.2) was drawn on the skull with a steril pencil, as well as the placement of the connectors. This is followed by a careful process of cutting the bone with a drill, until the bone piece can carefully be lifted to expose the dura mater, a thick membrane that is the outermost layer that surrounds the brain. To prevent cortical swelling, 2 ml/kg of mannitol i.v. was slowly injected over a period of 10 minutes. The dura is the final barrier between the

fragile brain/spinal cord and the outside world, and is essential to retaining the cerebrospinal fluid. It must be cut carefully with enough room from the edge to suture it back after the implantation is completed (Figure 4.4). The area is subsequently covered with an artificial transparent dura to secure the exposed cortical area while the connectors are placed and attached with titanium bone screws into the pre-drilled holes in the skull. The fragile wire bundles of the MEA are placed in a pre-drilled artificial groove leading from the connector to the exposed area. Once the connector is fixed and the MEA is ready for implantation, the artificial dura is removed, and the gold MEA wiring is teased into place with two specialized tweezers. Once the MEA is correctly resting on the target area, a pneumatically-actuated inserter (Array Inserter, Blackrock Microsystems) is used to implant the MEA into the cortical tissue, insuring minimal tissue damage. Once inserted, an artificial and non-absorbable dura (Preclude, Gore-tex) is placed on top of the exposed area with newly implanted MEA, and the natural dura is sutured shut and covered with a piece of an artificial absorbable dura (Seamdura, Codman). The bone flap is subsequently placed back onto the exposed area, and fixed with titanium plates (Bioplate, Codman) and with gelfoam in the edges that promotes bone growth. This is also the case for the groove with the exposed MEA wires, so that these will become encased in bone. Once finished, the skin is sutured back around the connector. The monkey received a full course of antibiotics and analgesics before returning to the home cage (~1-2 weeks recovery).

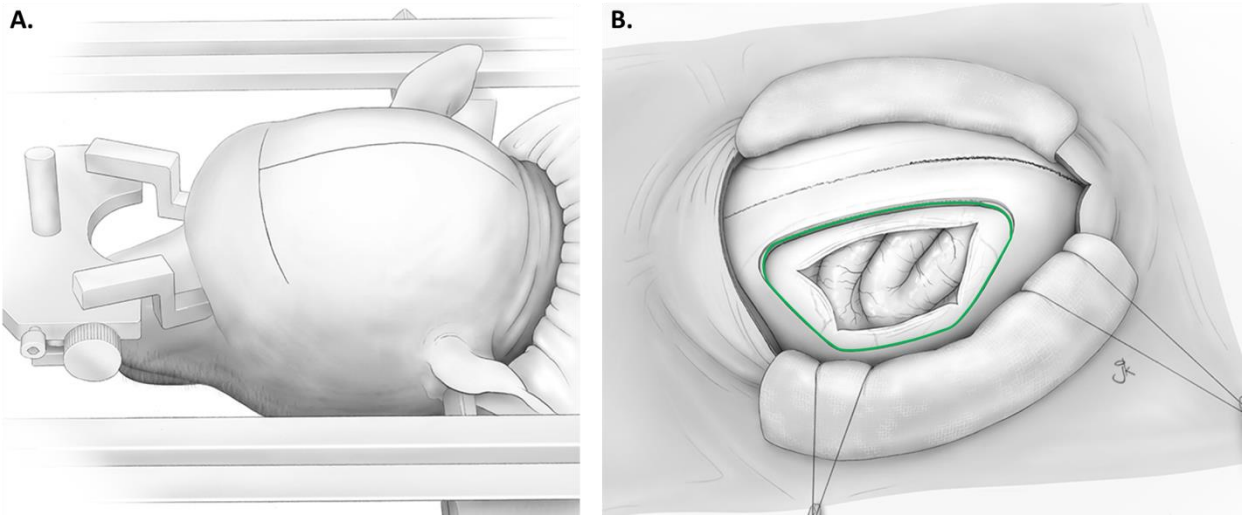

Figure 4.4: Craniotomy illustrations by Juna Kurihara (2011**)**. A) Monkey placed into stereotaxic instrument. B) Incised skin with drawn muscles and galea, and incised dura mater exposing the brain.

4.3 Results

The surgery outlined in the previous chapter reached the initial stages of implantation with monkey Y, but encountered complications at the point when the four separate MEAs from MEA2 were resting on the artificial dura mater ready to be implanted (Figure 4.5), with fatal consequences. The general consensus between surgical staff on the cause was an air embolism due to a strong bleeding of the skull during the craniotomy, leading to arrhythmia, heart chamber failure and ending in maximum circulatory arrest. In response, data from a previous study was made available to explore how single unit recordings from multiple MEAs could be analyzed in the framework of our Vision-for-Action project. We were particularly interested in exploiting the full potential of multi-electrode recordings, by looking at methods that allow us explore the functional interactions between individual neurons.

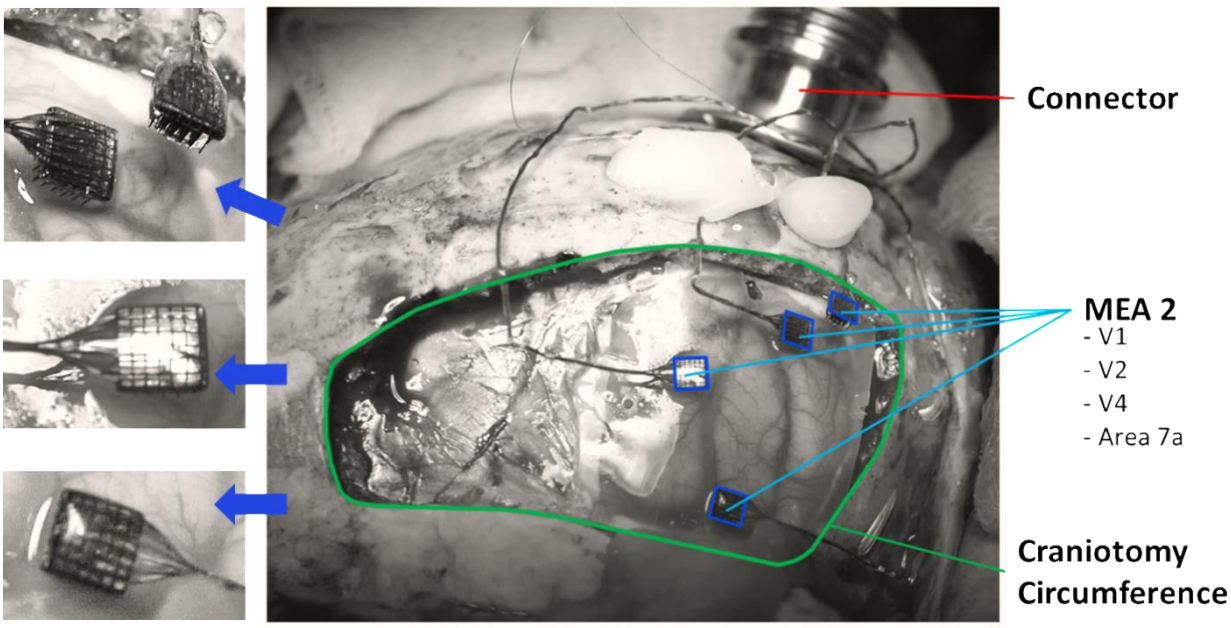

Figure 4.5: Craniotomy of monkey Y. The 4 MEAs (blue squares) resting on the artificial dura mater before final implantation. The MEAs are magnified in the left panels. The green circumference marks the borders the craniotomy. The connected in the back is temporarily attached with only a few screws before the final position is fastened.

5 NOISE CORRELATION

5.1 Introduction

The spiking activity of a single cortical neuron during repeated, controlled behavior or stimulus presentation is very variable. Even when the stimulus is the same across trials, the firing rate differs markedly from trial to trial (Perkel et al. 1967; Softky & Koch 1993; Arieli et al. 1996; Gutnisky & Dragoi 2008; Churchland et al. 2010). However, the combined activity of a number of neurons may show emergent properties of an ensemble which reflects aspects of sensory and/or motor variables. In sensory areas, for instance, encoding information is possible through neurons with the same responses to the same stimulus (redundant information), different responses to the same stimulus (independent information), or cooperative responses to encode more information between neurons than they do separately (synergistic information; Gawne & Richmond 1993). How this is carried out, and how these population codes contribute to computation of visually guided motor behavior for example is not fully understood. This is exacerbated further by the general variability of neurons, which means it would be difficult to estimate exactly what stimulus occurred if one were to investigate a noisy population response (Softky & Koch 1993; Stevens & Zador 1998; Averbeck et al. 2006). If this noise came from independent fluctuations in the activity modulation of one neuron around its average, the population code would be easier to understand, but noise in the brain can indeed be correlated, fundamentally affecting the outcome when combining activity in a neuronal pool (Shadlen & Newsome 1994). This shared variability of activity among neurons is known as *noise* correlation, and has been used to aid inferences about anatomical connectivity (Toyama et al. 1981b; Ts'o et al. 1986; Ko et al. 2011) and, more predominantly, used to determine the capacity of neurons to transmit information, i.e. representational capacity (Lee et al. 1998; Averbeck et al. 2006, Kanitscheidera et al. 2015). A common finding in studies exploring the underlying mechanisms of trial-by-trial fluctuations during periods of spontaneous or evoked activity in the visual cortex is the tendency of depressed correlation in the presence of visual input versus absence of stimulus (Smith & Kohn 2008).

Our aim here is to explore similar measurements in the motor cortex and expand on them, with behavioral epochs involving spontaneous activity, evoked activity by means of visual input, and evoked activity by means of motor output. Calculating noise correlation is done by

measuring the degree to which trial-to-trial fluctuations in response strength are correlated between two neurons (Cohen & Kohn 2011). This measure is known as *spike count correlation (r_{sc})* and requires large amounts of data from simultaneously recorded neurons, as well as a stringent control and understanding of the experimental and physiological factors. This measure is not to be confused with *signal* correlation, which measures the tuning similarity (redundant, independent, and synergistic information) between two neurons by correlating the mean responses of a neuron pair to different stimuli (Cohen & Kohn 2011). The term correlation in this chapter refers specifically to noise correlation, unless stated otherwise. A general finding based on multiple noise correlation studies predominantly in the visual areas (Table 5.1, Cohen & Kohn 2011) is that correlations between the firing of neurons within predefined analysis windows are small and positive (Schulz et al. 2015), which tend to be highest between neurons that are near to each other and have a high signal correlation, indicating similar functional properties or tuning. Noise correlation is also generally regarded as being restricted to subsets of neurons, as noise correlation between neurons from different hemispheres are close to zero (Cohen & Maunsell 2009). Poort and Roelfsema (2008) investigated how well V1 neurons distinguished different elements from an image that belong together from elements that do not belong together. The noise correlation coefficient was found to be consistent with previous studies (0.21), but a relationship between the strength of correlation and distance between recording sites was not found, and the authors found little influence of the stimulus on the strength of correlation. Finding a positive noise correlation (r_{sc}) between the activities of neurons with different stimulus selectivities allows for a subtraction of this common noise without signal loss, whereas positive correlations between the activities of neurons with same selectivity provides partially redundant information (Romo et al. 2003). It was concluded that these two effects of noise correlation cancel each other out, bringing the overall coding accuracy close to that without noise correlation, which means that noise correlations had no effect on the sensitivity of the population in this particular situation. In contrast, Cohen & Maunsell (2009) published findings that showed that attention influences noise correlations and did indeed improve population sensitivity in V4. Attention decreased noise correlation in V4 neurons in a change-detection task, improving the amount of sensory information encoded and, as a consequence, improving the performance.

In two studies exploring noise correlation in motor cortex, correlation coefficients (r_{sc}) were consistently lower than those found in visual areas, but showing different values in each

study, ranging from 0.1-0.2 in Maynard et al. (1999) and 0.02-0.04 in Lee et al. (1998). In both studies the same reaching task was used, a 8-direction center-out task, but other parameters were different, e.g. the mean firing rates considered (~20 spikes/s versus ~5 spikes/s), the duration of the analysis window (600ms versus 1000ms), the recording technology (chronically implanted 'Utah'-Arrays versus acutely inserted electrodes by using the 7-electrode Thomas-recording system), the species of macaque monkey (fascicularis versus mulatta) and the spike sorting approaches. These studies have different systematic bias influencing correlation estimates which, at least in part, causes these discrepancies. It is important to note that the correlational strength is in fact variable between studies regardless of the brain area, not just the motor areas, and still a point of contention. For example, in early visual studies recordings were performed from V1 in anesthetized animals and only moderate correlation has been reported (Reich et al. 2001: r_{sc} = 0.25; Kohn & Smith 2005: r_{sc} = 0.2; Smith & Kohn 2008: r_{sc} = 0.16), which was later shown to be likely dominated by coordinated fluctuations caused by opioid anesthesia (Ecker et al. 2014). After correcting for this factor, correlations dropped to levels similar to those observed in awake animals. In an earlier study Ecker and colleagues also challenged studies reporting a high degree of correlated variability between the activities of nearby neurons, by recording from awake monkeys with chronic tetrode arrays (Ecker et al. 2010). They found no shared variability between nearby neurons, even when they were similarly tuned, which in turn challenges the assumption proposed by Lee et al. (1998) and Smith & Kohn (2008) that a shared common input drives noise correlation. These and previous findings show that before noise correlation values are interpreted, careful framing of a controlled experiment is needed, taking into consideration the impact of task conditions, state of awareness of the animal, recording equipment, data processing and analysis techniques, systematic bias, size of the area recorded, and the location of recordings, i.e. brain region, even to the level of the cortical layer. It seems the theme in several review articles on the subject of correlational coding is to be extremely careful with interpreting results, emphasizing subtle pitfalls that bias findings significantly (Averbeck et al 2006; Cohen & Kohn 2011; Kohn et al. 2016).

With the massively parallel electrophysiological data generated by our Vision-for-Action project we will have the opportunity to measure noise correlation in different areas under the same experimental parameters. To gain proficiency with the measure of noise correlation known as spike count correlation (r_{sc}), data from three monkeys in an instructed-delay reach-to-grasp experiment was analyzed in collaboration with fellow PhD candidate Margaux Duret.

Table 5.1: Summary of studies measuring spike count correlations in primates (from Cohen & Kohn 2011)

Reference number	Area	Firing Rate (spikes/sec)	Duration (ms)	State (task, anesthesia, etc.)	r_{sc}
Kohn & Smith (2005)	V1	~25	2,560	Anesthetized	0.2
Smith & Kohn (2008)	V1	~8	1,280	Anesthetized	0.16
Reich et al. (2001)	V1	na	1,894	Anesthetized	0.25
Rasch et al. (2011)	V1	na	na	Anesthetized	0.26
Gutnisky & Dragoi (2008)	V1	~50	1,860	Fixation	0.25
Ecker et al. (2010)	V1	~3	500	Fixation	0.01
Poort & Roelfsema (2009)	V1	na	400	Tracing	0.18
Samonds et al. (2009)	V1	30	1,000	Discrimination	0.1
Cohen & Maunsell (2009)	V4	21	200	Attention/detection task	0.04
Mitchell et al. (2009)	V4	>5, ~20	800	Attention/tracking task	0.05
Huang & Lisberger (2009)	MT	~20	500	Fixation	0.1
Cohen & Newsome (2008)	MT	28.5	500	Discrimination	0.13
Bair et al. (2001)	MT	~20	1,000	Discrimination	0.15
Erickson et al. (2000)	Perirhinal	~12	200–500	Fixation/matching task	0.02
Averbeck & Lee (2006)	Supp. motor area	na	66 or 200	Serial reaching	0.013
Averbeck & Lee (2003)	Supp. motor area	~15	200	Reaching	0.02
Stark et al. (2008)	Premotor areas	~5	400	Grasping/imagery task	0.02
Maynard et al. (1999)	M1	~20	600	Reaching	0.1–0.2
Lee et al. (1998)	Motor/parietal; areas 2/5	~5	1,000	Reaching	0.02–0.04
Nevet et al. (2007)	Substantia nigra	58	500	Cue matching	0.01–0.04
Cohen et al. (2010)	FEF	~50	few hundred	Visual search	0.05–0.2
Bichot et al. (2001)	FEF	~20	~200	Visual search	0.09
Constantinidis & Goldman-Rakic (2002)	Prefrontal	~5	3,000	Delayed saccade task	0.08

From Cohen & Kohn 2011 (page 813): "These studies measured correlations in a variety of brain areas, behavioral and stimulus conditions, and measurement durations and between pairs of neurons that varied in the cortical distance and tuning similarity. When multiple values of correlations, firing rates and measurement windows were reported, Cohen & Kohn listed either the average or most common value that was listed in the text or estimated from summary figures".

Partially, the same data was used in a previous study to determine spike synchronization patterns in relation to behavior. It has been found that the percentage of neuron pairs with the same pattern of synchronous spikes (precision of 5ms) relative to the total number of neuron pairs decays with increasing distance between neurons (Torre et al. 2016, Figure 5B: 32% at 1mm, 21% at 4mm for monkey L; 40% at 1mm, 9% at 4mm for monkey N). This decay of neuron pairs with synchronous spike patterns is in line with distance effect findings in signal correlation and noise correlation (Smith & Kohn 2008, Kohn et al. 2016). Using methods outlined in the noise correlation papers in motor cortical areas mentioned before as a basis (Lee et al. 1998; Maynerd et al. 1999), we determined whether the amount of noise correlated

neuron pairs does indeed decrease with distance, as well as firing rate strength, and explored correlational strength and significance changes in a time-resolved manner across different epochs within a reach-to-grasp trial.

5.2 Methods

5.2.1 Data aqcuisition

Data was collected from a study investigating how information from largely segregated motor cortical networks that control hand shaping and grasp force is processed and integrated (Riehle et al. 2013). The data were recorded from single 'Utah' arrays (96 active electrodes) chronically implanted in the motor cortex of three monkeys during an instructed-delay reach-to-grasp task, monkey L, monkey N, and monkey E. The task protocol is described in detail in Riehle et al. (2013) and in Torre et al. (2016). To summarize, the monkey was trained in an instructed delay task. Each trial was initiated by resting the hand on a switch for 400ms, at which time a yellow light-emitting diode (LED) warned the monkey that the instruction cue will occur in 400ms. This cue informed by means of a 4 LED pattern about the type of *grip* to be used during this trial: a full-hand side grip (SG) or a two-finger precision grip (PG).

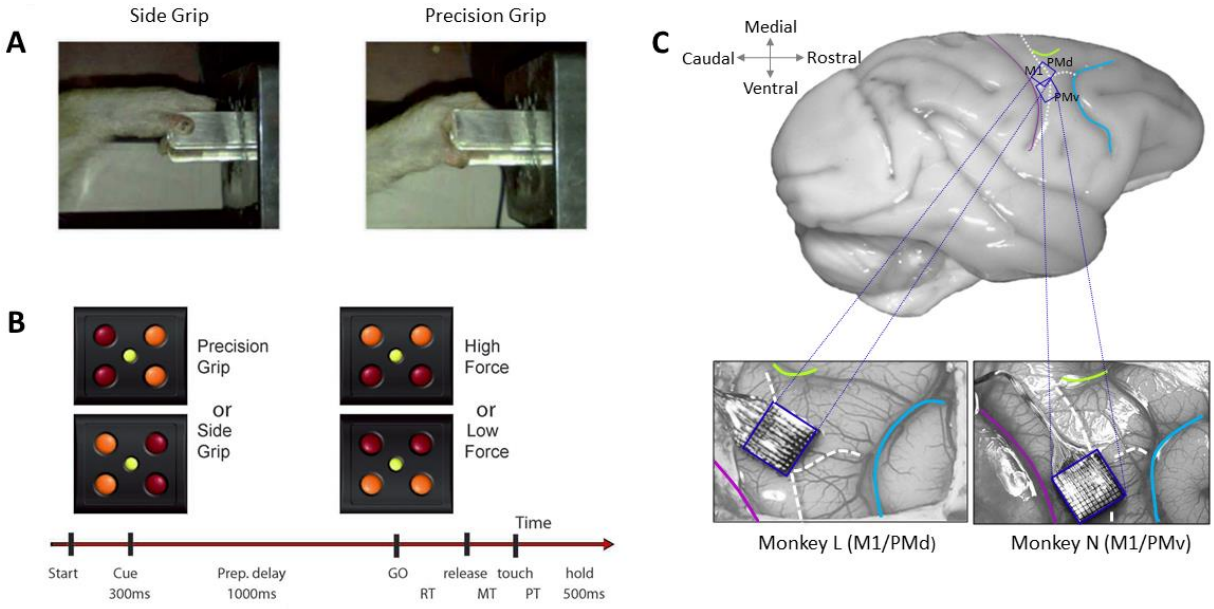

Figure 5.1: Experimental design. A) The type of grip the monkey must use to pull the object: side grip and precision grip. B) At Cue and GO two LEDS give the monkey trial information on the upcoming grip type and force type. The monkey must execute the correct grip type and anticipate the force required to get the reward. C) Implantation sites of monkey L and N. Adapted from Duret et al. (in preparation) and from Riehle et al. 2013. Note that this is a putative distinction from the location of the array on the cortical surface, there is no physiological (i.e intracranial microstimulation, or ICMS) or histological (post-mortem) control.

This instruction was given for another 300ms, after which a delay period of 1000ms started, where the hand of the monkey had to remain on the switch. At the end of the delay period, the final GO cue appeared by means of another 4 LED pattern informing what level of *force* has to be employed: low force (LF; 1N) or high force (HF; 2N). The monkey then had to release the switch (switch release; SR), grasp, pull and hold the object for 500ms to complete the trial and receive a apple sauce reward. Thus, the monkey had to perform 4 possible grip/force combinations: SGHF, SGLF, PGHF or PGLF (Figure 5.1A & B). The grip/force combinations were randomly presented within a session that lasted ~15 minutes, with a sequence of 100-200 successful trials. Once the monkey hit a performance level of 85% correct trials, a 100-electrode Utah array was surgically implanted contralateral to the working hand in the motor cortex, between the central sulcus and arcuate sulcus (See Figure 5.1C for implantation sites monkey L and N). Electrophysiological data was recorded at 30 kHz with the same 128-channel Cerebus DAQ system used as in our RIVER setup, in parallel with 1 kHz behavioral data (switch release, stimuli type and onset, force traces, and object displacement).

Electrophysiological recordings were subsequently filtered in two frequency bands, leaving the local field potential (LFP, 0.3-250 Hz) and spiking activity (0.25 – 7.5 kHz). Waveforms of potential spikes were sorted on each electrode using the Offline Spike Sorter (Plexon v3.3) into single-unit spiking activity (SUA). After selecting only neurons whose spike waveform had a signal-to-noise ratio > 2.5 (Hatsopoulos et al. 2004), we included 18 sessions from monkey L with 1556 neurons, 13 sessions from monkey N with 1741 neurons, and 13 sessions from monkey E with 1783 neurons.

5.2.2 Noise Correlation

The measure of noise correlation was calculated as follows: the number of spikes (spike count) of a neuron in a predefined time window across repeated trials, with identical stimuli and conditions (to exclude any possible bias due to signal correlation), was correlated with the spike count of another neuron recorded simultaneously during the same trials (Pearson's *r*). This measure is defined as *spike count* correlation, or r_{sc}, and measures the degree of shared trial-to-trial fluctuations between the activities of a pair of neurons during a specific time window of the trial. The length and occurrence of the analysis window across trials is generally coupled to a specific task-related event or behavioral event, but can also be explored

using a sliding window analysis if there is no *a priori* expectation of event-related impact on noise correlation.

5.2.3 Spike Count Correlation (r_{sc}) during Six Epochs

In our data we used similar analysis windows as those defined in Torre et al. (2016) where six epochs were identified to detect patterns of synchronous spikes during periods related to specific behavioral contexts. We used these 6 windows to explore spike count correlation (r_{sc}), each with a duration of 500ms and with data aligned to various events (GO-signal, switch release or reward):

1. **Start** from *Start*-250ms until *Start*+250ms, data aligned to event GO-signal. In this period the monkey had to sit quietly with the hand on the table switch awaiting the occurrence of the Cue. This period served as a 'baseline' condition for noise correlation.

2. **Cue** from *CueOn* until *CueOn*+500ms, data aligned to event GO-signal. In this period, visual stimuli provide information about the *grip* type.

3. **Early Delay** from *CueOff* until *CueOff*+500ms, data aligned to event GO-signal. During the first half of the preparatory delay of 1s, visual information concerning the *grip* type is to be processed.

4. **Late Delay** from *SR*-700ms until *SR*-200ms, data aligned to event SR (switch release = movement-onset; mvt in Figure 5.2). The second half of the preparatory delay, during which required movement has to be prepared.

5. **Movement** from *SR*-200ms until *SR*+300ms, data aligned to event SR. The period where visual information about the *force type* is given and the reaching movement is initiated, showing massive change in spiking activity related to movement onset.

6. **Object Hold** from *Reward*-500ms until *Reward*, data aligned to event Reward. Period during which the monkey must sustain object position until the reward is given.

Only data which had a minimum spiking activity of 2 spikes per analysis window were included in the analyses, as undersampling could lead to biased results (Cohen & Cohen 1983). Aligning the data correctly to the signals (Cue, Start, GO) and movement onset (SR) within each respective window is important in order to avoid unintended correlations.

5.2.4 *Fano factor (FF)*

In the next step of our analysis, we were interested in characterizing how the noise correlation of a neuron pair relates to the individual trial-to-trial firing rate variability of each individual neuron. This was done by calculating the Fano factor (FF), i.e. the ratio of the variance and the mean spike count of each neuron within each window (Shadlen & Newsome 1998; Nawrot et al. 2008). A high FF indicates a high variability across all trials, whereas a low FF indicates less variability across all trials. We compared the FF of pairs of neurons with the percentage of pairs with significant or insignificant r_{sc} values. For each given pair of neurons, the FF represented the geometric mean of the FF of two individual neurons.

5.2.5 *Spike Count Correlation as a function of Firing Rate & Distance between Neurons*

The distance between neurons may impact the strength of correlation, with neurons located nearby generally having a higher correlation than neurons further away (Kwan et al. 1987; Smith & Kohn 2008). Electrodes in the 'Utah' array are spaced 0.4mm from each other, placed in a 10x10 matrix on a surface area of 4x4mm. The maximum distance between electrodes (electrode 1 to electrode 100 for example), is ~5.5mm. However, the amount of possible neuron pairs at this maximum distance is very low, which exposes the inherent spatial bias: there are more neuron pair possibilities at half the surface area than possibilities of neuron pairs between neurons that are near each other or far apart. We therefore categorized neuron pairs based on the distances between the neurons into short (0.4mm to 1.5mm), medium (1.5mm to 3mm), and long (> 3mm) distances, and reported mean r_{sc} and the *n* for each group. Note, that we never analyzed neurons recorded on the same electrode; this could bias the spike count correlation, and drive the correlation upwards. In order to calculate the mean r_{sc}, the absolute individual correlation coefficients were transformed into Fisher's z, averaged, and the result re-transformed into Fisher's r. We used absolute correlation coefficients because the distribution of spike count correlations were equally positive and negative regardless of firing rate, and we were only interested both in the strength of correlation and in the amount of significant correlations. Had the distribution been asymmetric, with a weak negative tail and a heavy positive tail as was the case in V1 data of Schulz et al. (2015), this would not have been possible.

In parallel, we explored noise correlation as a function of firing rate, averaging in each analysis window the firing rate of the neuron pairs and grouping them into low (2-6 spks/window for monkey L & N; 2-5 spks/window for monkey E), medium (6-11

spks/window for monkey L & N; 5-9 spks/window for monkey E) or high (>11 spks/window for monkey L & N; >9 spks/window for monkey E), and reported the number of analyzed pairs of neurons (*n*) for each group. The firing rate was generally lower in the sessions of monkey E than in the sessions of monkey L and N (see Figure 5.5), which is why a lower threshold was used per firing rate group for monkey E. As in the case of the distance groups, the mean r_{sc} per firing rate group was calculated, as well as the percentage of significant correlations for the epochs.

5.2.6 Spike Count Correlation as a function of Spike Width

In the final step of our analysis we were interested to see if different neuron types are differently involved in noise correlation. For each neuron, we estimated the spike width from the trough-to-peak duration of the spike waveform. For each monkey, the distribution of spike widths of all neurons revealed to be bimodal. In order to categorize neurons by spike width, we defined two borders in the distributions of spike widths, splitting the neurons into groups of narrow spikes and broad spikes. Subsequently, we calculated the r_{sc} for neuron pairs that consisted of only putative interneurons (narrow-narrow pair), putative pyramidal neurons (broad-broad pair), and a mix of both (narrow-broad pair) in different periods.

5.3 Results

5.3.1 Firing rate profiles & the data set

Figure 5.2 shows that during the movement epoch, modulations of neuronal activity in each trial occur at the same time with respect to GO (Figure 5,2A) but at different time with respect to the GO (Figure 5.2B). In Figure 5.2A we see spike occurrences ("raster display") during 35 trials for neuron 1 on 'Utah'-array channel 56 (*Chan56.n1*, green markers), with the data aligned to the GO-signal (sorted by ascending reaction times, the time between the GO-signal and movement onset and indicated by the first set of red markers). Spike time markers for neuron 2 on channel 55 (*Chan55.n2*) and neuron 1 on channel 58 (*Chan58.n1*) are shown in blue, underneath *Chan56.n1* in Figure 5.2A. By comparing the spike occurrences we can already see that spiking activity in *Chan56.n1* decreases before movement onset ('Mvt' red markers) and strongly increases directly after it. In *Chan55.n2* a period of inhibition occurs around movement onset, followed by increased spiking activity, and in *Chan58.n1* no obvious increase or decrease in spiking activity is noticeable. These differences are more pronounced when we align the data to the behavioral event SR, shown in Figure 5.2B for the same

neurons. These three neuron examples illustrate the variability of firing rate profiles with respect to movement execution. In Figure 5.2C we show the six 500ms windows in the trial time as discussed above, with 1) Trial Start, Cue, and Early Delay aligned to the GO-signal, 2) Late Delay and Movement aligned to SR, and 3) Hold aligned to Reward.

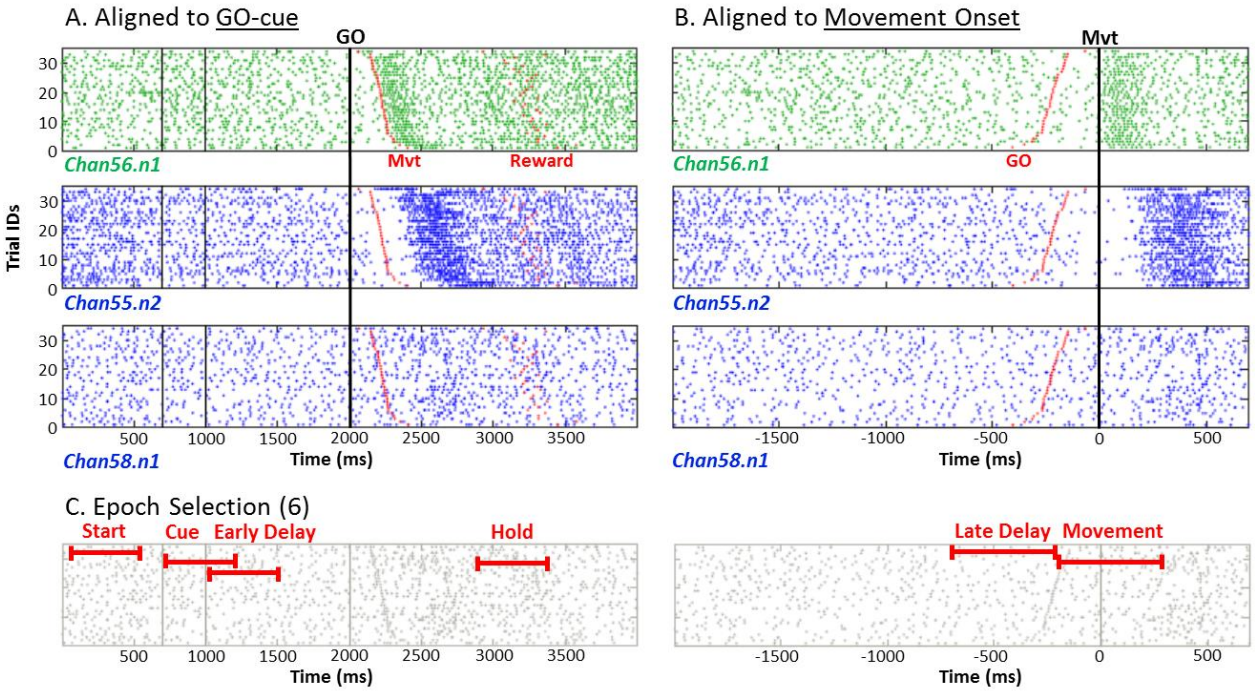

Figure 5.2: Examples of spiking activities of 3 neurons across 35 trials (*Chan56.n1, Chan55.n2, & Chan58.n1*), aligned to trial event GO-signal (A) and behavioral event SR (B). The six 500ms windows used to correlate between neurons are indicated with red bars in (C).

In Figure 5.3 the mean firing rates (spikes/second) of the same example neurons are shown: the green *Chan56.n1* and the two blue *Chan55.n2* and *Chan58.n1*.

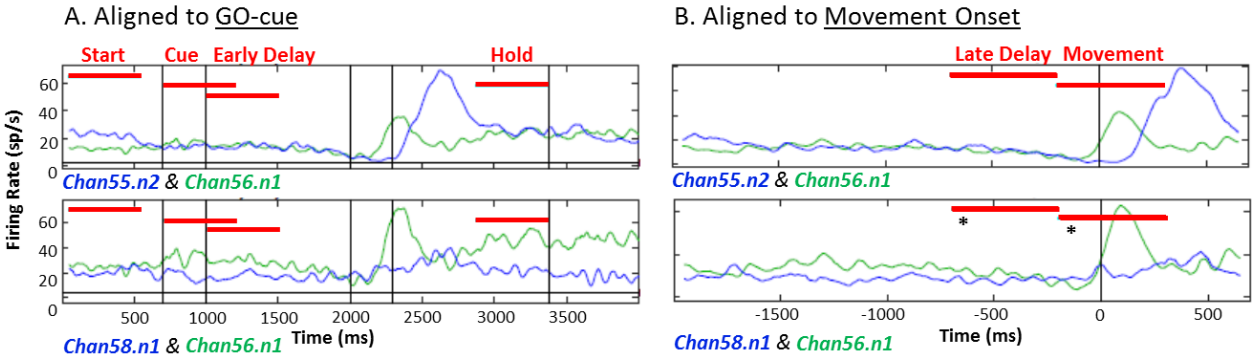

Figure 5.3: Average firing rate (sp/s) of example neurons: Chan56.n1 (green) and Chan55.n2/Chan58.n1 (blue). Red bars indicate six 500ms time window in which the average spike count is correlated between neurons. *Significant noise correlation ($p<0.05$).

For these three example neurons, we found a significant spike count correlation ($p < 0.05$) in the Late Delay and Movement period between *Chan56.n1* and *Chan58.n1*, which would indicate a shared variability between these neurons during these periods. The r_{sc} calculation used in our example neuron pairs in Figures 5.2 and 5.3 was repeated in the remaining neurons across all sessions within the six indicated 500ms windows for trial-type 'Side-Grip/High-Force' (SGHF), in all three monkeys. The three remaining trial-types, 'Side-Grip/Low-Force' (SGLF), 'Precision-Grip/High-Force' (PGHF), and 'Precision-Grip/Low-Force' (PGLF) showed similar results and no trial-type specific effect.

5.3.2 Spike Count Correlation (r_{sc}) during Six Epochs

The amount of correlated neuron pairs across all sessions within the six windows for all three monkeys is shown in Figure 5.4A. The activities of 6.5% to 12% of all neuron pairs were significantly correlated ($p < 0.05$) for monkey L, monkey N, and monkey E (Figure 5.4B).

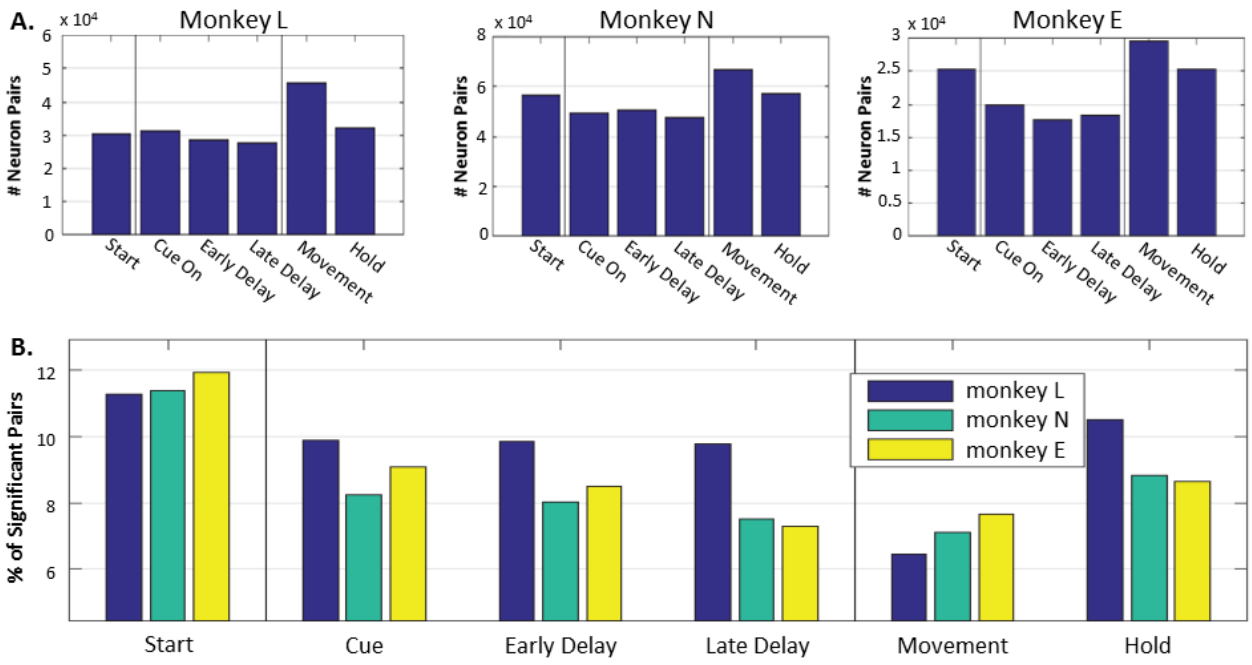

Figure 5.4: Number and percentage of correlated pairs. A) Number of analyzed pairs per time window. B) Percentages of significant noise correlation ($p < 0.05$) per time window, and per monkey.

When we grouped the significantly correlated and uncorrelated neuron pairs of all three monkeys together, the average percentage of significant pairs followed the trend expressed in Figure 5.4B, but with a substantially higher *n* of analyzed pairs in each window (Figure 5.5A).

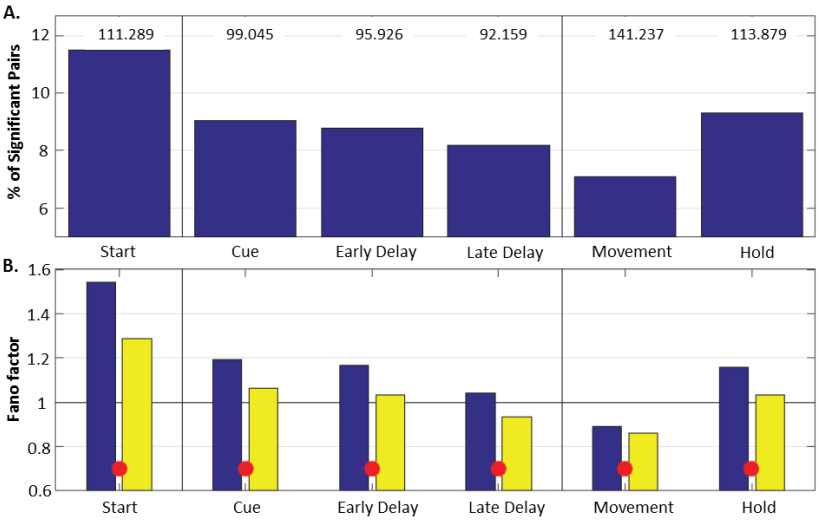

Figure 5.5: A) **Percentages of significant noise correlation** ($p < 0.05$). Number at the top of each bar indicates the amount of analyzed pairs of all 3 monkeys in this time window, during trial type SGHF. B) Fano factor as a function of the significance of noise correlation (all monkeys, red dot = significant difference, $p < 0.05$)

5.3.3 Fano Factor (FF)

In Figure 5.5B the average FF for all significantly correlated and uncorrelated neuron pairs is shown (blue/yellow bars, respectively). These results show that the FF, and therefore the spike count variability, was generally higher in the significantly correlated neuron pairs than in the uncorrelated pairs. More specifically, a higher percentage of neuron pairs was significantly noise correlated (11.5%), with a higher variability (FF=1.54) when the monkey was awaiting a cue in a task, than during a period of movement activity (7.1%, FF = 0.89). Though there was a significant difference in FF during the movement period between significantly correlated and uncorrelated neuron pairs, the difference was small (FF = 0.89 for significantly correlated pairs, FF = 0.86 for uncorrelated pairs). This difference was much more distinct in the 'Trial Start' period (FF = 1.54 for significantly correlated pairs, FF = 1.29 uncorrelated pairs).

5.3.4 Spike Count Correlation as a function of Firing Rate & Distance between Neurons

We focussed solely on the Trial Start and the Movement period in the next analysis: r_{sc} as a function of firing rate and distance between neurons. The mean r_{sc} was calculated in groups where neurons pairs had low, medium, or high firing rates during Trial Start period, represented by the blue bars in Figure 5.6A. The mean r_{sc} in groups with a short (0.4mm to 1.5mm), medium (1.5mm to 3mm), and long (> 3mm) distance between neurons was represented by the red bars in Figure 5.6A. The percentages of significant correlations are shown in Figure 5.6B for firing rate (red bars) and distance (blue bars). In Figure 5.7 the results for the same calculations are shown for the Movement period.

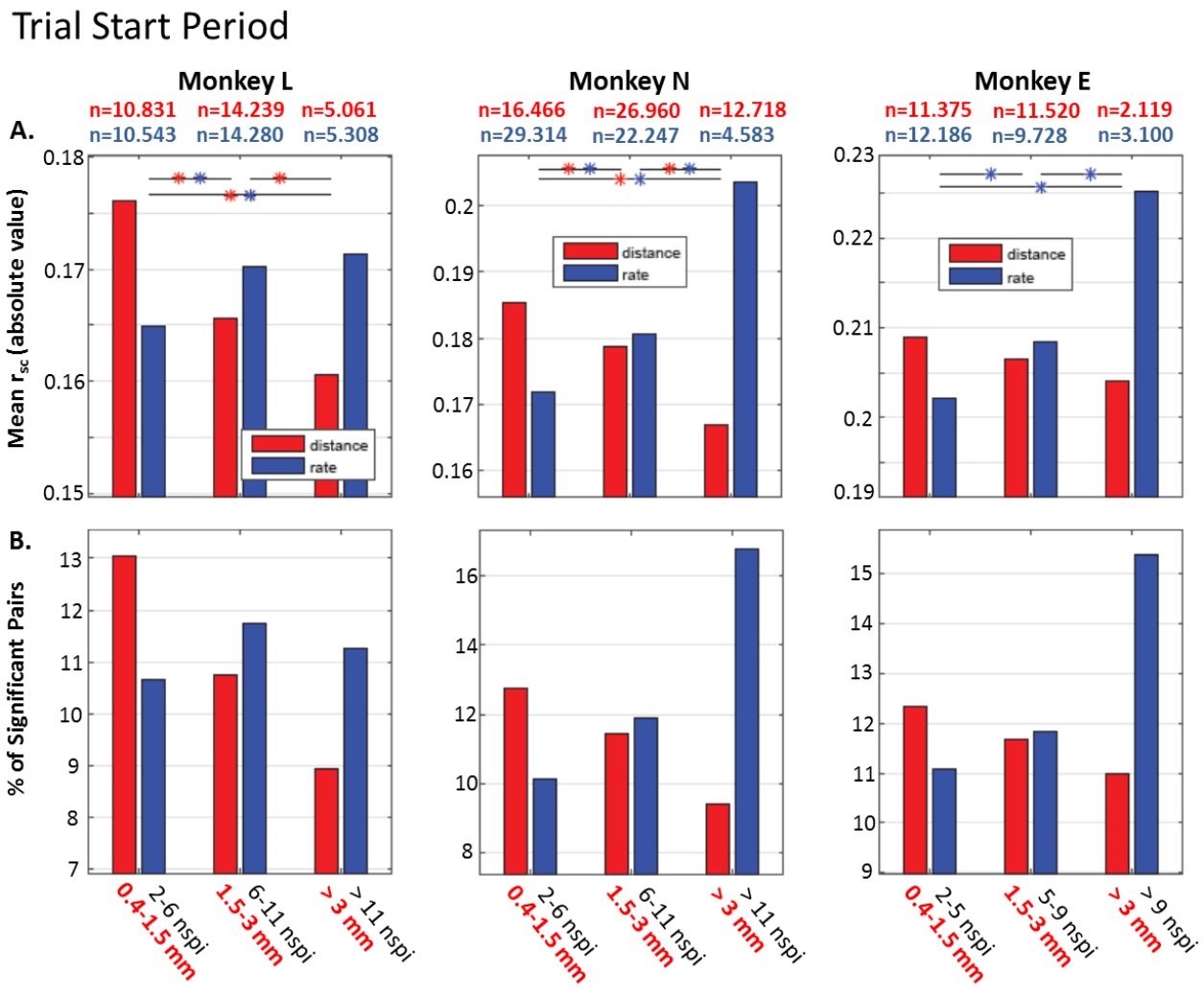

Figure 5.6: Firing rate and distance between neurons during Trial Start: spike count correlation as a function of distance (red bars, in mm) and firing rate (blue bars, in spikes/window, or nspi) during the Trial Start period. A) Mean spike count correlation coefficient (rsc) for distance (short-medium-long) and rate (low-medium-high). B) Percentage of neuron pairs that are significantly correlated for distance (short-medium-long) and rate (low-medium-high).

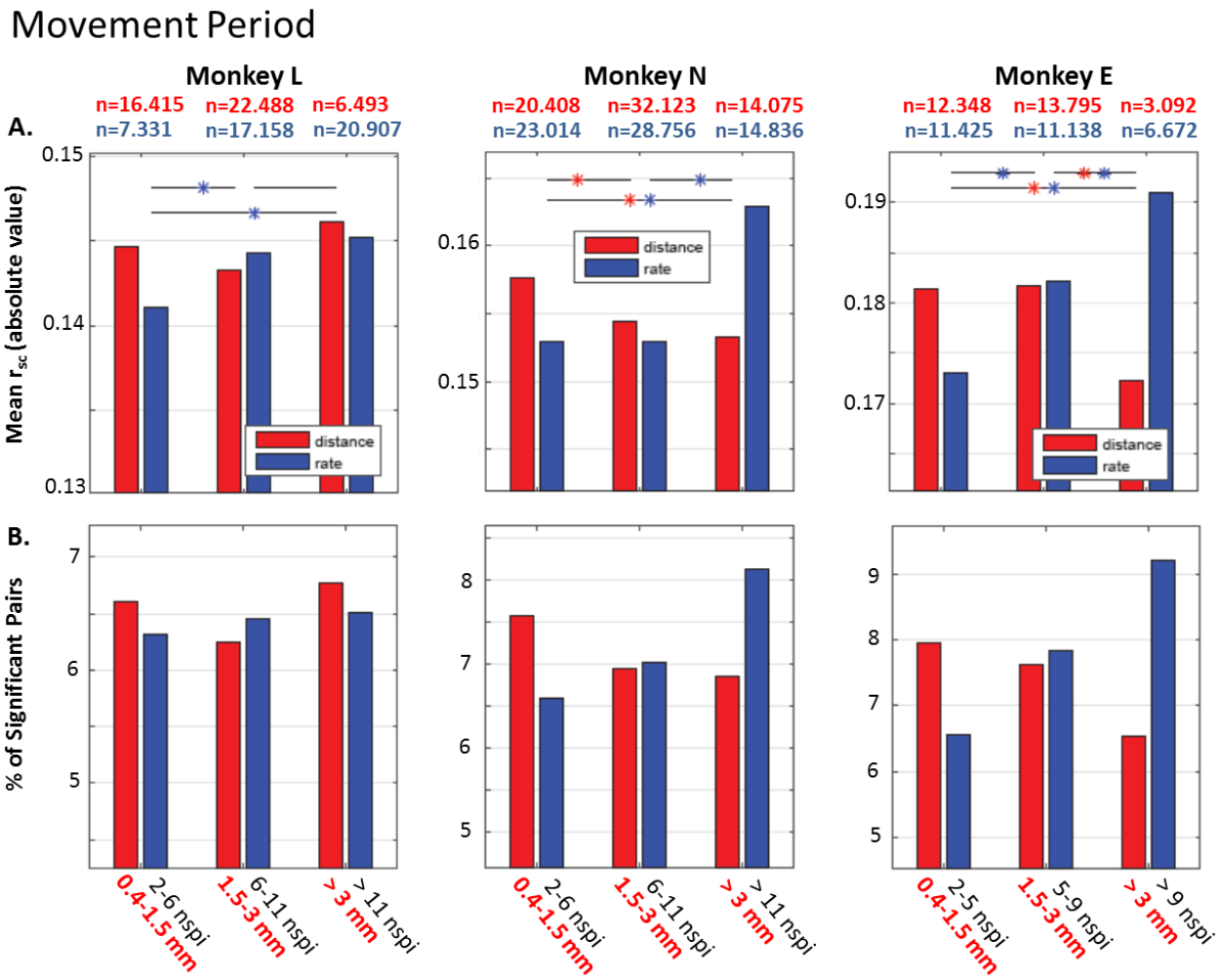

Figure 5.7: Firing rate and distance between neurons during Movement: spike count correlation as a function of distance (red bars, in mm) and firing rate (blue bars, in average spikes/window, or nspi) during the Movement period. A) Mean spike count correlation coefficient (rsc) for distance (short-medium-long) and rate (low-medium-high). B) Percentage of neuron pairs that are significantly correlated for distance (short-medium-long) and rate (low-medium-high).

5.3.5 Spike Count Correlation as a function of Spike Width

The bimodal distribution found in all three monkeys are shown in Figure 5.8A, where two borders in the distributions of spike widths split the neurons into groups of narrow spike neurons (left of the red line) and broad spike neurons (right of the blue line). For monkey L this gave us 927 neurons with an average spike width of 257µs (narrow) and 341 neurons with an average spike width of 439µs (broad). For monkey N this gave us 466 neurons with an average spike width of 277µs (narrow) and 515 neurons with an average spike width of 574µs (broad). Finally, for monkey E this gave us 555 neurons with an average spike width of 240µs (narrow) and 356 neurons with an average spike width of 450µs (broad). Figure 5.8B shows the mean firing rate (spikes/second), per monkey, of neurons categorized in either narrow (red) or broad (blue) spike group.

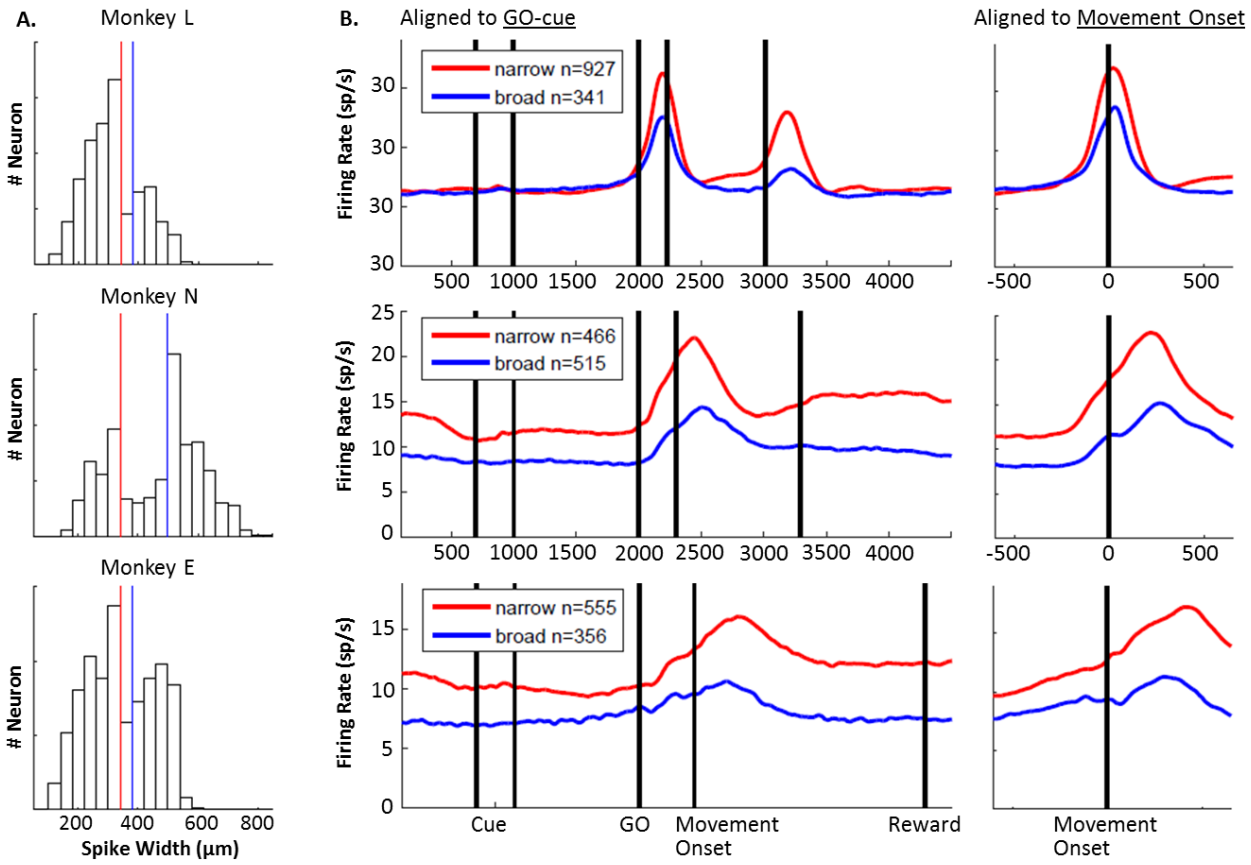

Figure 5.8: Bimodal Distributions. A) Frequency histogram of narrow/wide spike width categorization per monkey. B) Average firing rate for neurons with narrow (red) and broad (blue) spikes.

By grouping neurons into two spike width categories, we see a generally higher firing rate for narrow than broad spike neurons throughout the trial for monkey N and E, and during movement onset and reward periods of monkey L. For all three monkeys the mean firing rate started to increase after the onset of the GO signal, peaking at movement onset and reward onset of monkey L, and peaking later than movement onset in monkey N and E, without the same distinct peak at reward onset as monkey L.

The two different neuron types were then correlated amongst their own type and between types, yielding a relatively high percentage of significantly correlated number between narrow-narrow pairs (Figure 5.9, red bars), a relatively low percentage in broad-broad pairs (Figure 5.9, blue bars), and a percentage in the middle of both types when narrow-broad pairs were correlated (Figure 5.9, green bars). This distinction is most noticeable in the Time start period, with the percentages being much lower during the Movement period for all neuron pairs.

Figure 5.9: Percentage of significantly correlated neurons with respect to spike width. Narrow-narrow pairs (putative interneurons; red bars), broad-broad pairs (putative pyramidal neurons; blue bars), and narrow-broad pairs (mixed; green bars), for monkey L, N, and E, in the two trial epochs: Trial Start and Movement.

5.4 Discussion

We first focused on how the percentage of significant noise correlated neuron pairs changed for all three monkeys during different task epochs, in particular during the Trail Start and Movement period. In the Movement period a clear increase in the number of correlated neuron pairs was found in all three monkeys, relative to the other 500ms epochs. During this period, motor neurons involved in movement initiation and execution were highly active, increasing the number of neurons satisfying the firing rate criteria (>2 spikes/window) for the calculation of noise correlation, which in turns increased the number of observed correlated pairs (Figure 5.4A). However, when looking at the percentage of neurons that were *significantly* correlated, it was lowest during the Movement period (7.1%) compared to other epochs, reflected in Figure 5.4B for all three monkeys individually (averaged across monkeys in Figure 5.5A).

In contrast, the Trial Start period saw the highest percentage of significantly correlated pairs (11.5%). We can conclude that the percentage of significant noise correlation in the motor cortex is generally weak during different epochs of the reach-to-grasp task, but is strongest outside of the task with high spike count variability (FF = 1.54), and weakest during movements with low count variability (FF = 0.89). This finding shows a striking relationship between the variability of neuron pairs, known as the Fano factor (FF), and the percentage of significantly noise correlated pairs. We then separated neurons into categories defined by their spike width: narrow and broad. Narrow spike neurons were commonly defined as putative inhibitory interneurons, whereas broad spike neurons as putative excitatory pyramidal neurons (e.g., Mitchell et al. 2007; Song and McPeek 2010; Kaufman et al. 2013; Best et al. 2016; Vigneswaran et al. 2011).

By identifying different neuron types on the basis of their spike width, we were able to further investigate whether or not correlation properties differ for putative interneurons or putative pyramidal neurons. During the Trial Start period, when the monkey was waiting to start the trial, a higher percentage of narrow-narrow pairs were significantly correlated than broad-broad pairs, for all monkeys (Figure 5.10). The percentage of significantly correlated narrow-broad pairs was in between narrow-narrow and broad-broad pairs. In the Movement period, the differences between all three types of neuron pairs were much smaller. This is indicative of the general noise decorrelation seen during activity epochs, but narrow-narrow pairs still slightly exceeded both broad-broad and mixed pairs.

In a study by Schulz et al. (2015) the opposite was found, the strongest correlations were found between broad spike neurons in V1 of an anesthetized cat. The exception to this rule was during presentation of natural stimuli: narrow spiking neuron pairs would exceed correlation of broad spike pairs. The significance of this inversed phenomenon in awake monkey M1/PM neuron pairs and anesthetized cat V1 neuron pairs is unclear, because it is currently not known how different categories of neurons contribute to noise correlation. However, our results suggest that in the motor cortex the activity of putative interneurons provides the main contribution to noise correlation.

A recent finding showed that narrow spiking populations lead to a better offline decoding performance than several alternatives important to brain-machine interface (BMI) research (Best et al. 2016). Both narrow and wide response properties are undoubtedly important to normal movement generation, but the linear decoding model seems to be better suited for narrow spiking activity. Our own finding supports a more dichotomous change in noise correlation strength in narrow spiking populations in response to movement than wide of mixed spiking populations, which may be exploited when selecting neurons for the decoder.

Finally, our results show that *distance* has an effect on correlation strength between neurons. During the Trial Start period, the strength of correlation and the percentage of significant correlation pairs both decreased with distance, showing a significant difference between distance groups in monkey L and monkey N (Figure 5.6A & B, respectively, red bars). During the Movement period the overall correlation strength and percentage of significantly correlated pairs was lower than the Trial Start period, and had a far less prominent distance effect (Figure 5.7A & B, respectively, red bars). In contrast, the strength of noise correlation and the percentage of significant noise correlation both increased with *firing rate* in both

epochs for all monkeys, though not systematically (Figure 5.6 & 5.7, blue bars). This finding is less consistent in other studies, where some reported an increase of correlation with firing rate (Cohen and Maunsell 2009; Cohen and Kohn 2011) but others found no dependence (Kohn and Smith 2005).

6 CONCLUSION

My thesis combines scientific, technological and experimental approaches for the exploration of cortical network dynamics during visually-guided motor behavior. In the first part of this work, a continuous effort was made to survey functional and anatomical literature to better understand the neural underpinnings of visually-guided motor behavior, with a particular emphasize on the coordination between eye and hand movements. This directly encouraged the creation of the detailed Vision-for-Action connectivity map shown in chapter 1. The expansive involvement of many cortical and subcortical regions that contribute simultaneously to goal-directed behavior by means of indirect/direct and feedback/feedforward communication led to a broader and more contextual understanding of dozens of functionally connected brain structures, rather than a deep area-specific knowledge of a single region. This typified the general ambition of the Vision-for-Action project: to focus on the contextual function of multiple brain areas during their coordinated efforts to fulfill a single goal-directed behavior. With this philosophy in mind, my thesis had 3 main objectives: (i) to develop an experimental setup that meets our scientific objectives, (ii) to validate this setup through the analysis of pilot behavioral recordings, (iii) to explore potential methods for the analysis of multi-site, multi-electrode electrophysiological recordings during visually-guided behaviour.

The setup development required the use of embedded technology that was not available as a single experimental setup, and was therefore developed in-house as a cross-compatible platform for use in humans and monkeys: the *Real-time Integrated Visuomotor behavior & Electrophysiology Recording* (RIVER) setup (Figure 2.4; chapter 2). During its development, the monkey configuration of this setup (Figure 2.1A) was used and tested extensively with monkey Y (chapter 2 & 3) and is currently used by two other monkeys with promising results. Likewise, the human setup Figure 2.1D) has finished the testing phase, yielding similar preliminary behavioral data of eye and hand movements (Figure 3.12 & 3.13). The completion of the RIVER setup and training of specifically monkey Y became the focal point of my project, and overcame several technical and practical challenges that were met during the project, summarized as follows:

1) *Integration of proprietary systems:* in order collect eye and hand movement data, task and performance data, and electrophysiological data, three independent systems had to

be integrated hierarchically. Central to collecting eye (from EyeLink) and hand movement data in real-time was the KINARM system, which processes and controls all the aspects defined in the task executable in real-time, and continuously outputs all behavioral and event-based data via analog and digital channels to the data acquisition system Cerebus (Figure 6.1A & 2.1).

2) *Compatibility between setups, data formats, and labs*: we used the same platform to develop tasks in the monkey setup and extended it into the human configuration. This means that the behavioral data outputs are also structured in a similar fashion, using the same logic, event coding, temporal resolution, and signal processing of eye/hand movements. The electrophysiological recordings are different between species (EEG in humans and MEAs in monkeys), showcasing that certain parts of the RIVER setup can be swapped out and replaced with different or upgraded component without the need to create a new system from the ground up. Additionally, the behavioral data includes extensive information regarding qualitative features of the task, subject, material and environment, collectively known as metadata. This allows naive researchers from other labs to quickly understand how the data was acquired and processed, with access to qualitative conditions of the experiments, such as equipment, behavior, special circumstances, etc. (Figure 6.1D).

3) *Eye and hand movements in the same reference frame:* we discuss the influence of decoupled eye and hand movements on neural activity in chapter 1.5: even slight dissociations between eye and hand behavior can have far-reaching consequences on the neuronal responses. This required transforming eye movements into spatial coordinates compatible with hand and target positions in a horizontal plane. To facilitate this, an adaptive eye calibration was created to compensate for non-linearities caused by the horizontal orientation of the screen (Figure 6.1B & 2.5). One important advantage of this calibration method over standard pack-in methods is that it theoretically works in *any* orientation of the screen, not just horizontal as confirmed in our setups, but as long as there is a direct line of sight from the camera to the eye and a reasonable stability of the head, it will compensate for the geometrical deformation of the screen.

4) *Non-invasive Head Stabilization:* in order to minimize invasive surgical procedures to the implantation of multiple MEAs connected to two head connectors, we attempted a

form of non-invasive head stabilization with plastic masks (Figure 6.1C & 3.5). This approach has only recently become a practical avenue for head fixations (Slater et al. 2016), but was at the beginning of this project rarely used in other studies (Fairhall et al. 2006). As with any novel technique, it required steady, iterative development and testing, with realistic expectations.

Concurrently, the monkey was trained to exhibit a continuous visually-guided motor behavior we wished to record in conjunction with the electrophysiology. The core task design changed over time, but reached the final hexagon-shaped sequential pointing task presented in chapter 3 (Figure 3.10) and was used in both monkey and human participants. The preliminary behavioral analyses from chapter 3 allowed us to gain proficiency in understanding the interplay between eye and hand movements during a learned sequential pointing task. Coordinated behavior and the demands of a rule-based task exposed, in part, how eye and hand movements were scaled to fit the cognitive demands, such as the requirement for high positional accuracy of the hand, which induced a more dynamic involvement of the eye to accurately guide the hand feedback and get a reward.

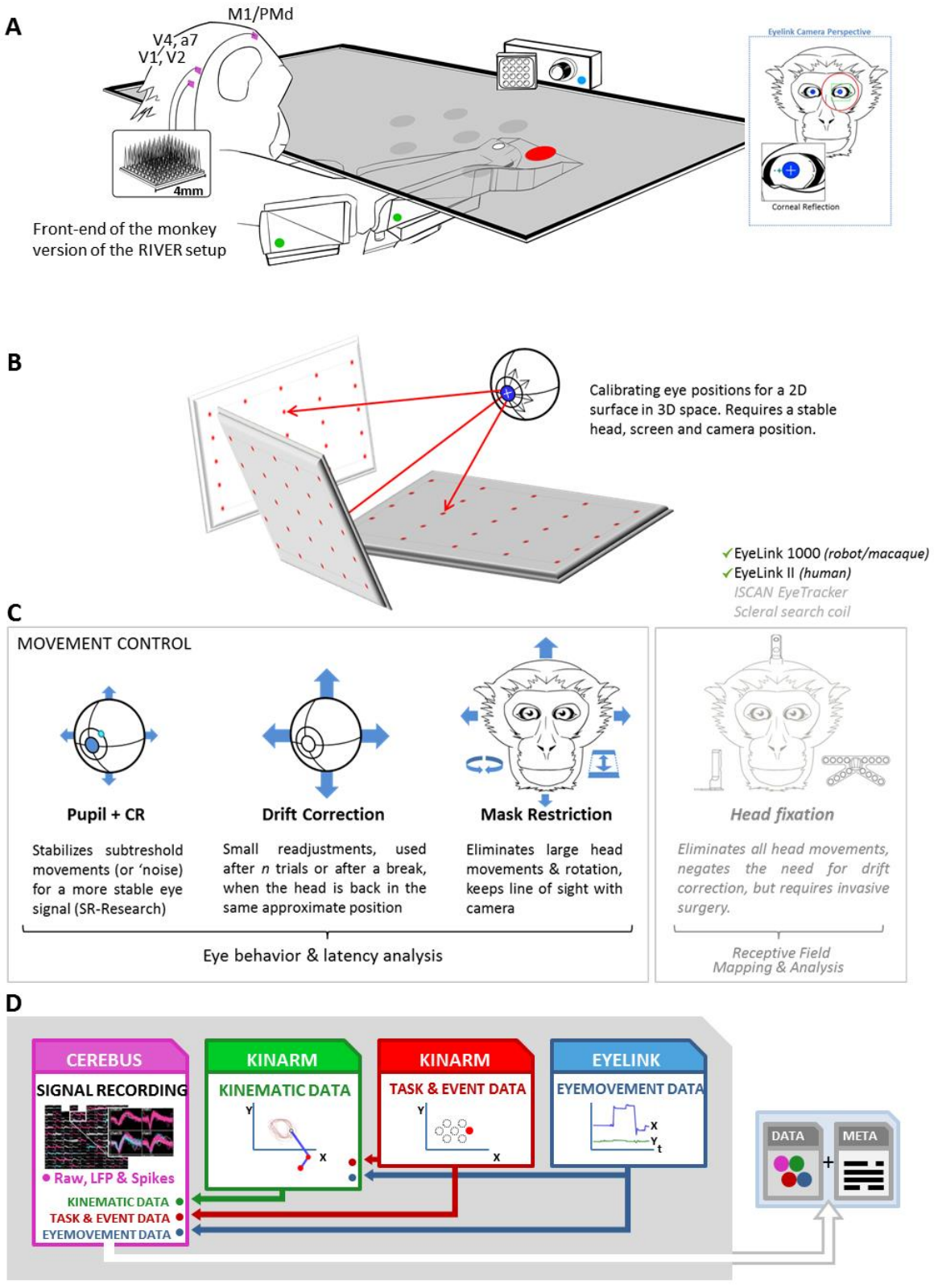

Figure 6.1: System Recap. A) Drawing of the front-end of the RIVER setup, depicting the monkey in the KINARM chair, the exoskeleton, the EyeLink 1000 camera, and the 10x10 MEA. B) Eye calibration method confirmed to work on horizontal screens, but theoretically compatible to other screen orientations. C) Several levels of non-invasive head stabilization used in our setup, with the more restraining yet invasive head post option (grey). D) Behavioral and electrophysiological data and metadata output.

The final step of the project involves recording multiple neurons from multiple areas and analyzed them in context of each other. This requires massively parallel electrophysiological recordings, temporal and spatial data of eye and hand movements, and the analysis method that allows us to quantify and interpret this coordination. The first analysis method we used to explore this kind of data was noise correlation, also known as spike count correlation (r_{sc}), which has so far been mostly implemented in neurons of the visual cortex, in conjunction with signal correlation. Unfortunately, due to monkey Y's passing during surgery we had to implement the method on data from another study, with the clear perspective in gaining proficiency with it in order to utilize it in future Vision-for-Action data. The results allowed us to make preliminary interpretations on the impact of active movement on 1) correlation strength versus a time period outside the trial, 2) the effect of distance between neurons and firing rate on correlation, 3) the relationship between cross-trial variability of a neuron (Fano factor, FF) and noise correlation, and 4) by differentiating neurons by spike width (narrow vs broad), allowed us to elucidate which type of putative neuron contributes the most to the average noise correlation strength (chapter 5).

In conclusion, this thesis presents the main results of a balanced PhD project, which required the scientific exploration of complex biological systems, significant technological developments pushing the frontier forward, learning the dynamics of training monkeys in a variety of conditions, and the acquisition and analysis of big data. To complete all of these scientific goals was ambitious, but significant headway was achieved in each of these goals independently, and with the RIVER setup being completed in both species with preliminary data yielding insights into monkey eye-hand coordination and neuronal correlation during different trial epochs, the stage is set for extraordinary scientific exploration.

ACKNOWLEDGEMENTS

This project received funding from the European Union's Horizon 2020 research and innovation program under grant agreement No. 720270)(HBP), the Helmholtz Association through the Helmholtz Portfolio Theme "Supercomputing and Modeling for the Human Brain (SMHB)", the Deutsche Forschungsgemeinschaft Grant GR 1753/4-2 Priority Program (SPP 1665). The project was supported by the Computational and Systems Neuroscience (INM-6) & Theoretical Neuroscience (IAS-6) labs, the Laboratoire International Associé (LIA, International Lab Vision-for-Action), and the Institut de Neurosciences de la Timone (INT), which provided hosting of the project and the required support for monkey housing and care.

I am deeply grateful for the continued support and supervision of Dr. Alexa Riehle (INT) throughout my project and thesis, giving me invaluable lessons and insights into the complexity of behavioral and electrophysiological experimentation in monkeys, sharing her extensive knowledge and experience each step of the way, and creating a work environment that allowed for true innovation and scientific variety.

Likewise, I would like to extend my sincere gratitude to Prof. Dr. Sonja Grün (INM-6) who gave me the opportunity to confer a doctorate in such a multifaceted and ambitious thesis. Her direction and supervision has driven all aspects of my project forward, and provided a platform for me to pursue excellence in science.

I would like to thank Dr. Thomas Brochier (INT) for giving his council with depth and enthusiasm. His support, suggestions, curiosity, and command of the topics has guided me and my project into what it is today, and he will hopefully continue to do so in the future.

I am indebted to my colleague Dr. Frédéric Barthélemy (INT/INM-6) with whom I worked closely to meet all the technological and engineering challenges. He has been a patient and diligent teacher, and I am grateful to have had his friendship and guiding hand.

I have greatly benefited from the conversations, presentations and contributions of Dr. Bjørg Kilavik (INT), and thank her sincerely for sharing her valuable experience and frank insights during our parallel monkey training sessions and general conversation.

A special thanks to my lab mate and collaborator Margaux Duret, whose humor, openness and optimism were a great source of support and discourse.

From the INT, I would like to generally thank my fellow lab mates and researchers in the open area and offices of the 3rd floor. Discussions, seminars, journal clubs and debates across topics and projects allowed for students to benefit from each other's insight and opinions, helping us to grow as researchers. Many have come and gone, bringing a unique perspective and character to the group each time.

From the INM-6, I would like to extend the same general gratitude to my fellow lab mates, even though we only saw each other sporadically, a great wealth of knowledge was passed between us in the open market place of ideas. Besides these insights of higher learning, I have enjoyed their artistic expression (Vahid), anime expertise (Alper), cocktail craft (Carlos), stoic intelligence (Junji), mad hack skills (Michael B.), italian hand signals (Emiliano), blue hair (Julia), and bone-dry humor (Michael D.).

I would like to thank Dr. Lyuba Zehl (INM-6) in particular as the only other biologist in the INM-6, we shared a common background and interest from the get-go, and our open conversations and mutual support have always been natural extensions of our friendship.

A special thank you to Dr. Sacha van Albada (INM-6), who's simple and kind act of placing me in contact with Sonja initiated the adventure that followed.

My heartfelt appreciation also extends to my family for supporting me throughout my project, accepting the choices I make, and understanding the paths I take.

I dedicate this thesis to my love Aisha, who has been by my side every step of the way, sharing and enhancing every aspect of my life and work, and my other love, my son Dax, whose arrival marked the beginning of exquisite joy and exhaustion beyond compare.

BIBLIOGRAPHY

Adams, D. L., Horton, J. C. (2003). A Precise Retinotopic Map of Primate Striate Cortex Generated from the Representation of Angioscotomas. Journal of Neuroscience: 23 (9) 3771-3789

Albright, T. D. (1984) Direction and orientation selectivity of neurons in visual area MT of the macaque. Journal of Neurophysiology:52(6):1106-30

Andersen, R. A., & Buneo, C. A. (2002). Intentional Maps in Posterior Parietal Cortex. Annual Review of Neuroscience, 25(1), 189-220. doi:10.1146/annurev.neuro.25.112701.142922

Andersen, R. A., Mountcastle, V. B. (1983). The influence of the angle of gaze upon the excitability of the light-sensitive neurons of the posterior parietal cortex. Journal of Neuroscience, 3(3):532-48

Andersen, R. A., Snyder, L. H., Li, C., & Stricanne, B. (1993). Coordinate transformations in the representation of spatial information. Current Opinion in Neurobiology, 3(2), 171-176. doi:10.1016/0959-4388(93)90206-e

Andersen, R., Andersen, K., Hwang, E., & Hauschild, M. (2014). Optic Ataxia: From Balint's Syndrome to the Parietal Reach Region. Neuron, 81(5), 967-983. doi:10.1016/j.neuron.2014.02.025

Andersen, R., Essick, G., & Siegel, R. (1985). Encoding of spatial location by posterior parietal neurons. Science, 230(4724), 456-458. doi:10.1126/science.4048942

Andersen, R.A., Bracewell, R.M., Barash, S., Fogassi, L., & Gnadt, J.W. (1990). Eye position effects on visual, memory, and saccade-related activity in areas LIP and 7a of macaque. The Journal of neuroscience, 10 4, 1176-96

Anderson, J. C., & Martin, K. A. (2009). The Synaptic Connections between Cortical Areas V1 and V2 in Macaque Monkey. Journal of Neuroscience, 29(36), 11283-11293. doi:10.1523/jneurosci.5757-08.2009

Anikeeva, P., Andalman, A. S., Witten, I., Warden, M., Goshen, I., Grosenick, L., . . . Deisseroth, K. (2011). Optetrode: a multichannel readout for optogenetic control in freely moving mice. Nature Neuroscience, 15(1), 163-170. doi:10.1038/nn.2992

Archambault, P. S., Caminiti, R., & Battaglia-Mayer, A. (2009). Cortical Mechanisms for Online Control of Hand Movement Trajectory: The Role of the Posterior Parietal Cortex. Cerebral Cortex, 19(12), 2848-2864. doi:10.1093/cercor/bhp058

Arend, I., Rafal, R., & Ward, R. (2008). Spatial and temporal deficits are regionally dissociable in patients with pulvinar lesions. Brain, 131(8), 2140-2152. doi:10.1093/brain/awn135

Arieli, A., Sterkin, A., Grinvald, A., & Aertsen, A. (1996). Dynamics of Ongoing Activity: Explanation of the Large Variability in Evoked Cortical Responses. Science, 273(5283), 1868-1871. doi:10.1126/science.273.5283.1868

Averbeck, B. B., Latham, P. E., & Pouget, A. (2006). Neural correlations, population coding and computation. Nature Reviews Neuroscience, 7(5), 358-366. doi:10.1038/nrn1888

Averbeck, B.B. & Lee, D. (2003). Neural noise and movement-related codes in the macaque supplementary motor area. Journal of Neuroscience, 23, 7630–7641

Badan, M., Hauert, C.-A., Mounoud, P. (2000). Sequential pointing in children and adults. Journal of Experimental Child Psychology, 75, 43-69

Bair, W. & O'Keefe, L.P. (1998). The influence of fixational eye movements on the response of neurons in area MT of the macaque. Visual Neuroscience, 15, 779–786

Baker, J. T., Donoghue, J. P., Sanes, J. N. (1999) Gaze direction modulates finger movement activation patterns in human cerebral cortex. Journal of Neuroscience: 19:10044–10052

Barash, S., Bracewell, R. M., Fogassi, L., Gnadt, J. W., Andersen, R. A. (1991). Saccade-Related Activity in the Lateral Intraparietal Area I. Temporal Properties; Comparison With Area 7a. Journal of Neurophysiology: Vol. 66, No. 3

Bastos, A., Vezoli, J., Bosman, C., Schoffelen, J., Oostenveld, R., Dowdall, J., . . . Fries, P. (2015). Visual Areas Exert Feedforward and Feedback Influences through Distinct Frequency Channels. Neuron, 85(2), 390-401. doi:10.1016/j.neuron.2014.12.018

Battaglia-Mayer, A., Ferraina, S., Genovesio, A., Marconi, B., Squatrito, S., Molinari, M., . . . Caminiti, R. (2001). Eye-Hand Coordination during Reaching. II. An Analysis of the Relationships between Visuomanual Signals in Parietal Cortex and Parieto-frontal Association Projections. Cerebral Cortex, 11(6), 528-544. doi:10.1093/cercor/11.6.528

Beck, M. R., Hong, S. L., Lamsweerde, A. E., & Ericson, J. M. (2014). The Effects of Incidentally Learned Temporal and Spatial Predictability on Response Times and Visual Fixations during Target Detection and Discrimination. PLoS ONE, 9(4). doi:10.1371/journal.pone.0094539

Bédard, P., Thangavel, A., & Sanes, J. N. (2008). Gaze influences finger movement-related and visual-related activation across the huan brain. Experimental Brain Research, 188(1), 63-75. doi:10.1007/s00221-008-1339-3

Best, M. D., Suminski, A. J., Takahashi, K., Brown, K. A., & Hatsopoulos, N. G. (2016). Spatio-Temporal Patterning in Primary Motor Cortex at Movement Onset. Cerebral Cortex. doi:10.1093/cercor/bhv327

Best, M. D., Takahashi, K., Suminski, A. J., Ethier, C., Miller, L. E., & Hatsopoulos, N. G. (2016). Comparing offline decoding performance in physiologically defined neuronal classes. Journal of Neural Engineering, 13(2), 026004. doi:10.1088/1741-2560/13/2/026004

Bichot, N.P., Thompson, K.G., Chenchal Rao, S. & Schall, J.D. (2001). Reliability of macaque frontal eye field neurons signaling saccade targets during visual search. Journal of Neuroscience, 21, 713–725

Biguer, B., Jeannerod, M., & Prablanc, C. (1982). The coordination of eye, head, and arm movements during reaching at a single visual target. Experimental Brain Research, 46(2), 301-304. doi:10.1007/bf00237188

Bock, O., & Arnold, K., (1993). Error accumulation and error correction in sequential pointing movements. Experimental Brain Research, 95, 111–117

Boussaoud, D., Barth, T., & Wise, S. (1993). Effects of gaze on apparent visual responses of frontal cortex neurons. Experimental Brain Research, 93(3). doi:10.1007/bf00229358

Boussaoud, D., Jouffrais, C., Bremmer, F. (1998). Eye position effects on the neuronal activity of dorsal premotor cortex in the macaque monkey. Journal of Neurophysiology, 80 (1998), 1132-1150

Bowman, M. C., Johannson, R. S., & Flanagan, J. R. (2009). Eye–hand coordination in a sequential target contact task. Experimental Brain Research, 195(2), 273-283. doi:10.1007/s00221-009-1781-x

Bray, S., Almas, R., Arnold, A. E., Iaria, G., & Macqueen, G. (2015). Intraparietal Sulcus Activity and Functional Connectivity Supporting Spatial Working Memory Manipulation. Cerebral Cortex, 25(5), 1252-1264. doi:10.1093/cercor/bht320

Breveglieri, R., Bosco, A., Galletti, C., Passarelli, L., & Fattori, P. (2016). Neural activity in the medial parietal area V6A while grasping with or without visual feedback. Scientific Reports, 6(1). doi:10.1038/srep28893

Bridge, H., Leopold, D. A., & Bourne, J. A. (2016). Adaptive Pulvinar Circuitry Supports Visual Cognition. Trends in Cognitive Sciences, 20(2), 146-157. doi:10.1016/j.tics.2015.10.003

Brotchie, P. R., Andersen, R. A., Snyder, L. H., Goodman, S. J. (1995). Head position signals used by parietal neurons to encode locations of visual stimuli. Nature, 375: 232–235.

Brunner, C., Birbaumer, N., Blankertz, B., Guger, C., Kübler, A., Mattia, D., . . . Müller-Putz, G. R. (2015). BNCI Horizon 2020: towards a roadmap for the BCI community. Brain-Computer Interfaces, 2(1), 1-10. doi:10.1080/2326263x.2015.1008956

Buneo, C. A., & Andersen, R. A. (2006). The posterior parietal cortex: Sensorimotor interface for the planning and online control of visually guided movements. Neuropsychologia, 44(13), 2594-2606. doi:10.1016/j.neuropsychologia.2005.10.011

Butler, A. B. (2000) Chordate evolution and the origin of craniates: an old brain in a new head. The Anatomical Record; 261(3):111-25

Buxhoeveden, D. P., & Casanova, M. F. (2002). The minicolumn hypothesis in neuroscience. Brain, 125(5), 935-951. doi:10.1093/brain/awf110

Caminiti, R., Ferraina, S., & Mayer, A. B. (1998). Visuomotor transformations: early cortical mechanisms of reaching. Current Opinion in Neurobiology, 8(6), 753-761. doi:10.1016/s0959-4388(98)80118-9

Campbell, P., Jones, K., Huber, R., Horch, K., & Normann, R. (1991). A silicon-based, three-dimensional neural interface: manufacturing processes for an intracortical electrode array. IEEE Transactions on Biomedical Engineering, 38(8), 758-768. doi:10.1109/10.83588

Casagrande, V. (1994). A third parallel visual pathway to primate area V1. Trends in Neurosciences, 17(7), 305-310. doi:10.1016/0166-2236(94)90065-5

Casanova, C., Merabet, L., Desautels, A., & Minville, K. (2001). Chapter 5 Higher-order motion processing in the pulvinar. Progress in Brain Research Vision: From Neurons to Cognition, 71-82. doi:10.1016/s0079-6123(01)34006-2

Cattell, J. M., & Fullerton, F. S. (1892). The Psychophysics of Movement. Mind NS 1: 447-452

Charvet, G., Billoint, O., Gharbi, S., Heuschkel, M., Georges, C., Kauffmann, T., . . . Guillemaud, R. (2010). A modular 256-channel Micro Electrode Array platform for in vitro and in vivo neural stimulation and recording: BioMEA™. 2010 Annual International Conference of the IEEE Engineering in Medicine and Biology. doi:10.1109/iembs.2010.5626403

Chase, S. M., Kass, R. E., & Schwartz, A. B. (2012). Behavioral and neural correlates of visuomotor adaptation observed through a brain-computer interface in primary motor cortex. Journal of Neurophysiology, 108(2), 624-644. doi:10.1152/jn.00371.2011

Cheung, K. C., Renaud, P., Tanila, H., & Djupsund, K. (2007). Flexible polyimide microelectrode array for in vivo recordings and current source density analysis. Biosensors and Bioelectronics, 22(8), 1783-1790. doi:10.1016/j.bios.2006.08.035

Chouinard, P. A. (2006). Different Roles of PMv and PMd during Object Lifting. Journal of Neuroscience, 26(24), 6397-6398. doi:10.1523/jneurosci.1481-06.2006

Chouinard, P. A., & Paus, T. (2006). The Primary Motor and Premotor Areas of the Human Cerebral Cortex. The Neuroscientist, 12(2), 143-152. doi:10.1177/1073858405284255

Churchland, M. M., Yu, B. M., Cunningham, J. P., Sugrue, L. P., Cohen, M. R., Corrado, G. S., . . . Shenoy, K. V. (2010). Stimulus onset quenches neural variability: a widespread cortical phenomenon. Nature Neuroscience, 13(3), 369-378. doi:10.1038/nn.2501

Cisek, P., & Kalaska, J. F. (2002). Simultaneous Encoding of Multiple Potential Reach Directions in Dorsal Premotor Cortex. Journal of Neurophysiology, 87(2), 1149-1154. doi:10.1152/jn.00443.2001

Cisek, P., & Kalaska, J. F. (2005). Neural Correlates of Reaching Decisions in Dorsal Premotor Cortex: Specification of Multiple Direction Choices and Final Selection of Action. Neuron, 45(5), 801-814. doi:10.1016/j.neuron.2005.01.027

Cohen, J. & Cohen, P. (1983). Applied multiple regression/correlation analysis for the behavioral sciences (2nd ed.)

Cohen, J. Y., Crowder, E. A., Heitz, R. P., Subraveti, C. R., Thompson, K. G., Woodman, G. F., & Schall, J. D. (2010). Cooperation and Competition among Frontal Eye Field Neurons during Visual Target Selection. Journal of Neuroscience, 30(9), 3227-3238. doi:10.1523/jneurosci.4600-09.2010

Cohen, M. R., & Kohn, A. (2011). Measuring and interpreting neuronal correlations. Nature Neuroscience, 14(7), 811-819. doi:10.1038/nn.2842

Cohen, M. R., & Maunsell, J. H. (2009). Attention improves performance primarily by reducing interneuronal correlations. Nature Neuroscience, 12(12), 1594-1600. doi:10.1038/nn.2439

Cohen, Y. E. & Andersen, R. A. (1998). The parietal reach area (PRR) encodes reaches to auditory targets in an eye-centered reference frame. Soc. Neurosci. Abstr. 24: 262, 1998

Cohen, Y. E., & Andersen, R. A. (2002). A common reference frame for movement plans in the posterior parietal cortex. Nature Reviews Neuroscience, 3(7), 553-562. doi:10.1038/nrn873

Colby, C. L., Duhamel, J. R., Goldberg, M. E. (1993) Ventral intraparietal area of the macaque: anatomic location and visual response properties. Journal of Neurophysiology: 69(3):902-14

Colby, C. L., Gattass, R., Olson, C. R., & Gross, C. G. (1988). Topographical organization of cortical afferents to extrastriate visual area PO in the macaque: A dual tracer study. The Journal of Comparative Neurology, 269(3), 392-413. doi:10.1002/cne.902690307

Connolly, J. D., Goodale, M. A., DeSouza, J. F. X., Menon, R.S., Vilis, T. (2000). A comparison of frontoparietal fMRI activation during anti-saccades and anti-pointing. Journal of Neurophysiology 1645-1655.

Constantinidis, C. & Goldman-Rakic, P.S. (2002). Correlated discharges among putative pyramidal neurons and interneurons in the primate prefrontal cortex. Journal of Neurophysiology, 88, 3487–3497

Crawford, J. D., Medendorp, W.P., Marotta, J. J. (2004). Spatial Transformations for Eye-Hand Coordination. Journal of Neurophysiology, 92(1), 10-19. doi:10.1152/jn.00117.2004

Crawford, J., Henriques, D., Medendorp, W., & Khan, A. (2003). Ocular kinematics and eye-hand coordination. Strabismus, 11(1), 33-47. doi:10.1076/stra.11.1.33.14094

Crist, R., & Lebedev, M. (2007). Multielectrode Recording in Behaving Monkeys. Methods for Neural Ensemble Recordings, Second Edition Frontiers in Neuroscience, 169-188. doi:10.1201/9781420006414.ch9

Daniel, P. M., & Whitteridge, D. (1961). The representation of the visual field on the cerebral cortex in monkeys. The Journal of Physiology, 159(2), 203-221. doi:10.1113/jphysiol.1961.sp006803

Dean, H. L., Marti, D., Tsui, E., Rinzel, J., & Pesaran, B. (2011). Reaction Time Correlations during Eye-Hand Coordination: Behavior and Modeling. Journal of Neuroscience, 31(7), 2399-2412. doi:10.1523/jneurosci.4591-10.2011

Dekker, T., Mareschal, D., Sereno, M. I., & Johnson, M. H. (2011). Dorsal and ventral stream activation and object recognition performance in school-age children. NeuroImage, 57(3), 659-670. doi:10.1016/j.neuroimage.2010.11.005

Derjean, D., Moussaddy, A., Atallah, E., St-Pierre, M., Auclair, F., Chang, S., . . . Dubuc, R. (2010). A Novel Neural Substrate for the Transformation of Olfactory Inputs into Motor Output. PLoS Biology, 8(12). doi:10.1371/journal.pbio.1000567

DeSouza, J. F. X., Dukelow, S. P., Gati, J. S., Menon, R. S., Andersen, R. A., Vilis, T. (2000). Eye Position Signal Modulates a Human Parietal Pointing Region during Memory-Guided Movements. Journal of Neuroscience, 20 (15) 5835-5840

Donkelaar, P. V. (1997). Eye–hand interactions during goal-directed pointing movements. NeuroReport, 8(9), 2139-2142. doi:10.1097/00001756-199707070-00010

Donoghue, J., Suner, S., & Sanes, J. (1990). Dynamic organization of primary motor cortex output to target muscles in adult rats II. Rapid reorganization following motor nerve lesions. Experimental Brain Research, 79(3). doi:10.1007/bf00229319

Dragoi, V., & Tsuchitani, C. (2007). Visual Processing: Cortical Pathways. Retrieved March 1, 2017, from http://neuroscience.uth.tmc.edu/s2/chapter14.html

Dubner, R., & Zeki, S. (1971). Response properties and receptive fields of cells in an anatomically defined region of the superior temporal sulcus in the monkey. Brain Research, 35(2), 528-532. doi:10.1016/0006-8993(71)90494-x

Dum, R. P., Strick, P. L. (1996) Spinal cord terminations of the medial wall motor areas in macaque monkeys. Journal of Neurophysiology, 16, 6513–6525

Ecker, A. S., Berens, P., Cotton, R. J., Subramaniyan, M., Denfield, G. H., Cadwell, C. R., . . . Tolias, A. S. (2014). State dependence of noise correlations in macaque primary visual cortex. Neuron 82(1).

Ecker, A. S., Berens, P., Keliris, G. A., Bethge, M., Logothetis, N. K., & Tolias, A. S. (2010). Decorrelated Neuronal Firing in Cortical Microcircuits. Science, 327(5965), 584-587. doi:10.1126/science.1179867

Erickson, C.A., Jagadeesh, B. & Desimone, R. (2000). Clustering of perirhinal neurons with similar properties following visual experience in adult monkeys. Nature Neuroscience, 3, 1143–1148

Fairhall, S. J., Dickson, C. A., Scott, L., & Pearce, P. C. (2006). A non-invasive method for studying an index of pupil diameter and visual performance in the rhesus monkey. Journal of Medical Primatology, 35(2), 67-77. doi:10.1111/j.1600-0684.2005.00135.x

Felleman, D. J., & Essen, D. C. (1991). Distributed Hierarchical Processing in the Primate Cerebral Cortex. Cerebral Cortex, 1(1), 1-47. doi:10.1093/cercor/1.1.1

Fernández, E., Greger, B., House, P. A., Aranda, I., Botella, C., Albisua, J., . . . Normann, R. A. (2014). Acute human brain responses to intracortical microelectrode arrays: challenges and future prospects. Frontiers in Neuroengineering, 7. doi:10.3389/fneng.2014.00024

Ferraina, S., Garasto, M. R., Battaglia-Mayer, A., Ferraresi, P., Johnson, P. B., Lacquaniti, F., & Carniniti, R. (1997). Visual Control of Hand-reaching Movement: Activity in Parietal Area 7m. European Journal of Neuroscience, 9(5), 1090-1095. doi:10.1111/j.1460-9568.1997.tb01460.x

Ferraina, S., Pare, M., Wurtz, R. H. (2002) Comparison of Cortico-Cortical and Cortico-Collicular Signals for the Generation of Saccadic Eye Movements. Journal of Neurophysiology, 87: 845–858, 2002;10.1152/jn.00317.2001

Fraser, G. W., & Schwartz, A. B. (2011). Recording from the same neurons chronically in motor cortex. Journal of Neurophysiology, 107(7), 1970-1978. doi:10.1152/jn.01012.2010

Freeman, J., & Simoncelli, E. P. (2011). Metamers of the ventral stream. Nature Neuroscience, 14(9), 1195-1204. DOI: 10.1038/nn.2889

Gail, A., Klaes, C., & Westendorff, S. (2009). Implementation of Spatial Transformation Rules for Goal-Directed Reaching via Gain Modulation in Monkey Parietal and Premotor Cortex. Journal of Neuroscience, 29(30), 9490-9499. doi:10.1523/jneurosci.1095-09.2009

Galletti, C., Battaglini, P. P., & Fattori, P. (1995). Eye Position Influence on the Parieto-occipital Area PO (V6) of the Macaque Monkey. European Journal of Neuroscience, 7(12), 2486-2501. doi:10.1111/j.1460-9568.1995.tb01047.x

Galletti, C., Fattori, P., Battaglini, P. P., Shipp, S., & Zeki, S. (1996). Functional Demarcation of a Border Between Areas V6 and V6A in the Superior Parietal Gyrus of the Macaque Monkey. European Journal of Neuroscience, 8(1), 30-52. doi:10.1111/j.1460-9568.1996.tb01165.x.

Galletti, C., Fattori, P., Gamberini, M., & Kutz, D. (2004). The Most Direct Visual Pathway to the Frontal Cortex. Cortex, 40(1), 216-217. doi:10.1016/s0010-9452(08)70956-0

Galletti, C., Fattori, P., Kutz, D. F., & Gamberini, M. (1999). Brain location and visual topography of cortical area V6A in the macaque monkey. European Journal of Neuroscience, 11(2), 575-582. doi:10.1046/j.1460-9568.1999.00467.x

Galletti, C., Gamberini, M., Kutz, D. F., Fattori, P., Luppino, G., & Matelli, M. (2001). The cortical connections of area V6: an occipito-parietal network processing visual information. European Journal of Neuroscience, 13(8), 1572-1588. doi:10.1046/j.0953-816x.2001.01538.x

Garcia, S., Guarino, D., Jaillet, F., Jennings, T., Pröpper, R., Rautenberg, P. L., . . . Davison, A. P. (2014). Neo: an object model for handling electrophysiology data in multiple formats. Frontiers in Neuroinformatics, 8. doi:10.3389/fninf.2014.00010

Gardner, J. (2013). A history of deep brain stimulation: Technological innovation and the role of clinical assessment tools. Social Studies of Science, 43(5), 707-728. doi:10.1177/0306312713483678

Gattass, R., Gross, C.G. & Sandell, J.H. (1981). Visual topography of V2 in the macaque. Journal of Computational Neurology, 201, 519–539

Gattass, R., Lima, B., Soares, J. G., & Ungerleider, L. G. (2015). Controversies about the visual areas located at the anterior border of area V2 in primates. Visual Neuroscience, 32. doi:10.1017/s0952523815000188

Gattass, R., Sousa, A.P. & Gross, C.G. (1988). Visuotopic organization and extent of V3 and V4 of the macaque. Journal of Neuroscience, Neurosci. 8, 1831–1845

Gawne, T. J., Richmond, B.J. (1993). How independent are the messages carried by adjacent inferior temporal cortical neurons? Journal of Neuroscience: 13 (7) 2758-2771

Gebhardt, C., Baier, H., & Bene, F. D. (2013). Direction selectivity in the visual system of the zebrafish larva. Frontiers in Neural Circuits, 7. doi:10.3389/fncir.2013.00111

Gegenfurtner K. R., Kiper D. C., Levitt J. B. (1997). Functional Properties of Neurons in Macaque Area V3. Journal of Neurophysiology 77 (4), 1906-1923. 4 1997

Georgopoulos, A. P., Kalaska, J. F., Caminiti, R., Massey, J.T. (1982) On the relations between the direction of two-dimensional arm movements and cell discharge in primate motor cortex. Journal of Neuroscience, 2(11):1527-37

Gess, R. W., Coates, M. I., & Rubidge, B. S. (2006). A lamprey from the Devonian period of South Africa. Nature, 443(7114), 981-984. doi:10.1038/nature05150

Gillebert, C. R., Mantini, D., Thijs, V., Sunaert, S., Dupont, P., & Vandenberghe, R. (2011). Lesion evidence for the critical role of the intraparietal sulcus in spatial attention. Brain, 134(6), 1694-1709. doi:10.1093/brain/awr085

Goodale, M. A. (2011). Transforming vision into action. Vision Research, 51(13), 1567-1587. doi:10.1016/j.visres.2010.07.027

Goodale, M. A., & Milner, A. (1992). Separate visual pathways for perception and action. Trends in Neurosciences, 15(1), 20-25. doi:10.1016/0166-2236(92)90344-8

Goodale, M. A., Milner, A. D., Jakobson, L. S., & Carey, D. P. (1991). A neurological dissociation between perceiving objects and grasping them. Nature, 349(6305), 154-156. doi:10.1038/349154a0

Gorbet, D. J., Staines, W. R., & Sergio, L. E. (2004). Brain mechanisms for preparing increasingly complex sensory to motor transformations. NeuroImage, 23(3), 1100-1111. doi:10.1016/j.neuroimage.2004.07.043

Graham, R. B., (1990). Physiological psychology. Belmont, CA: Wadsworth.

Granek, J. A., Gorbet, D. J., & Sergio, L. E. (2010). Extensive video-game experience alters cortical networks for complex visuomotor transformations. Cortex, 46(9), 1165-1177. doi:10.1016/j.cortex.2009.10.009

Graybiel, A., Aosaki, T., Flaherty, A., & Kimura, M. (1994). The basal ganglia and adaptive motor control. Science, 265(5180), 1826-1831. doi:10.1126/science.8091209

Grefkes, C., & Fink, G. R. (2005). REVIEW: The functional organization of the intraparietal sulcus in humans and monkeys. Journal of Anatomy, 207(1), 3-17. doi:10.1111/j.1469-7580.2005.00426.x

Greger, B., Kateb, B., Gruen, P., & Patterson, P. H. (2007). A chronically implantable, hybrid cannula–electrode device for assessing the effects of molecules on electrophysiological signals in freely behaving animals. Journal of Neuroscience Methods, 163(2), 321-325. doi:10.1016/j.jneumeth.2007.03.017

Grewe, J., Wachtler, T., & Benda, J. (2011). A Bottom-up Approach to Data Annotation in Neurophysiology. Frontiers in Neuroinformatics, 5. doi:10.3389/fninf.2011.00016

Gribble, P. L., Everling, S., Ford, K., & Mattar, A. (2002). Hand-eye coordination for rapid pointing movements. Experimental Brain Research, 145(3), 372-382. doi:10.1007/s00221-002-1122-9

Grieve, K. L., Acuña, C., & Cudeiro, J. (2000). The primate pulvinar nuclei: vision and action. Trends in Neurosciences, 23(1), 35-39. doi:10.1016/s0166-2236(99)01482-4

Grillner, S., Cangiano, L., Hu, G., Thompson, R., Hill, R., & Wallén, P. (2000). The intrinsic function of a motor system — from ion channels to networks and behavior. Brain Research, 886(1-2), 224-236. doi:10.1016/s0006-8993(00)03088-2

Gutnisky, D. A., & Dragoi, V. (2008). Adaptive coding of visual information in neural populations. Nature, 452(7184), 220-224. doi:10.1038/nature06563

Hatsopoulos, N. (2004). Decoding Continuous and Discrete Motor Behaviors Using Motor and Premotor Cortical Ensembles. Journal of Neurophysiology, 92(2), 1165-1174. doi:10.1152/jn.01245.2003

Hawkins, K. M., Sayegh, P., Yan, X., Crawford, J. D., & Sergio, L. E. (2013). Neural Activity in Superior Parietal Cortex during Rule-based Visual-motor Transformations. Journal of Cognitive Neuroscience, 25(3), 436-454. doi:10.1162/jocn_a_00318

Hayhoe, M. M., Shrivastava, A., Mruczek, R., & Pelz, J. B. (2003). Visual memory and motor planning in a natural task. Journal of Vision, 3(1), 6. doi:10.1167/3.1.6

Hendry, S. H., & Reid, R. C. (2000). The Koniocellular Pathway in Primate Vision. Annual Review of Neuroscience, 23(1), 127-153. doi:10.1146/annurev.neuro.23.1.127

Herman, R., Herman, R., & Maulucci, R. (1981). Visually triggered eye-arm movements in man. Experimental Brain Research, 42-42(3-4). doi:10.1007/bf00237504

Himmelbach, M., & Karnath, H. (2005). Dorsal and Ventral Stream Interaction: Contributions from Optic Ataxia. Journal of Cognitive Neuroscience, 17(4), 632-640. doi:10.1162/0898929053467514

Holmqvist, K., Nyström, M., Andersson, R., Dewhurst, R., Jarodzka, H., van de Weijer, J. (2011) Eye tracking: A comprehensive guide to methods and measures. Oxford: Oxford University Press

Hoshi, E., & Tanji, J. (2004). Functional specialization in dorsal and ventral premotor areas. Progress in Brain Research Brain Mechanisms for the Integration of Posture and Movement, 507-511. doi:10.1016/s0079-6123(03)43047-1

Huang, X. & Lisberger, S.G. (2009). Noise correlations in cortical area MT and their potential impact on trial-by-trial variation in the direction and speed of smooth-pursuit eye movements. Journal of Neurophysiology. 101, 3012–3030

Hubel, D. H., & Wiesel, T. N. (1959). Receptive fields of single neurones in the cats striate cortex. The Journal of Physiology, 148(3), 574-591. doi:10.1113/jphysiol.1959.sp006308

Hubel, D. H., & Wiesel, T. N. (1968). Receptive fields and functional architecture of monkey striate cortex. The Journal of Physiology, 195(1), 215-243. doi:10.1113/jphysiol.1968.sp008455

Hubel, D. H., & Wiesel, T. N. (1974). Sequence regularity and geometry of orientation columns in the monkey striate cortex. The Journal of Comparative Neurology, 158(3), 267-293. doi:10.1002/cne.901580304

Hubel, D. H., Wiesel, T. N., & Stryker, M. P. (1977). Orientation columns in macaque monkey visual cortex demonstrated by the 2-deoxyglucose autoradiographic technique. Nature, 269(5626), 328-330. doi:10.1038/269328a0

Hutchins, K.D., Martino, A.M. & Strick, P.L. Exp Brain Res (1988) 71: 667. doi:10.1007/BF00248761

Hwang, E. J., Hauschild, M., Wilke, M., & Andersen, R. A. (2014). Spatial and Temporal Eye-Hand Coordination Relies on the Parietal Reach Region. Journal of Neuroscience, 34(38), 12884-12892. doi:10.1523/jneurosci.3719-13.2014

Ilg, U. J. (2008). The role of areas MT and MST in coding of visual motion underlying the execution of smooth pursuit. Vision Research, 48(20), 2062-2069. doi:10.1016/j.visres.2008.04.015

Ingle, D. (1973). Two Visual Systems in the Frog. Science, 181(4104), 1053-1055. doi:10.1126/science.181.4104.1053

Ito, J., Maldonado, P., Singer, W., & Grun, S. (2011). Saccade-Related Modulations of Neuronal Excitability Support Synchrony of Visually Elicited Spikes. Cerebral Cortex, 21(11), 2482-2497. doi:10.1093/cercor/bhr020

Jeannerod, M. (1995). Mental imagery in the motor context. Neuropsychologia, 33(11), 1419-1432. doi:10.1016/0028-3932(95)00073-c

Johnson, P. B., Ferraina, S., Bianchi, L., & Caminiti, R. (1996). Cortical Networks for Visual Reaching: Physiological and Anatomical Organization of Frontal and Parietal Lobe Arm Regions. Cerebral Cortex, 6(2), 102-119. doi:10.1093/cercor/6.2.102

Johnson, P., Ferraina, S., & Caminiti, R. (1993). Cortical networks for visual reaching. Experimental Brain Research, 97(2). doi:10.1007/bf00228707

Jonikaitis, D., & Deubel, H. (2011). Independent Allocation of Attention to Eye and Hand Targets in Coordinated Eye-Hand Movements. Psychological Science, 22(3), 339-347. doi:10.1177/0956797610397666

Kaas, J. H., & Lyon, D. C. (2007). Pulvinar contributions to the dorsal and ventral streams of visual processing in primates. Brain Research Reviews, 55(2), 285-296. doi:10.1016/j.brainresrev.2007.02.008

Kaas, J. H., Gharbawie, O. A., & Stepniewska, I. (2011). The Organization and Evolution of Dorsal Stream Multisensory Motor Pathways in Primates. Frontiers in Neuroanatomy, 5. doi:10.3389/fnana.2011.00034

Kakei, S., Hoffman, D. S., Strick, P. L. (1999). Muscle and Movement Representations in the Primary Motor Cortex. Science, 285(5436), 2136-2139. doi:10.1126/science.285.5436.213

Kalaska, J. F., Scott, S. H., Cisek, P., & Sergio, L. E. (1997). Cortical control of reaching movements. Current Opinion in Neurobiology, 7(6), 849-859. doi:10.1016/s0959-4388(97)80146-8

Kandel, E. R., Schwartz, J. H. 1., & Jessell, T. M. (2000). Principles of neural science (4th ed.), Chapter 21: Coding of sensory information. New York: McGraw-Hill, Health Professions Division.

Kanitscheider, I., Coen-Cagli, R., & Pouget, A. (2015). Origin of information-limiting noise correlations. Proceedings of the National Academy of Sciences, 112(50). doi:10.1073/pnas.1508738112

Kaufman, M. T., Churchland, M. M., & Shenoy, K. V. (2013). The roles of monkey M1 neuron classes in movement preparation and execution. Journal of Neurophysiology, 110(4), 817-825. doi:10.1152/jn.00892.2011

Kelly, R. C., Smith, M. A., Samonds, J. M., Kohn, A., Bonds, A. B., Movshon, J. A., & Lee, T. S. (2007). Comparison of Recordings from Microelectrode Arrays and Single Electrodes in the Visual Cortex. Journal of Neuroscience, 27(2), 261-264. doi:10.1523/jneurosci.4906-06.2007

Khan, A. Z., Song, J., & Mcpeek, R. M. (2011). The eye dominates in guiding attention during simultaneous eye and hand movements. Journal of Vision, 11(1), 9-9. doi:10.1167/11.1.9

Kim, J., Ghaffari, R., & Kim, D. (2017). The quest for miniaturized soft bioelectronic devices. Nature Biomedical Engineering, 1(3), 0049. doi:10.1038/s41551-017-0049

Ko, H., Hofer, S. B., Pichler, B., Buchanan, K. A., Sjöström, P. J., & Mrsic-Flogel, T. D. (2011). Functional specificity of local synaptic connections in neocortical networks. Nature, 473(7345), 87-91. doi:10.1038/nature09880

Kohn, A. & Smith, M.A. (2005). Stimulus dependence of neuronal correlation in primary visual cortex of the macaque. Journal of Neuroscience: 25, 3661–3673

Kohn, A., Coen-Cagli, R., Kanitscheider, I., & Pouget, A. (2016). Correlations and Neuronal Population Information. Annual Review of Neuroscience, 39(1), 237-256. doi:10.1146/annurev-neuro-070815-013851

Kwan, H. C., Murphy, J. T., & Wong, Y. C. (1987). Interaction between neurons in precentral cortical zones controlling different joints. Brain Research, 400(2), 259-269. doi:10.1016/0006-8993(87)90625-1

Lacquaniti, F., Caminiti, R. (1998). Visuo-motor transformations for arm reaching. European Journal of Neuroscience, 10(1), 195-203. doi:10.1046/j.1460-9568.1998.00040.x

Lebedev, M. A., & Nicolelis, M. A. (2017). Brain-Machine Interfaces: From Basic Science to Neuroprostheses and Neurorehabilitation. Physiological Reviews, 97(2), 767-837. doi:10.1152/physrev.00027.2016

Lee, D., Poizner, H., Corcos, D. M., & Henriques, D. Y. (2013). Unconstrained reaching modulates eye–hand coupling. Experimental Brain Research, 232(1), 211-223. doi:10.1007/s00221-013-3732-9

Lee, D., Port, N. L., Kruse, W., Georgopoulos, A. P. (1998). Variability and Correlated Noise in the Discharge of Neurons in Motor and Parietal Areas of the Primate Cortex. Journal of Neuroscience: 18 (3) 1161-1170

Lehmann, S. J., & Scherberger, H. (2013). Reach and Gaze Representations in Macaque Parietal and Premotor Grasp Areas. Journal of Neuroscience, 33(16), 7038-7049. doi:10.1523/jneurosci.5568-12.2013

Lemon, R. N. (2008). Descending Pathways in Motor Control. Annual Review of Neuroscience, 31(1), 195-218. doi:10.1146/annurev.neuro.31.060407.125547

Lenci, F., Ghetti, F., & Song, P. (2001). Chapter 17 Photomovement in ciliates. Comprehensive Series in Photosciences Photomovement, 475-503. doi:10.1016/s1568-461x(01)80021-1

Lent, R., Azevedo, F. A., Andrade-Moraes, C. H., & Pinto, A. V. (2011). How many neurons do you have? Some dogmas of quantitative neuroscience under revision. European Journal of Neuroscience, 35(1), 1-9. doi:10.1111/j.1460-9568.2011.07923.x

Lynch, J. C., Mountcastle, V. B., Talbot, W. H., Yin, T. C. (1977). Parietal lobe mechanisms for directed visual attention. Journal of Neuroscience, 40(2):362-89

Mante, V., Carandini, M. (2005). Mapping of Stimulus Energy in Primary Visual Cortex. Journal of Neurophysiology, 94(1), 788-798. doi:10.1152/jn.01094.2004

Mantini, D., Hasson, U., Betti, V., Perrucci, M. G., Romani, G. L., Corbetta, M., . . . Vanduffel, W. (2012). Interspecies activity correlations reveal functional correspondence between monkey and human brain areas. Nature Methods, 9(3), 277-282. doi:10.1038/nmeth.1868

Mascaro, M., Battaglia-Mayer, A., Nasi, L., Amit, D. J., Caminiti, R. (2003). The Eye and the Hand: Neural Mechanisms and Network Models for Oculomanual Coordination in Parietal Cortex. Cerebral Cortex, 13(12), 1276-1286. doi:10.1093/cercor/bhg075

Matelli, M., Luppino, G., Rizzolatti, G. (1985). Patterns of cytochrome oxidase activity in the frontal agranular cortex of the macaque monkey. Behavioural Brain Research, 18: 125-136

Maunsell, J.H., van Essen, D.C. (1983).The connections of the middle temporal visual area (MT) and their relationship to a cortical hierarchy in the macaque monkey. Journal of Neurophysiology: 3(12):2563-86

Maynard, E. M., Hatsopoulos, N. G., Ojakangas, C. L., Acuna, B. D., Sanes, J. N., Normann, R. A., Donoghue, J. P. (1999). Neuronal interactions improve cortical population coding of movement direction. Journal of Neuroscience: 19:8083–8093

Mcfarland, J. M., Bondy, A. G., Saunders, R. C., Cumming, B. G., & Butts, D. A. (2015). Saccadic modulation of stimulus processing in primary visual cortex. Nature Communications, 6, 8110. doi:10.1038/ncomms9110

Mchugh, M. L. (2011). Multiple comparison analysis testing in ANOVA. Biochemia Medica, 203-209. doi:10.11613/bm.2011.029

Michaels, J. A., Dann, B., Intveld, R. W., & Scherberger, H. (2015). Predicting Reaction Time from the Neural State Space of the Premotor and Parietal Grasping Network. Journal of Neuroscience, 35(32), 11415-11432. doi:10.1523/jneurosci.1714-15.2015

Milekovic, T., Truccolo, W., Grün, S., Riehle, A., & Brochier, T. (2015). Local field potentials in primate motor cortex encode grasp kinetic parameters. NeuroImage, 114, 338-355. doi:10.1016/j.neuroimage.2015.04.008

Milner, D., & Goodale, M. (2006). The Visual Brain in Action (Revision of the book of the same name from 1995). doi:10.1093/acprof:oso/9780198524724.001.0001

Mirabella, G., Bertini, G., Samengo, I., Kilavik, B. E., Frilli, D., Libera, C. D., & Chelazzi, L. (2007). Neurons in Area V4 of the Macaque Translate Attended Visual Features into Behaviorally Relevant Categories. Neuron, 54(2), 303-318. doi:10.1016/j.neuron.2007.04.007

Mitchell, J. F., Sundberg, K. A., & Reynolds, J. H. (2007). Differential Attention-Dependent Response Modulation across Cell Classes in Macaque Visual Area V4. Neuron, 55(1), 131-141. doi:10.1016/j.neuron.2007.06.018

Mitchell, J.F., Sundberg, K.A. & Reynolds, J.H. (2009). Spatial attention decorrelates intrinsic activity fluctuations in macaque area V4. Neuron 63, 879–888

Mooshagian, E., Wang, C., Ferdoash, A., & Snyder, L. H. (2014). Movement order and saccade direction affect a common measure of eye-hand coordination in bimanual reaching. Journal of Neurophysiology, 112(3), 730-739. doi:10.1152/jn.00234.2014

Mountcastle, V. B., Lynch, J.C., Georgopoulos, A., Sakata, H., Acuna, C. (1975) Posterior parietal association cortex of the monkey: command functions for operations within extrapersonal space. Journal of Neuroscience, 38(4):871-908

Mustari, M. J., Ono, S., & Das, V. E. (2009). Signal Processing and Distribution in Cortical-Brainstem Pathways for Smooth Pursuit Eye Movements. Annals of the New York Academy of Sciences, 1164(1), 147-154. doi:10.1111/j.1749-6632.2009.03859.x

Nachev, P., Kennard, C., & Husain, M. (2008). Functional role of the supplementary and pre-supplementary motor areas. Nature Reviews Neuroscience, 9(11), 856-869. doi:10.1038/nrn2478

Nachev, P., Wydell, H., O'Neill, K., Husain, M., & Kennard, C. (2007). The role of the pre-supplementary motor area in the control of action. NeuroImage, 36. doi:10.1016/j.neuroimage.2007.03.034

Nawrot, M. P., Boucsein, C., Molina, V. R., Riehle, A., Aertsen, A., & Rotter, S. (2008). Measurement of variability dynamics in cortical spike trains. Journal of Neuroscience Methods, 169(2), 374-390. doi:10.1016/j.jneumeth.2007.10.013

Neggers, S. F., Bekkering, H. (2001) Gaze anchoring to a pointing target is present during the entire pointing movement and is driven by a non-visual signal. Journal of Neuroscience, 86(2):961-70

Neggers, S.F., Bekkering, H. (2000) Ocular gaze is anchored to the target of an ongoing pointing movement. Journal of Neurophysiology, 83(2):639-51

Nevet, A., Morris, G., Saban, G., Arkadir, D. & Bergman, H. (2007). Lack of spike-count and spike-time correlations in the substantia nigra reticulata despite overlap of neural responses. Journal of Neurophysiology, 98, 2232–2243

Nicolelis, M. A., Ghazanfar, A. A., Faggin, B. M., Votaw, S., & Oliveira, L. M. (1997). Reconstructing the Engram: Simultaneous, Multisite, Many Single Neuron Recordings. Neuron, 18(4), 529-537. doi:10.1016/s0896-6273(00)80295-0

Nordhausen, C. T., Maynard, E. M., & Normann, R. A. (1996). Single unit recording capabilities of a 100 microelectrode array. Brain Research, 726(1-2), 129-140. doi:10.1016/0006-8993(96)00321-6

Overgaard, M. (2012). Blindsight: recent and historical controversies on the blindness of blindsight. Wiley Interdisciplinary Reviews: Cognitive Science, 3(6), 607-614. doi:10.1002/wcs.1194

Paik, S., & Ringach, D. L. (2011). Retinal origin of orientation maps in visual cortex. Nature Neuroscience, 14(7), 919-925. doi:10.1038/nn.2824

Parton, A., Nachev, P., Hodgson, T. L., Mort, D., Thomas, D., Ordidge, R., . . . Husain, M. (2007). Role of the human supplementary eye field in the control of saccadic eye movements. Neuropsychologia, 45(5), 997-1008. doi:10.1016/j.neuropsychologia.2006.09.007

Paus, T. (1996). Location and function of the human frontal eye-field: A selective review. Neuropsychologia, 34(6), 475-483. doi:10.1016/0028-3932(95)00134-4

Pelz, J., Hayhoe, M., & Loeber, R. (2001). The coordination of eye, head, and hand movements in a natural task. Experimental Brain Research, 139(3), 266-277. doi:10.1007/s002210100745

Perkel, D. H., Gerstein, G. L., & Moore, G. P. (1967). Neuronal Spike Trains and Stochastic Point Processes. Biophysical Journal, 7(4), 419-440. doi:10.1016/s0006-3495(67)86597-4

Pitzalis, S., Sereno, M., Committeri, G., Fattori, P., Galati, G., Tosoni, A., & Galletti, C. (2013). The human homologue of macaque area V6A. NeuroImage, 82, 517-530. doi:10.1016/j.neuroimage.2013.06.026

Polanen, V. V., & Davare, M. (2015). Interactions between dorsal and ventral streams for controlling skilled grasp. Neuropsychologia, 79, 186-191. doi:10.1016/j.neuropsychologia.2015.07.010

Poort, J., & Roelfsema, P. R. (2009). Noise Correlations Have Little Influence on the Coding of Selective Attention in Area V1. Cerebral Cortex, 19(3), 543-553. doi:10.1093/cercor/bhn103

Poort, J., Raudies, F., Wannig, A., Lamme, V., Neumann, H., & Roelfsema, P. (2012). The Role of Attention in Figure-Ground Segregation in Areas V1 and V4 of the Visual Cortex. Neuron, 75(1), 143-156. doi:10.1016/j.neuron.2012.04.032

Prablanc, C., Echallier, J. E., Jeannerod, M., & Komilis, E. (1979). Optimal response of eye and hand motor systems in pointing at a visual target. Biological Cybernetics, 35(3), 183-187. doi:10.1007/bf00337063

Rand, M. K. (2014). Segment interdependency and gaze anchoring during manual two-segment sequences. Experimental Brain Research, 232(9), 2753-2765. doi:10.1007/s00221-014-3951-8

Rand, M. K., & Stelmach, G. E. (2010). Effects of hand termination and accuracy constraint on eye–hand coordination during sequential two-segment movements. Experimental Brain Research, 207(3-4), 197-211. doi:10.1007/s00221-010-2456-3

Rasch, M.J., Schuch, K., Logothetis, N.K. & Maass, W. (2011). Statistical comparison of spike responses to natural stimuli in monkey area V1 with simulated responses of a detailed laminar network model for a patch of V1. Journal of Neurophysiology: 105, 757–778

Rasmussen, T., Penfield, W. (1948). Movement of head and eyes from stimulation of human frontal cortex. Research publications - Association for Research in Nervous and Mental Disease: 27: 346–361, 1948

Rathelot, J. A., Strick, P.L. (2006). Muscle representation in the macaque motor cortex: an anatomical perspective. Proceedings of the National Academy of Sciences of the United States America, 103(21):8257-62

Reich, D.S., Mechler, F. & Victor, J.D. (2001). Independent and redundant information in nearby cortical neurons. Science 294: 2566–2568

Reina, G., & Schwartz, A. B. (2003). Eye–hand coupling during closed-loop drawing: Evidence of shared motor planning? Human Movement Science, 22(2), 137-152. doi:10.1016/s0167-9457(02)00156-2

Rétaux, S., Kano, S. (2010) Midline Signaling and Evolution of the Forebrain in Chordates: A Focus on the Lamprey Hedgehog Case. Integr Comp Biol; 50 (1): 98-109. doi: 10.1093/icb/icq032

Riehle, A., Wirtssohn, S., Grün, S., & Brochier, T. (2013). Mapping the spatio-temporal structure of motor cortical LFP and spiking activities during reach-to-grasp movements. Frontiers in Neural Circuits, 7. doi:10.3389/fncir.2013.00048

Rizzolatti, G., & Matelli, M. (2003). Two different streams form the dorsal visual system: anatomy and functions. Experimental Brain Research, 153(2), 146-157. doi:10.1007/s00221-003-1588-0

Rizzolatti, G., Riggio, L., Dascola, I., and Umiltà, C. (1987). Reorienting attention across the horizontal and vertical meridians: evidence in favor of a premotor theory of attention. Neuropsychologia, 25, 31–40.

Roe, A. W., & Ts'O, D. Y. (1997). The Functional Architecture of Area V2 in the Macaque Monkey. Extrastriate Cortex in Primates Cerebral Cortex, 295-333. doi:10.1007/978-1-4757-9625-4_7

Roe, A., Chelazzi, L., Connor, C., Conway, B., Fujita, I., Gallant, J., . . . Vanduffel, W. (2012). Toward a Unified Theory of Visual Area V4. Neuron, 74(1), 12-29. doi:10.1016/j.neuron.2012.03.011

Rogal, L., Reible, G., & Fischer, B. (1985). Reaction times of the eye and the hand of the monkey in a visual reach task. Neuroscience Letters, 58(1), 127-132. doi:10.1016/0304-3940(85)90341-6

Romo, R., Hernández, A., Zainos, A., & Salinas, E. (2003). Correlated Neuronal Discharges that Increase Coding Efficiency during Perceptual Discrimination. Neuron, 38(4), 649-657. doi:10.1016/s0896-6273(03)00287-3

Rosenbluth, D., & Allman, J. M. (2002). The Effect of Gaze Angle and Fixation Distance on the Responses of Neurons in V1, V2, and V4. Neuron, 33(1), 143-149. doi:10.1016/s0896-6273(01)00559-1

Rubehn, B., Bosman, C., Oostenveld, R., Fries, P., & Stieglitz, T. (2009). A MEMS-based flexible multichannel ECoG-electrode array. Journal of Neural Engineering, 6(3), 036003. doi:10.1088/1741-2560/6/3/036003

Sailer, U. (2005). Eye-Hand Coordination during Learning of a Novel Visuomotor Task. Journal of Neuroscience, 25(39), 8833-8842. doi:10.1523/jneurosci.2658-05.2005

Sakata, H., Shibutani, H., Kawano, K., & Harrington, T. L. (1985). Neural mechanisms of space vision in the parietal association cortex of the monkey. Vision Research, 25(3), 453-463. doi:10.1016/0042-6989(85)90070-7

Salinas, E., & Sejnowski, T. J. (2001). Book Review: Gain Modulation in the Central Nervous System: Where Behavior, Neurophysiology, and Computation Meet. The Neuroscientist, 7(5), 430-440. doi:10.1177/107385840100700512

Samonds, J.M., Potetz, B.R. & Lee, T.S. (2009). Cooperative and competitive interactions facilitate stereo computations in macaque primary visual cortex. Journal of Neuroscience. 29, 15780–15795

Sandwell, D. T. (1987). Biharmonic spline interpolation of GEOS-3 and SEASAT altimeter data. Geophysical Research Letters, 14(2), 139-142. doi:10.1029/gl014i002p00139

Sarlegna, F., Blouin, J., Bresciani, J., Bourdin, C., Vercher, J., & Gauthier, G. M. (2003). Target and hand position information in the online control of goal-directed arm movements. Experimental Brain Research, 151(4), 524-535. doi:10.1007/s00221-003-1504-7

Sayegh, P. F., Hawkins, K. M., Neagu, B., Crawford, J. D., Hoffman, K. L., & Sergio, L. E. (2013). Differences in spectral profiles between rostral and caudal premotor cortex when hand-eye actions are decoupled. Journal of Neurophysiology, 110(4), 952-963. doi:10.1152/jn.00764.2012

Sayegh, P. F., Hawkins, K. M., Neagu, B., Crawford, J. D., Hoffman, K. L., & Sergio, L. E. (2014). Decoupling the actions of the eyes from the hand alters beta and gamma synchrony within SPL. Journal of Neurophysiology, 111(11), 2210-2221. doi:10.1152/jn.00793.2013

Schenk, T., & Mcintosh, R. D. (2010). Do we have independent visual streams for perception and action? Cognitive Neuroscience, 1(1), 52-62. doi:10.1080/17588920903388950

Schmid, M. C., Mrowka, S. W., Turchi, J., Saunders, R. C., Wilke, M., Peters, A. J., . . . Leopold, D. A. (2010). Blindsight depends on the lateral geniculate nucleus. Nature, 466(7304), 373-377. doi:10.1038/nature09179

Schneider, G. E. (1969). Two Visual Systems. Science, 163(3870), 895-902. doi:10.1126/science.163.3870.895

Schulz, D. P., Sahani, M., & Carandini, M. (2015). Five key factors determining pairwise correlations in visual cortex. Journal of Neurophysiology, 114(2), 1022-1033. doi:10.1152/jn.00094.2015

Schwartz, A. B. (2004). Differential Representation of Perception and Action in the Frontal Cortex. Science, 303(5656), 380-383. doi:10.1126/science.1087788

Scott, S. H. (1999). Apparatus for measuring and perturbing shoulder and elbow joint positions and torques during reaching. Journal of Neuroscience Methods, 89(2), 119-127. doi:10.1016/s0165-0270(99)00053-9

Shadlen, M. N., & Newsome, W. T. (1994). Noise, neural codes and cortical organization. Current Opinion in Neurobiology, 4(4), 569-579. doi:10.1016/0959-4388(94)90059-0

Shadmehr, R., & Wise, S. P. (2005). The computational neurobiology of reaching and pointing: a foundation for motor learning. Cambridge, MA: MIT Press.

Shipp, S., & Zeki, S. (2002). The functional organization of area V2, I: Specialization across stripes and layers. Visual Neuroscience, 19(02), 187-210. doi:10.1017/s0952523802191164

Shipp, S., Blanton, M., & Zeki, S. (1998). A visuo-somatomotor pathway through superior parietal cortex in the macaque monkey: cortical connections of areas V6 and V6A. European Journal of Neuroscience, 10(10), 3171-3193. doi:10.1046/j.1460-9568.1998.00327.x

Sincich, L. C., Jocson, C. M., & Horton, J. C. (2010). V1 Interpatch Projections to V2 Thick Stripes and Pale Stripes. Journal of Neuroscience, 30(20), 6963-6974. doi:10.1523/jneurosci.5506-09.2010

Slater, H., Milne, A. E., Wilson, B., Muers, R. S., Balezeau, F., Hunter, D., . . . Petkov, C. I. (2016). Individually customisable non-invasive head immobilisation system for non-human primates with an option for voluntary engagement. Journal of Neuroscience Methods, 269, 46-60. doi:10.1016/j.jneumeth.2016.05.009

Smith, M. A., & Kohn, A. (2008). Spatial and Temporal Scales of Neuronal Correlation in Primary Visual Cortex. Journal of Neuroscience, 28(48), 12591-12603. doi:10.1523/jneurosci.2929-08.2008

Smith, M.A. & Kohn, A. (2008).Spatial and temporal scales of neuronal correlation in primary visual cortex. Journal of Neuroscience: 28, 12591–12603

Snyder, L. H., Batista, A. P., & Andersen, R. A. (1997). Coding of intention in the posterior parietal cortex. Nature, 386(6621), 167-170. doi:10.1038/386167a0

Softky, W., & Koch, C. (1992). Cortical Cells Do NOT Perform Temporal Integration of Small EPSPs. International Journal of Neural Systems, 03(Supp01), 169-173. doi:10.1142/s0129065792000498

Song, J. H., & Mcpeek, R. M. (2010). Roles of Narrow- and Broad-Spiking Dorsal Premotor Area Neurons in Reach Target Selection and Movement Production. Journal of Neurophysiology, 103(4), 2124-2138. doi:10.1152/jn.00238.2009

Stark, E., Globerson, A., Asher, I. & Abeles, M. (2008). Correlations between groups of premotor neurons carry information about prehension. Journal of Neuroscience, 28, 10618–10630

Steinmetz, M. A., Connor, C. E., Constantinidis, C., McLaughlin, J. R. (1994). Covert attention suppresses neuronal responses in area 7a of the posterior parietal cortex. Journal of Neurophysiology: 72:1020–1023

Stevens, C. F., & Zador, A. M. (1998). Input synchrony and the irregular firing of cortical neurons. Nature Neuroscience, 1(3), 210-217. doi:10.1038/659

Swisher, J. D., Halko, M. A., Merabet, L. B., Mcmains, S. A., & Somers, D. C. (2007). Visual Topography of Human Intraparietal Sulcus. Journal of Neuroscience, 27(20), 5326-5337. doi:10.1523/jneurosci.0991-07.2007

Takahashi, K., Kim, S., Coleman, T. P., Brown, K. A., Suminski, A. J., Best, M. D., & Hatsopoulos, N. G. (2015). Large-scale spatiotemporal spike patterning consistent with wave propagation in motor cortex. Nature Communications, 6, 7169. doi:10.1038/ncomms8169

Tanaka, K., Hikosaka, K., Saito, H., Yukie, M., Fukada, Y., Iwai, E. (1986). Analysis of local and wide-field movements in the superior temporal visual areas of the macaque monkey. Journal of Neuroscience: 6 (1) 134-144

Tanné, J., Boussaoud, D., Boyer-Zeller, N., & Rouiller, E. M. (1995). Direct visual pathways for reaching movements in the macaque monkey. NeuroReport, 7(1), 267-272. doi:10.1097/00001756-199512290-00064

Thura, D., Hadj-Bouziane, F., Meunier, M., & Boussaoud, D. (2008). Hand position modulates saccadic activity in the frontal eye field. Behavioural Brain Research, 186(1), 148-153. doi:10.1016/j.bbr.2007.07.035

Tolias, A. S., Moore, T., Smirnakis, S. M., Tehovnik, E. J., Siapas, A. G., & Schiller, P. H. (2001). Eye Movements Modulate Visual Receptive Fields of V4 Neurons. Neuron, 29(3), 757-767. doi:10.1016/s0896-6273(01)00250-1

Tootell, R. B. H., Mendola, J. D., Hadjikhani, N. K., Ledden, P. J., Liu, A. K., Reppas, J. B., . . . Dale, A. M. (1997). Functional Analysis of V3A and Related Areas in Human Visual Cortex. Journal of Neuroscience, 17 (18) 7060-7078

Torre, E., Quaglio, P., Denker, M., Brochier, T., Riehle, A., & Grun, S. (2016). Synchronous Spike Patterns in Macaque Motor Cortex during an Instructed-Delay Reach-to-Grasp Task. Journal of Neuroscience, 36(32), 8329-8340. doi:10.1523/jneurosci.4375-15.2016

Torrecillos, F., Alayrangues, J., Kilavik, B. E., & Malfait, N. (2015). Distinct Modulations in Sensorimotor Postmovement and Foreperiod -Band Activities Related to Error Salience Processing and Sensorimotor Adaptation. Journal of Neuroscience, 35(37), 12753-12765. doi:10.1523/jneurosci.1090-15.2015

Toyama, K., Kimura, M., & Tanaka, K. (1981). Cross-Correlation Study Of The Cats Visual Cortex. Regulatory Functions of the CNS Subsystems, 69-78. doi:10.1016/b978-0-08-027371-6.50013-6

Trevarthen, C. B. (1968). Two mechanisms of vision in primates. Psychologische Forschung, 31(4), 299-337. doi:10.1007/bf00422717

Ts'o, D. Y., Gilbert, C. D., Wiesel, T. N. (1986). Relationships between horizontal interactions and functional architecture in cat striate cortex as revealed by cross-correlation analysis. Journal of Neuroscience: 6 (4) 1160-1170

Ungerleider, L. G., & Desimone, R. (1986). Cortical connections of visual area MT in the macaque. The Journal of Comparative Neurology, 248(2), 190-222. doi:10.1002/cne.902480204

Ungerleider, L. G., & Mishkin, M. (1982). Two cortical visual systems. In D. J. Ingle, M. A. Goodale, & R. J. W. Mansfield (Eds.), Analysis of visual behavior (pp. 549-586). Cambridge: MIT Press.

Ungerleider, L. G., Galkin,T. W., Desimone, R., Gattass, R. (2008) Cortical connections of area V4 in the macaque. Cerebral Cortex:18(3):477-99

Vercher, J., Magenes, G., Prablanc, C., & Gauthier, G. (1994). Eye-head-hand coordination in pointing at visual targets: spatial and temporal analysis. Experimental Brain Research, 99(3). doi:10.1007/bf00228987

Vernet, M., Quentin, R., Chanes, L., Mitsumasu, A., & Valero-Cabre, A. (2014). Corrigendum: Frontal eye field, where art thou? Anatomy, function, and non-invasive manipulation of frontal regions involved in eye movements and associated cognitive operations. Frontiers in Integrative Neuroscience, 8. doi:10.3389/fnint.2014.00088

Vigneswaran, G., Kraskov, A., & Lemon, R. N. (2011). Large Identified Pyramidal Cells in Macaque Motor and Premotor Cortex Exhibit "Thin Spikes": Implications for Cell Type Classification. Journal of Neuroscience, 31(40), 14235-14242. doi:10.1523/jneurosci.3142-11.2011

Weiskrantz, L., & Cowey, A. (1963). Striate cortex lesions and visual acuity of the rhesus monkey. Journal of Comparative and Physiological Psychology, 56(2), 225-231. doi:10.1037/h0043778

Werner, W., Dannenberg, S., & Hoffmann, K. (1997). Arm-movement-related neurons in the primate superior colliculus and underlying reticular formation: comparison of neuronal activity with EMGs of muscles of the shoulder, arm and trunk during reaching. Experimental Brain Research, 115(2), 191-205. doi:10.1007/pl00005690

Wise, S. P., Boussaoud, D., Johnson, P. B., & Caminiti, R. (1997). PREMOTOR AND PARIETAL CORTEX: Corticocortical Connectivity and Combinatorial Computations. Annual Review of Neuroscience, 20(1), 25-42. doi:10.1146/annurev.neuro.20.1.25

Wise, S. P., Pellegrino, G. D., & Boussaoud, D. (1996). The premotor cortex and nonstandard sensorimotor mapping. Canadian Journal of Physiology and Pharmacology, 74(4), 469-482. doi:10.1139/y96-035

Woodworth, R. S. (1899). The accuracy of voluntary movement. Psychological Review, 3, (3, Suppl. 13), 1-119

Wu, C., Kwon, O., & Kowler, E. (2010). Fitts's Law and speed/accuracy trade-offs during sequences of saccades: Implications for strategies of saccadic planning. Vision Research, 50(21), 2142-2157. doi:10.1016/j.visres.2010.08.008

Wunderlich, G., Marshall, J., Amunts, K., Weiss, P., Mohlberg, H., Zafiris, O., . . . Fink, G. (2002). The importance of seeing it coming: a functional magnetic resonance imaging study of motion-in-depth towards the human observer. Neuroscience, 112(3), 535-540. doi:10.1016/s0306-4522(02)00110-0

Yttri, E. A., Liu, Y., & Snyder, L. H. (2013). Lesions of cortical area LIP affect reach onset only when the reach is accompanied by a saccade, revealing an active eye-hand coordination circuit. Proceedings of the National Academy of Sciences, 110(6), 2371-2376. doi:10.1073/pnas.1220508110

Yttri, E. A., Wang, C., Liu, Y., & Snyder, L. H. (2014). The parietal reach region is limb specific and not involved in eye-hand coordination. Journal of Neurophysiology, 111(3), 520-532. doi:10.1152/jn.00058.2013

Zehl, L., Jaillet, F., Stoewer, A., Grewe, J., Sobolev, A., Wachtler, T., . . . Grün, S. (2016). Handling Metadata in a Neurophysiology Laboratory. Frontiers in Neuroinformatics, 10. doi:10.3389/fninf.2016.00026